Masters Thesis in
Mechanical Engineering
November 2010

The Development and Optimisation of a Low Cost Optical Chemical Sensing Platform

Dylan Orpen, BEng

November 2010

A thesis submitted to Dublin City University in partial fulfilment of the requirements for the degree of Master of Engineering.

CLARITY Research Centre:
The Centre for Sensor Web Technologies
National Centre for Sensor Research
School of Mechanical and Manufacturing Engineering
Dublin City University
Dublin 9, Ireland

Declaration

I hereby certify that this material, which I now submit for assessment on the programme of study leading to the award of Masters in Engineering is entirely my own work, that I have exercised reasonable care to ensure that the work is original, and does not to the best of my knowledge breach any law of copyright, and has not been taken from the work of others save and to the extent that such work has been cited and acknowledged within the text of my work.

Dylan Orpen
Student ID No: 54382293
Date: November-2010

Contact Information:
Author: Dylan Orpen
E-mail: orpend2@gmail.com

University Supervisor:
Dr. Brian Corcoran
Lecturer
Mechanical and Manufacturing Engineering
Dublin City University
Dublin 9
Ireland
Internet: www.dcu.ie
Phone: +353 1 700 8040

Research Group Supervisor:
Prof. Dermot Diamond
Principle Investigator
CLARITY
Dublin City University
Dublin 9
Ireland
Internet: www.clarity-centre.org
Phone: +353 1 700 5404

Acknowledgements

I would like to take this opportunity to thank those that helped me on the road to completing this thesis. Firstly I would like to extend my thanks to the extended CLARITY family who were continuously generous with their time and expertise; namely, Cormac, Damien, Steve, Breda, Emer, Martina, John, the list goes on. Without their help and direction the completion of this work would not have been possible.

I would also like to thank those outside of the CLARITY group who went out of their own way to facilitate work that was required within the project; namely Dr. Karl Crowley, the inkjet printing supremo and Dr. Tony Cafolla, the AFM wizard.

Lastly I am indebted to my supervisors, Dr. Brian Corcoran, and Prof. Dermot Diamond. Thank you for giving me the opportunity to further my studies to the point where I am now able to present this thesis. It has been a personally developing experience where I was given the chance to broaden my education through working in new areas with some truly talented people, and for this I am extremely grateful.

Lastly this research has been supported by Science Foundation Ireland (SFI) under the grant 07/CE/I1147.

Abstract

With recent improvements in wireless sensor network hardware it is logical there should be a concurrent push to develop the sensors that are compatible in terms of price and performance. Wireless sensor networks are made up of a multitude of low power sensing nodes and are typically deployed in a scatter web configuration. A key concept is that the nodes are so low cost and are spread so densely, that the failure of any one node will not be a cause for great concern. The sensed data collected from wireless sensing networks have advantages over other traditional sensing methods. For example, the accuracy of any one particular node is not critical to the system; however, there must be reproducibility in the data from one node relative to the next. Therefore, when data is compared from multiple nodes one can deduce if the signal is increasing or decreasing and, hence, develop a directional sense to the response. This is something that cannot be achieved using traditional single point grab sampling.

The chemical sensor optimised as part of this project is based on the use of two light emitting diodes (LEDs), as both the light source and photodetector. This light sensor, when coupled with a PET slide coated with a pH sensitive colorimetric dye realises a simple gas sensor. Such setups have been successfully used to detect both acetic acid and ammonia. To date the sensors are already low cost due to their operating principle being based on the use of off the shelf LEDs, but flaws include a lack of reproducibility in sensed data. This is partly due to a reliance on poor manufacturing methods. Such inaccuracies have led to the requirement of an expensive individual node by node calibration.

The goal of this work is to improve the system performance through redesign. This will be accomplished by integration of the device into a flowcell platform, and the automation of the sensor creation process. The redesign of the sensor will improve sensor performance and It is hoped that this will increase accuracy in collected data and also increase the reproducibility of the created sensors. This reproducibility increase will be achieved through this careful control of deposited film thickness, and through the utilization of the highly reproducible inkjet printing process. The enhanced reproducibility between sensors opens the potential of calibration free use.

Table of Contents

List of Figures

List of Tables

List of Acronyms

ABS	-	Acrylonitrile butadiene styrene
ADC	-	Analog-to-digital converter
AFM	-	Atomic force microscopy
BPB	-	Bromophenol Blue
CAD	-	Computer-aided design
CNC	-	Computer numerically controlled
DOD	-	Drop on demand
FDM	-	Fused deposition modelling
FID	-	Flame ionization detector
GC-MS	-	Gas chromatography-mass spectrometry
GUI	-	Graphical user interface
I/O	-	Input/Output
ISE	-	Ion selective electrode
LED	-	Light emitting diode
LOD	-	Limit of detection
MEMS	-	Microelectromechanical systems
NPNA	-	Normalized protein equivalent of total nitrogen appearance
PCB	-	Printed circuit board
PEDD	-	Paired emitter detector diode
PET	-	Polyethylene terephthalate
PID	-	Photo ionisation detector
POC	-	Proof of concept
PMMA	-	Polymethylmethacrylate
PTFE	-	Polytetrafluoroethylene
PPB	-	Parts per billion
PPM	-	Parts per million
PVC	-	Polyvinylchloride
PVDF	-	Polyvinylidene fluoride

RF	-	Radio frequency
RSD	-	Relative standard deviation
SNR	-	Signal-to-noise ratio
SOP	-	Standard operating procedure
THABR	-	Tetra hexyl ammonium bromide
TVB-N	-	Total volatile base nitrogen
UV	-	Ultraviolet
WSN	-	Wireless sensor network

Publications

Relevant Publications

Journal Articles

Orpen, D., Fay, C., Beirne, S., Corcoran, B and Diamond, D. (2010), "The optimisation of a paired emitter detector diode optical pH sensing device", Sensor and Actuators: B Chemical/doi:10.1016/j.snb.2010.10.007.

Conference Posters

Orpen, D., Fay, C., Beirne, S., Corcoran, B and Diamond, D. (2010), "The development of optical chemical sensors using inkjet printing – key parameters include accuracy, reproducibility and cost", Sensor Systems for Environmental Monitoring, 14th November, Burlington House, Piccadilly, London UK.

Other Publications

Journal Articles

Naher, S., Orpen, D., Brabazon, D and Morshed, M.N. (2010) "An overview of microfludic mixing applications", Advanced Materials Research, Vol 83 – 86, pp 931-939. (Published)

Orpen, D., Naher, S., Brabazon, D., Clause, P., and Morshed, M.M. (2010) "Effects of geometry on microfluidic mixing", Journal of Simiulation of Modelling Practice and Theory. (Submitted)

1

1.1. Chemical and Optical Sensing

The chemical sensing field has been a developing research area since its inception post WWI, where chemical warfare was used with devastating effect. More recently research in the area has been fuelled by the projected figure that the chemical sensor market will grow to $4 billion worldwide within the next 10 years [1]. Some of the primary motivations behind the development of these sensors include "the monitoring and controlling of environmental pollution; improved diagnostics for point of care medical applications; reductions in measurement time, sensor size, and power consumption; improvement in measurement precision and accuracy; and improved detection limits for security, battlefield environments, and process and quality control of industrial applications" [1].

The sensing requirements for each of these applications are similar. They all desire accuracy, precision, short measurement times, and low detection limits, and as a result it is crucial that technologies are developed to meet these criteria.

One type of chemical sensing striving to meet these requirements is optical chemical sensing. Development of optical sensors has been driven by factors such as the "availability of low-cost miniature optoelectronic light sources and detectors, the need for multianalyte array-based sensors, particularly in the area of biosensing, advances in microfluidics and imaging technology, and the trend toward sensor networks to which optical sensors are well suited" [2]. One of the most widely used techniques employed in optical chemical sensors is optical absorption and luminescence [3,4,5], but many sensors based on other spectroscopies have also been realised, such as utilizing refractive index [6] and reflectivity [7] to sense chemical changes.

Within this project a prototype optical sensor, already developed in this research group will be further developed for improved detection of acetic species, and then optimised to improve its performance characteristics. The developed prototype optical sensor is an indirect colorimetric pH sensor, sensitive to acetic acid detection. Colorimetric pH sensors sense using organic pH indicators, the absorbance of which is modified by the pH of their surrounding environment. The pKa of these indicators indicates the centre of the measurable pH range, for example, cresol red, bromophenol blue, and bromocresol purple respond to acidic pH (pH < 7), while cresol red, naphtholbenzene, and phenolphthalein respond at alkaline pH (pH > 7) [2]. The colour change range of the bromophenol blue based dye in this project is similar to that of the bromocresol green shown in Figure 1. Similarly, bromophenol blue is blue in its base alkaline deprotonated state, and becomes yellow in its protonated acetic state. Optical sensors based on the use of these colorimetric dyes are low cost, accurate and appear ideal for the development of low-cost sensing systems.

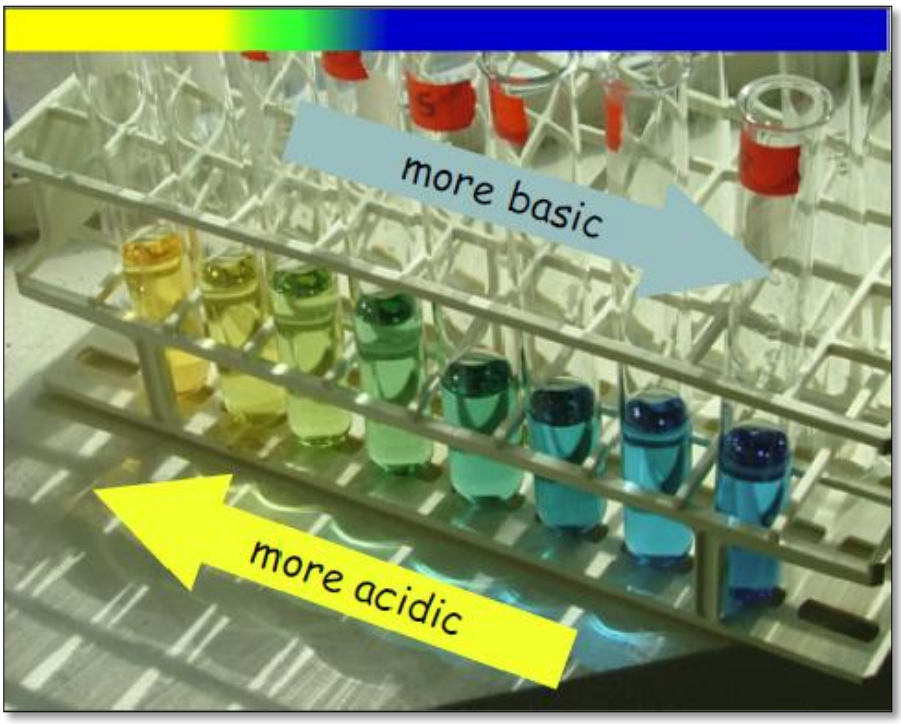

Figure 1: The pH range of the indicator chemical bromocresol green above, and in solution below [8]

Optical sensing devices developed using light emitting diodes (LEDs) offer promise in that they are small, ultra low power, are accurate and are less expensive than conventional sensors. Optical sensors developed using LEDs as both the light source and the light detector are referred to as paired emitter detector diode sensors (PEDD). When such an optical capture system is coupled with a colorimetric coating to modulate the light passing through it, a simple chemical sensor is realised. The colorimetric coatings are developed to change between a light and dark colour in the presence of a chemical contaminant and as this colour change takes place the amount of light falling from the emitter LED onto the detector LED is measured and provides an indirect measurement of the amount of the chemical concentration present.

1.2. Wireless Sensor Networks

A wireless sensor network (WSN) is a collection of nodes organized into a cooperative network [9]. Each node consists of a processor, a transceiver, a power source and a sensor (i.e., a chemical sensor), so, each node can fully support itself in terms of power, sensing and communication. The nodes communicate wirelessly and often self-organize after being deployed in an ad hoc fashion. Systems of 1000s or even 10,000 nodes are anticipated. Such systems have been predicted to revolutionize the way we live and work and interact with the physical world [10]. A simple graphical representation can be seen in the schematic in Figure 2.

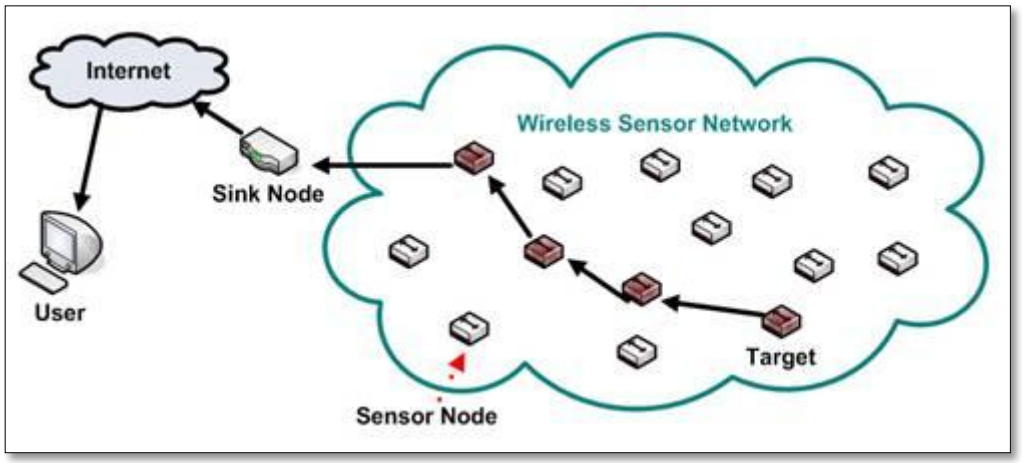

Figure 2: An example of the ad hoc nature of a WSN, and the direction of data flow [11]

Currently, WSNs are beginning to be deployed at an accelerating pace. It is not unreasonable to anticipate that within 10 - 15 years, there will be a dramatic increase in the use of WSNs in our daily lives [9]. These sensors will be automated and access the physical world on our behalf, sensing all types of physical data. It is anticipated this information will be fed autonomously onto the internet, creating a merge between the physical and virtual worlds. This new technology is exciting and when combined with different transducers, application areas are vast, including monitoring and control of environmental pollution, machine health monitoring, industrial monitoring, water quality monitoring, landfill gas monitoring, vehicle detection, traffic management and green house monitoring.

Sensing the physical world with WSNs has inherent advantages over traditional sensing methods (i.e., manual single point sampling/grab sampling). For example, WSNs when configured become autonomous; sensing and relaying data, which can be accessed remotely on demand. Another positive is that networks can include nodes capable of sensing multiple targets and, hence, generate smart sets of data, where trends are easier to identify and display. WSNs can also sense in a directional way and track moving plumes of chemical species, due to the nature of their deployment, whereby following the direction of increasing or decreasing intensities the direction of movement can be calculated and quantified. This concept is central to the use of wireless sensor actuator networks (WSANs), particularly in relation to sensing airborne contaminants. The real time data can be examined autonomously. If certain thresholds are reached, action plans can be triggered (i.e., a mine ventilation shaft could be opened, a subway entrance closed, a purge cycle initiated).

For the effective implementation of large scale WSNs the requirements can be separated out into two categories; hardware development and sensor development. In terms of hardware, it's imperative they consume little power, avoid collisions (have reliability), are implemented with small code size, include robust radio technology, run on low-cost and energy-efficient processors, have flexible signal inputs/outputs and a flexible open source development platform [12]. Many of these requirements have been reached in terms of performance. It is therefore logical, that chemical sensors which could potentially be the nodes in these networks be developed in parallel.

1.3. Inkjet Printing

Printing has long been an industry process relied upon for the creation of cheap reliable devices. Printing is in fact suggested as one of the tools that will be used to realise the goal of WSNs with more than 50,000 nodes. This will be possible when the electronics are printed instead of being wired; meaning a large size and price reduction, where repeatability is still preserved [13]. However, printing is also potentially an ideal deposition method for the creation of chemical sensors. If both sets of components could be printed it would be a large step towards realising the deployment of large WSNs where price could be kept minimal and reliability could be enhanced.

The effective implementation of inkjet printing for sensor creation would offer the ability to be able to generate a very large number of sensors which are robust, reproducible and of low cost. Already, inkjet printing has been successfully implemented for sensor creation. For example polyanaline nanotubes [13,14,15] and carbon nanotubes [16,17] have both been printed and function as sensors with relative success. Such printed nanotubes can be seen in Figure 3 (b), Figure 3 (a) demonstrates an inkjet printed solar cell.

Colorimetric optical sensors have not been printed with the same frequency, but successful printing has been achieved [4]. Historically, printed sensors were fabricated using thick film technologies, namely screen printing. Although, this is still a powerful tool, a range of printing techniques are now being applied to printing devices. The main drivers behind the utilization of inkjet printing for sensor fabrication were the cost reduction and miniaturization from traditional ion selective electrodes (ISEs), increased reducibility, automation, and the ability for mass production.

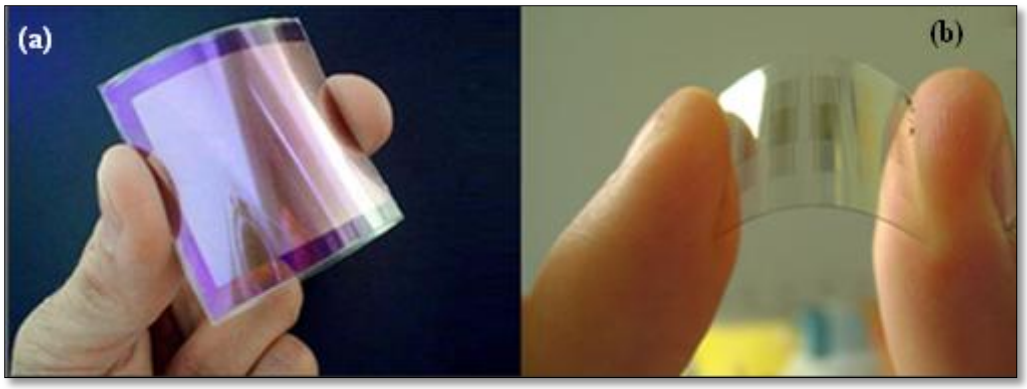

Figure 3: Examples of inkjet printed technologies; (a) a solar cell [18] and (b) inkjet printed carbon nanotubes [19]

1.4. Aims and Objectives of the Study

An ultra low cost PEDD colorimetric sensor was developed previously in DCU as a proof of concept project. The proof of concept configuration has been reported for the detection of acetic acid on a scale of parts per million in ambient air [5]. This project is a further development and optimisation study, of this PEDD sensor, where the chemical sensing device will be redesigned and optimised. For this improvement, the following goals were set out:

- To improve as many performance characteristics of the sensor as possible. (i.e., the limit of detection, speed of response, sensitivity);
- To redesign the device as a standalone device with potential for field trials;
- To incorporate a slide into the device to provide immobilization of the colorimetric coating, allowing for the testing of more controlled deposition methods. This change will also facilitate the quick changing of the sensing film, potentially changing the operation of the device to sense a totally different target;
- Investigate the possibility of creating a slide coating on two sides, potentially doubling the sensitivity and the resolution. A comparison of slides coated on one side against slides coated on both sides could be made.
- Carry out evaluative testing on suitable substrates with potential for immobilising of the colorimetric coating, in order to evaluate what chemical formulation or substrate combination, would work most effectively;

- Investigate inkjet printing as a method for the coating of slides and compare it against the methods currently being utilized (drop casting, dip coating, and painting).
- Investigate the reproducibility of created sensors and test the concept that with a sufficient level of reproducibility batch calibration could be carried out. In this approach, the calibration parameters (baseline, slope, linear range etc.) are transferrable across an entire batch of sensors provided they are very reproducible. This means that only one sensor per batch needs to be calibrated, which is a dramatic improvement on the current practice, which is to individually calibrate every electrode. Batch-wide, transferrable calibration parameters' arising from highly reproducible sensors is a direct consequence of highly automated device fabrication. Both of these combined will drive down the cost of chemical sensors, opening the way to massively scaled up deployments, which is the ultimate goal of our research.

2

2.1. Overview

This literature review will begin with a broad introduction to chemical sensors. This section will track the advancements made since the first discovery of universal indicators dyes which were harvested from lichen mosses [20], through to where the technology has advanced to today with colorimetric coatings being integrated into chemical sensor actuator networks [21,22], where responses are dependent on chemical triggers.

In section 2.2 the various methods of chemical sensing will be introduced and summarised, as will the applications for the technologies. An effort will be made to highlight the key results and also the shortcomings of any of the research work. Within section 2.3 the focus will be on optical sensors and particularly colorimetric sensors, as they are the areas of investigation in this project.

Section 2.4 of the literature review the use of LEDs as sensors will be detailed. This sensor configuration is the platform upon which this project is based. Finally the various applications utilising LEDs as sensors will be examined and the results of the various studies will be analysed.

Section 2.5 explains the history and development of WSNs, including their applications and short comings. The final section, section 2.6 will introduce the printing of chemical coatings, focusing on inkjet printing, a technique central to this study.

2.2. Chemical Sensors

A "chemical sensor" is defined by R. W. Catterall's in his book titled "Chemical Sensors" as a device which "responds to a particular analyte in a selective way through a chemical reaction and can be used for the qualitative or quantitative determination of the analyte. Such a sensor is concerned with detecting and measuring a specific chemical substance or set of chemicals." There are a variety of chemical sensors ranging from very sensitive to broadly sensitive. This range in sensitivity has an implication in cost. Very sensitive chemical sensors which can detect and quantify individual chemical species (i.e., GCMS is prohibitively expensive and usually found as bench top instruments. Therefore, the detection of changes in the chemical environment, such as changes in pH, can be indirectly used to detect the presence of chemical species.

A particular chemical compound is not being sensed as part of this study but rather pH in general. pH is the most commonly measured, chemical variable [23], pH is defined as "*a measure of the acidity or alkalinity of a solution equal to the common logarithm of the reciprocal of the activity of the hydrogen ions in moles per cubic decimetre of solution*" [24]. This highlights that pH measurement is actually a measurement of the concentration of hydrogen ions in a sample. The traditional pH scale which we know today ranges from 0 (acidic) to 14 (alkaline), a scale conceived by Soren Sorensen in 1909.

2.2.1. Chemical Sensing Techniques

Gas chromatography is one of a family of highly efficient (chromatographic) separation techniques [25]. However, gas chromatography cannot fully identify the particular volatiles present in a sample gas. Therefore, the technique is often used in conjunction with other techniques in order to fully analyse samples. Coupling a mass spectrometer with a gas chromatography system (GC-MS) allows for the identification of separate unknown compounds by accurately calculating their molecular weight [26]. This technique can deliver analysis of chemical species down to the ppb (parts per billion) level [25], but has drawbacks, namely the price of the equipment (upwards of $30,000 [27]) and the time it takes to analyse a sample.

Other lab based techniques used for the detection of gas species include flame ionisation detection (FID) and photoionisation detection (PID) which work on a similar concept. The FID system works by burning the sample gas in a hydrogen flame and the ions produced are measured at the sensor electrode. The sensitivity is in the ppm (parts per million) range so it is not as sensitive as the GC-MS system [28]. The PID system has a similar method of operation, where the sample is ionised by UV light source. Again, the current produced by the ions is measured, indicating the concentration of species present. The sensitivity of this technique is in the ppb range. However, with both techniques neither can fully distinguish all species, giving a lack of sensitivity [28]. Similar to the precision laboratory measurement equipment necessary for GC/MS, FID and PID sensing techniques, there are portable handheld devices based upon all of these techniques, but due to the complexity of the techniques they aren't viable as the basis of a network of chemical sensing nodes. However, the PID technique is considered low cost in relation to FID [28].

Sensor systems and individual sensors, based on infrared technology are readily available and are popular as "off the shelf" sensors. These sensors provide gas detection with excellent selectivity and reliability. Infrared sensors are target specific, the wavelength of the sensor can be tuned to a specific band or bands of interest for target gases including hydrocarbons, carbon dioxide, carbon monoxide and ammonia [29]. An alternative form of chemical sensor is the semiconductor sensor, which have been around since the 1970s. These sensors use metal oxides prepared from transition metals (i.e., tin or aluminium), to sense the target gas species. In the presence of the target gas, the metal oxide film causes the gas to dissociate into charged ions producing a current. This change in conductivity produces a signal which indicates the concentration of the target species present. Solid state sensors are very low cost unlike infrared sensors. However, not to the extent that they suit development into WSN with very large node sizes and issues also exist with cross contamination of solid state sensors.

Another family of commercially available sensors are electrochemical sensors. These sensors work by reaction of the target gas at the sensing electrode which produces an electrical signal proportional to the gas concentration present. The main components of an electrochemical sensor are the sensing electrode (target specific)

and the counter electrode, separated by a layer of electrolyte. Electrochemical sensors do have some interference from other gases, and none are completely specific. Electrochemical sensors require the least amount of power of all the gas sensors described in this review, making them the most ideal sensor for development into WSNs. However, electrochemical sensors have a limited shelf life, limited operation time, and possess a narrow temperature range which is subject to several interfering gases such as hydrogen [30].

So, it becomes clear, concluding this section of the review that although there are many gas and pH sensing techniques in use, there are not many techniques which suit development for WSNs. Optical sensors have been widely accepted as a front runner for development with WSNs. Therefore the following section will discuss optical and colorimetric sensors in more detail.

2.3. Optical and Colorimetric Sensors

An optical sensor is a device that converts light energy into electronic signals. These electronic signals can, in turn, be interpreted by a processor unit. When a change in signal occurs, it will result in either an increase or decrease of the electrical output. Research and development in optical sensors has been driven by the fact that optical sensors have inherent advantages over traditional sensing methods. For example, they exhibit good sensitivity, have a wide dynamic range, and have multiplexing capabilities [31].

Optical sensors based on the use of LEDs also possess additional advantages. For example they are low power, can operate in both polarities and are of exceptionally low cost [32]. Optical sensor development has also recently been exploiting the capabilities of fibre optics to send and receive optical signals over long distance. Using fibre optics avoids having to convert between electronics and photonics separately at each sensing site, thereby reducing costs and increasing flexibility [33].

The origins of colorimetric sensing stretches back to the 16th century when chemists extracted dyes from lichen mosses, to create early versions of a universal indicator [20]. These indicator dyes contained substances which change colour depending on

the hydrogen ion concentration in a sample, showing if it is acidic or alkaline. The use of litmus or indicator paper means that when measuring pH, the need for precise amounts of sample and reagent were removed. It also removed the possibility of destroying a sample by getting this measurement wrong. This advancement in the technology made testing quicker, cheaper and easier.

In recent years, these colour changing reagents have been extensively explored and have been immobilised in various polymers, both natural and synthetic. Polymers like gelatin, albumin, and cellulose have been used, depending on the characteristics and requirements of the sensors [34]. These optically responsive materials are being integrated with various other components to create new types of optical sensors. Such sensors have been applied to measure various kinds of chemical samples, such as gases [4,5,19,35], electrolytes [36] and neutral biomolecules [37,38]. This colorimetric form of optical sensing also presents advantages over more traditional sensing methods. For example it is fully non-destructive, does not consume any of the sample, is repeatable, is low cost, is easy to use and is reliable [34].

2.3.1. Applications

Colorimetric dyes, such as thymol blue and metacresol purple have been used in the detection of carbon dioxide gas [39,40] and 2,6-dichloroindophenol has been used in research sensing oxygen [41], Bromophenol blue dye has been utilised in the detection of both ammonia and acetic acid [4,5,42]. The simplicity of the developed devices, contributes to their low cost, low power nature making them attractive for use in low-cost, large-scale chemical sensing networks. The resulting colour changes these indicators undergo is representative of the amount of the target species present. In litmus paper the colour change is compared against a colour chart and the pH is deduced. In this study and with the paired LED emitter detector diode setup the colour change is measured using a reverse biased LED as a photo detector [4,5].

2.4. Light Emitting Diodes as Sensors

As mentioned in the previous paragraph one potential technique to perform colour intensity measurements is the use of LEDs as light detectors. The principle of operation is discussed in the following subsection; as it is this principle that the low cost chemical sensors developed in this study are based upon. Therefore, the concept will be developed, explained and its applications examined.

2.4.1. Method of Operation of LEDs

An LED is fundamentally a photodiode and is therefore, also a light detector. Dietz *et al.* [43] investigated the use of LEDs for ambient illumination sensing and the principle of this measurement method is discussed in the following paragraphs. It was oncluded that although LEDs are not optimised for light detection, they do operate very successfully in that role. During the 1970's, Mims began investigating the use of LEDs for light detection and in switching between light emission and detection [44,45].

In normal light emitting mode, if an LED is connected between two digital I/O pins in series with resistor, when a voltage is supplied through the LEDs anode, through a resistor to ground, the LED will light up. But as well as being a light emitting device, an LED can also function as a light detector. To operate in this configuration the LED is initially wired in reverse bias (i.e., when the LEDs cathode is connected to a pin in logic high state (output mode), the LEDs internal capacitance is charged). When the state of the I/O is reversed, it causes its junction capacitance to discharge; this discharge is carried out at a rate proportional to the light falling upon the LED [3].

In order to perform a light intensity measurement, the I/O pin is checked over a fixed number of processor counts. A microprocessor count is done across the I/O pins to see how long the voltage takes to decay to logic zero, from the moment the capacitance starts to decay. The voltage threshold point is dependent on the type of circuitry components being used. If the time required for this discharge is accurately measured, we can then measure the diode photocurrent, meaning we have indirectly

measured the incoming light from the emitter LED. This method of operation has been used extensively in modern optical sensor research, and is explained in more detail by O'Toole *et al.* [46,47].

When a colorimetric chemical is immobilised and placed between the emitter and detector LED's to modulate the amount of light passing through dependant on the level of chemical contaminant present, a simple gas sensor is realised (concept shown in Figure 4). This concept has been the basis of many colorimetric optical sensors that have been developed [3,5,35,42,48,49] and is the working principle of this study.

The colour change can be calibrated to accurately describe the level of the target in the environment directly surrounding the coated slide. Limits of detection are reportedly in the ppm [4,5] or even ppb level [50] where a trade off is often made by having a slow reaction time.

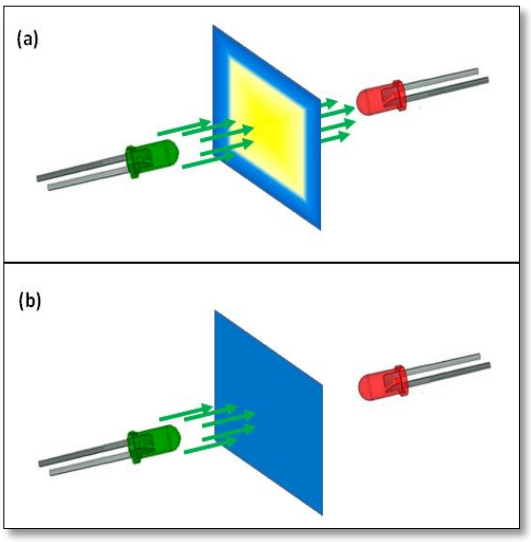

Figure 4: (a) shows the system in the presence of an acetic species, inducing a yellow colour change, (b) shows the setup with no target present and little light permeating

2.4.2. Applications

There are many examples of the implementation of colorimetric coatings in chemical sensing and the utilization of LEDs as light emitters and detectors. Byrne *et al.* [42] have reported the development of a colorimetric amine sensor that is used in the detection of amine spoilage products in packaged fish. The sensor consists of a pH indicator dye immobilised on a polymer film. As the fish ages, the total volatile basic nitrogen (TVB-N) shifts to a higher pH. The sensor effectively measures the spoilage of the fish in a non-invasive or non-destructive fashion. The results of which can be autonomously read using an LED probe or alternatively by a customer through comparison against a printed colour chart.

Sadeghi and Doosti have created an optical test strip to examine uranium levels, particularly in drinking water [51]. The sensor is based on the immobilization of C.I. Mordant Blue 29 (Chromazurol S)/cetyl N,N,N-trimethyl ammonium bromide ion pair on a triacetyl cellulose membrane. The project successfully managed to detect uranium levels in there samples however it was also noted by the autor that batch to batch sensor repeatability suffered due to reliance on the dip coating process (in the creation of the strips). Dip coating is also an immobilisation method which leads to sensors which are very prone to leaching, one of the downfalls of many colorimetric sensors [52].

One application of colorimetric sensing where leaching of sensors is less of a concern is gas sensing. Shepherd *et al.* presented work where a polymer coating was set up between two LED's [53]. The LEDs were utilised as both the emitter and detector. Results were presented from sensors employing an ammonia sensitive film and demonstrated detection of this target in the parts per million (ppm) range. The configuration is highlighted as being applicable to a wide range of colorimetric based gas sensing devices using different coatings for different target gases (i.e., for ammonia detection the reagent used was p-Nitrophenylnitrosamine). The coating process in this study (painting using a craft brush directly onto the LED surface) was again highlighted as a cause for concern highlighted by a lack of reproducibility in the created sensors [52].

Baldwin *et al.* similarly utilize LEDs as an optical detection system, creating an iron sensor based on the colorimetric reaction of divalent iron with ligand-1, 10-phenanthroline [49]. A limit of detection of 5 ppb was achieved with a residual standard deviation (RSD) of 0.08%, but more importantly results found showed that the system was relatively free from interference.

Sheperd *et al.* Also demonstrated in their work that by using dual LED sensors coupled with a colorimetric coating, a wireless chemical sensing network could also be implemented [53]. Although the networks functioned, accuracy in trials was reported as the weak point of the work, but only because no effort was made to control the fabrication of the nodes. Despite this, the data clearly showed the direction of the plume of acetic acid in real time and the manner in which the test chamber topography influenced the path of the plume. However, it was noted that it was difficult to interpret the concentrations of the gas due to a lack of reproducibility of the colorimetric coating on the LED surface.

The Sheperd *et al*. [53] study will be developed and expanded upon within this work. It is hoped that through the introduction of a more reproducible deposition method it will be possible to show that multiple chemical sensing nodes could potentially be made and operated from the same calibration and concentration data will be interpretable through close control of the thickness of deposited sensor films.

2.5. Wireless Sensor Networks

In our world there exists an endless quantity of variables, within different environments, which people have a desire to monitor. With traditional single point manual sampling, all the data we desire from the physical world simply cannot be continuously monitored. It is suggested that WSNs will give us the capability of merging the divide between the physical and digital worlds [54].

A sensor network is deemed as being composed of a large number of nodes which are deployed densely, and in close proximity to the phenomenon to be monitored. Each of these nodes collects data and its purpose is to route this information back to a sink. The network must possess self-organizing capabilities since the positions of

individual nodes are not predetermined. Cooperation among nodes is the dominant feature of this type of network, where groups of nodes cooperate to relay information captured back to the user through the network, as seen below in Figure 5.

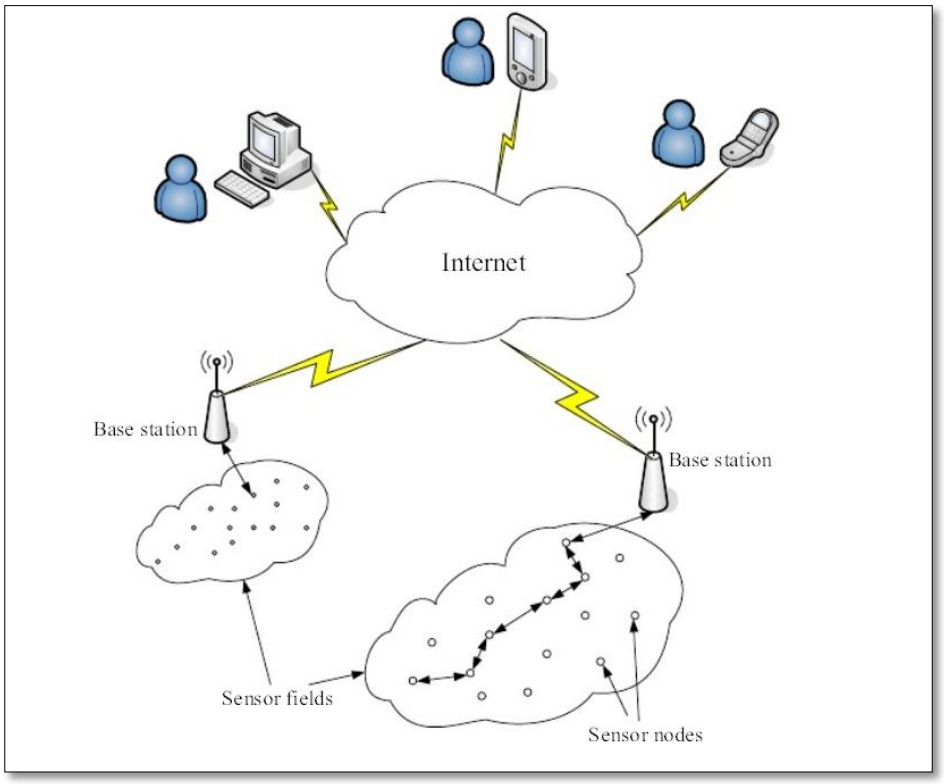

Figure 5: A graphical representation of the data flow within a WSN [66]

WSN development has been the centre of much research and development (R&D) over the last number of years. The large amount of research carried out in the area is due to the diverse range of potential applications for the technology. Target applications include building security [55], wildlife monitoring [56], manufacturing performance [57], machinery monitoring [58], monitoring of traffic [59], pollution [60,61], wildfires [62], water and air quality [63] and power usage monitoring [64,65].

The large research effort is clear from the amount of developed wireless communication platforms emerging from many of the world's top universities. UC Berkeley's developed motes (Mica family was released in 2001), include the Mica, Mica2, Mica2Dot, and the MicaZ, UCLA have developed the Medusa, and the WINS mote, and MIT have developed MIT's µAMPS-1. All the developed motes

are based upon processors from Atmel, Intel, and Texas Instruments [64]. As well as a focused research effort from universities, the release of the ZigBee protocol (one which was specifically designed for short range and low data rate wireless networks) resulted in the emergence of many commercial sensor node products, including MicaZ [67], Telos [68], Ember [69], and Xbee. Specifications and reliability of these wireless transmitting modules has much improved over the course of their development. The Xbee boasts "out-of-the-box RF communication", an outdoor/RF line-of-sight range of up to 1 mile, a RF LOS operating frequency of 2.4 GHz, and receiver sensitivity: -92 dBm [70].

With such impressive off the shelf wireless transmitting modules already available it's imperative that a focused research effort is made to develop the nodes to populate these networks. Nodes must be robust, cheap, consume little power, sensitive and reliable [54]. The development of such a chemical sensing node is the core focus of this body of work.

2.5.1. Applications and Recent Studies

A multitude of applications are already exploiting wireless sensor technology and mining high quality data. Fei Ding *et al.* successfully deployed a WSN during field *trials setup to detect radioactivity [71]. The system nodes communicated using ZigBee radios but had a limited deployment time of just 20 hours. This short life span was due to the heavy power draw from the Geiger tubes sensors running off rechargeable lithium batteries. Similarly Peng Jiang *et al.* implemented a WSN in an artificial lake monitoring pH and temperature, again utilising ZigBee radios for communication [72]. The sensors used in the nodes were commercially available sensors and, although, the accuracy reported was good, they are too expensive to be considered a realistic option for large scale sensor networks (over €100 each). These two studies validated the use of ZigBee technology for WSN communications but both had separate concerns about sensors used within their respective studies.

C. Becher *et al.* successfully demonstrated in their work that the chemical trace of individuals could be tracked within a test corridor built in a tent during a military tech-demo in Eckernförde, Germany [73]. They achieved this by using metal oxide

gas sensors and coupled the data with tracking data from laser range scanners and video systems. They concluded that “due to the need of a high number of chemical sensors they need to be small, cheap, and robust and they should have low maintenance costs.” This is a key concept in the development of nodes for WSNs and is a concept central to this study.

In order to create vast WSNs one of the main inhibiting factors is node cost. The creation of novel sensing methods and novel sensing nodes is one way of overcoming this problem. Kwang-Yong Choi *et al.* have reported the successful development of micro gas sensors fabricated using MEMS technology [74]. The fabricated micro platforms for NO_2, NH_3, and xylene gas showed good thermal stability and durability during the experiments and good sensitivity but like many new technologies many aspects of the sensing method were undesirable (i.e., sensors exhibited a large amount of thermal drift). Also the sensor fabrication method included a low pressure chemical vapour deposition process and sputter coating suggesting a possible lack of reproducibility between sensors.

One of the many drawbacks to the development of WSNs is the idea of fully automating a complex task currently controlled manually. J.A. López Riquelme *et al.* describe their experience during the introduction and deployment of an experimental sensor network at an ecological horticultural enterprise in the semiarid region of Murcia [22].

The networks autonomously collected various soil characteristics such as temperature, volumetric moisture content and salinity. The potential exists for the user to setup predefined responses to various results, such as irrigation of certain plots or the opening of air vents etc. However, in this horticultural study the sensor network was not setup as a WSAN which initiates responses, but as a network that just solely collected high quality data for the users to interpret. They concluded that the network had the ability to successfully monitor a crop of ecological cabbage for the entire growing season with the required precision. However, they also concluded that the implementation of such a network had some obstacles, e.g., “lack of experienced staff for troubleshooting, high cost for the sensors, and the power supply are of great concern” [22].

Within this study it is expected that the low cost, low power, nature of the sensor can be improved upon and its reproducibility improved. It is also planned that the study will culminate in the demonstration of all these aspects exhibiting the potential of the nodes for use within WSNs, and in time even within WSAN.

2.6. Printing Sensors

The dual LED sensor configuration has proven very successful when combined with a colorimetric polymer to detect the presence of target gases [3,5,44,51]. The gas concentration can be evaluated easily, but a problem arises when an attempt is made to compare the readings against similar sensors due to lack of uniformity in created sensors.

The chemically selective layer is fundamental to the operation of a sensing device. It affects the selectivity, the sensitivity, the lifetime, and the response time of the device. It is logical to say that an ideal sensor should be completely reproducible and consistent throughout the complete layer.

Beirne used a craft brush to paint his coatings onto LED's in his work [5]; while Byrne drop cast his sensors [42]. Both methods reportedly led to uneven layer thickness in the coatings and hence a lack of reproducibility within the sensors. In the work of Shepherd *et al.* a mix of NPNA and PVC in cyclohexanone was prepared which was coated onto the detector LED lens by applying a small volume from a pipette [33]. Similar problems were encountered where a lack of consistency in the process led to a lack of reproducibility with groups of multiple sensors (the inaccuracies that can come from casting are seen in Figure 6). It is a project goal to achieve reproducibility in the device's chemically selective layer.

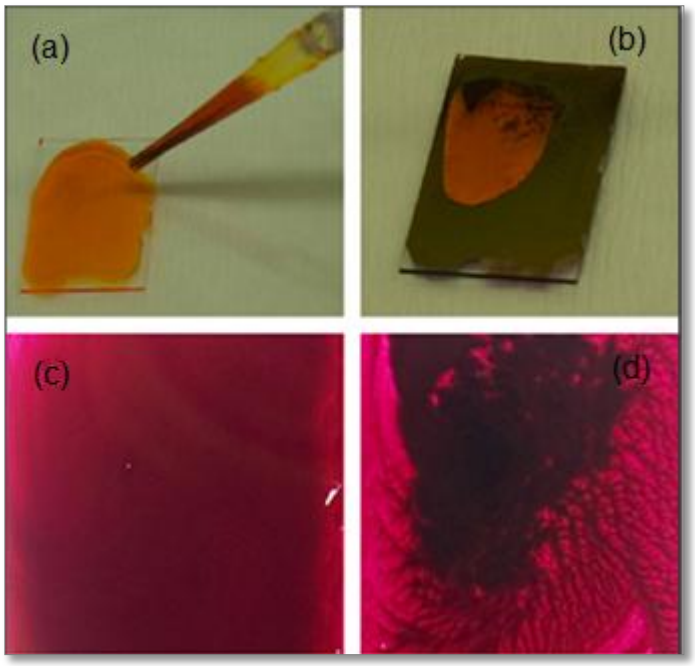

Figure 6: (a) Typical drop casting of a film (b) inhomogeneous drying with crystallisation (c) shows a successfully cast film showing a very good homogeneity (d) shows some common drying issues (i.e., picture framing, and precipitation) [73]

2.6.1. Casting and Printing Techniques

In order to achieve the deposition of homogenous layers many different casting and printing techniques have been employed in different research projects and areas. This is because each different material will possess different composition characteristics, and as a result will behave differently when it is being deposited or when it is drying after deposition.

Casting is one of the simplest deposition techniques. The procedure is to simply cast a solution onto a substrate and allow it to dry. While it is possible to prepare films of good quality and also thick films the technique suffers from a lack of control over the film thickness and often picture framing effects are observed near the edges of the film or precipitation during drying [75]. Having a picture effect or "coffee ring" effect is not always detrimental to the operation of the film, depending on how much of its surface is being used in its operation, and whether or not the film is being cut down further from its casting size. The inability to control film thickness accurately is a big drawback to the use of casting within this study, considering an effort will be made to create batches of reproducible slides.

Another casting process is spin coating. It can be used to create very homogenous films as thick as 30 cm. The process is commonly used in research to fabricate solar cells [76]. The technique is not viable for the creation of ultra thin films and also requires the employment of a viscous coating material. Spin coating will, therefore, be ignored for the purpose of this study despite its ability to create reproducible films. Similarly screen printing requires your ink to exhibit high viscosity and low volatility which is again a limiting factor for the low viscosity dye being used in this study.

Inkjet printing is a process that lends itself to research. This is because the system can handle a wide range of dyes as the head is ceramic and hence strongly resistant to organic solvents [77]. The technique also exhibits high resolution and can handle printing films of low thickness making it ideal for use in this study.

2.6.2. Inkjet Printing and its Applications

Recent years have seen inkjet printing emerging as a tool that can be used in various manufacturing processes to deposit minute quantities of materials [77.]. Inkjet printers operate either on a continuous or drop-on-demand (DOD) mode. In continuous mode inkjet printing, ink is pumped through a nozzle to form a liquid jet. Uniformly spaced and uniformly sized droplets are obtained by imposing a periodic perturbation, leading to surface tension driven jet breakup, an effect known as the Rayleigh-Tomotika instability [77].

Continuous inkjet printing is widely used in industry to print coding, marking and labelling, where speed is essential. However, the majority of activity in inkjet printing today is devoted to DOD methods, which are superior due to the smaller drop size (as low as picoliters), higher accuracy and fewer restrictions on ink properties [77]. In DOD mode, an acoustic pulse ejects ink droplets from a reservoir through a nozzle. The pulse can be generated either thermally or piezo-electrically.

The material requirements for inkjet printing focus on surface tension and viscosity, where inkjet printing is only viable with materials where the surface tension is low and the viscosity is high [78]. This is to ensure the nozzle doesn't block and that the small piezoelectric charge will be sufficiently powerful to move the droplets.

The improved reproducibility achievable through the use of inkjet printing was displayed by O' Toole *et al.* [4] in a study of inkjet printing of colorimetric gas sensors directly onto surface mount LEDs. A 91.8% decrease in a ten sensor batch relative standard deviation was generated over ten drop cast sensors.

J. Courbat *et al.* [48] reported a study of ammonia colorimetric gas sensors. They employed three different pH indicators and immobilised them in a polymer; then added a plasticiser to ensure they could be spin coated. As expected, the thick films that were generated had slow response times (i.e., 2 hours for a full response). They concluded that the indicator bromophenol blue functioned best and that by using "other deposition methods such as spray coating or inkjet printing could be easily considered by tuning the viscosity and the surface tension of those solutions by choosing the adequate solvents and their concentrations, leading to low-cost printed devices".

Similarly, L. Setti *et al.* [79] used thermal inkjet printing to print an amperometric glucose biosensor. They successfully printed their sensors and concluded that in comparison to screen printing, it allowed for the deposition of small material amounts, and was more versatile in terms of what substrate you could deposit on. It also was cheaper, making it ideal for their application.

The reproducibility improvements are obvious in most research work that has utilized inkjet printing as a deposition method, almost regardless of what materials were being deposited. This reproducibility increase was seen in the work of Pekkanen *et al.* [80] in their printing of detailed silver nano particles based circuitry. They carried out a design of experiments on the performance variables with the inkjet printing process and optimum settings were discovered and implemented. The optimum settings resulted in a desired drop velocity being attained with minimum deviation between firing nozzles, culminating in a visibly high resolution being

achieved. It was also the opinion of the author that optimisation of the inkjet printing was a time consuming process due to the multilevel nature of the fabrication of the device. It was also suggested that using statistical model- based methods, such as linear regression, do not describe the relationship between different manufacturing stages explicitly. To ensure effective process control and monitoring, engineering knowledge must be taken into account in multistage process modelling (i.e. D.O.Es). The multilevel nature of the fabrication stages in the study by Pekkanen was not something expected within this study because the fabrication will be a one stage process.

So throughout the literature inkjet printing has been highlighted as a technique which yields high accuracy, high reproducibility, with a low wastage of expensive materials. However there is a need to justify the use of inkjet printing due to the difficult optimisation stages required in its use. It is hoped that this kind of justification will not be a requirement of this study given the relative simplicity of the fabrication stages of the devices which will be explained in more detail in Chapter 3.

2.7. Summary

It can be concluded from the literature survey, that extensive research is required into the development of robust, reliable, cheap, accurate, low power sensors is the goal of developing fully autonomous WSNs or WSANs are to be realised. Dual LED sensors look like an obvious choice for development for these applications due to their low power, low cost nature, and their simple method of operation. There has been extensive testing carried out on the use of dual LED sensors in conjunction with colorimetric chemical sensing coatings, but the colorimetric coatings have not been immobilised on a separate slide. By immobilising the coating separately from the LED it may be possible to open up a variety of more reliable deposition techniques in order to improve sensor to sensor reproducibility. Coating onto a separate slide also opens the possibility of coating a slide on both sides, potentially increasing resolution as well as sensitivity.

Inkjet printing has presented itself as a highly robust process, and one that can be optimised for almost all inks and substrates providing the viscosity is in the correct region. With the demand for WSNs ever increasing, and with the development of low cost communications platforms, it is logical that research overcomes problems in the production of sensing nodes. A major inhibitor to the use of developed chemical sensors in a large scale (<100), is their cost. Sensors developed to date from LEDs have had a very low unit cost; the cost arises in the need for an individual calibration on each sensor due to a lack of reproducibility in their creation methods. The current study determines a suitable deposition process to increase reproducibility to a point where batch to batch calibration is possible, driving the sensor end cost down, making it possible to deploy a network of chemical sensors with the end cost still low.

3

3.1. Development of a Test Rig

Before a design could be finalised for the new flowcell a series of design testing had to be carried out. From this testing a number of key design parameters were discovered. These design parameters included the distance between the emitter and detector LEDs, the distance between the emitter and coating slide, and the distance between the detector and coating slide.

Previously the colorimetric ink had been drop cast or printed directly onto the LED surface, [4,5] however, within this study the colorimetric coating was immobilised onto a separate substrate, this had to be facilitated in the newly designed sensor. Initially to design the test sensor a series of design concepts were developed with the 3D CAD modelling software package Pro Engineering Wildfire 4.0®. These concepts were then exported and rendered and are visible in Figure 7 below.

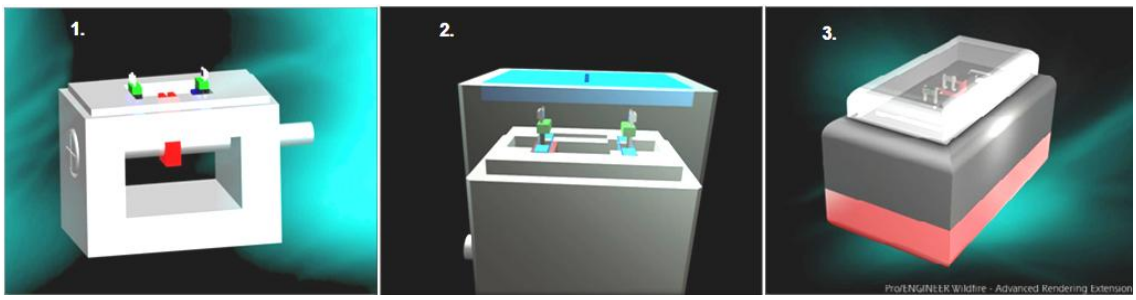

Figure 7: Test rig concepts - rendered 3D visualisations of each designed concept

The first concept labelled 1 in Figure 7, though basic; satisfies many of the design requirements. It is based on an adjustable lead screw that dictates the position of the coating slide. Both of the LEDs sit on tracking where they can be moved to a desired location and fixed. However, Concept 1 did little to shroud the LEDs from

environmental light sources. Similarly it was felt that with the fixed LEDs unnecessary restriction had been placed on the range of experimentation possible using this configuration. Concept 2 labelled 2 in Figure 7 was a further development of Concept 1. Some changes were noticeable, implemented to increase the functionality of the device and meet more of the key design requirements. Firstly the design was fitted with a cap which acted as a light shroud. The cap is only transparent for the purpose of demonstration in the render. This design facilitates the use of different caps in order to alter the position of the coating slide. The emitter LED is fixed in position; the detector LED in contrast is adjustable by means of the lead screw. However the distance between the lead screw and the track on which the detector LED runs on, was looked on as a design error. The unnecessarily long distance could potentially cause the detector LED holder to snag in operation.

Concept 3 was an improved version of Concept 2. Firstly, through mounting of the surface mount LEDs on 90º header pins the LEDs could be adjusted to be nearly in complete contact, and as far apart as 20 mm. The distance between the lead screw and the track the detector LED ran on was heavily reduced by a factor of 75%. The design of the tracks design was also altered. Instead of running on top of a grooved track, each LED holder was designed with a vertical profile across it. This meant that once assembled both LED holders were restricted so they could only move in a horizontal plane. Concept 3 meets all the design requirements as outlined in Table 1 below and hence was selected for testing and manufacture.

Table 1: Design requirements and whether each concept meets these requirements

	Shrouds from external light	Adjustable distance between LEDs	Moveable yet secured coated slide
Concept 1	×	×	✓
Concept 2	✓	×	✓
Concept 3	✓	✓	✓

3.2. Manufacturing of the Test Rig

The test rig was manufactured using a Dimension sst 768 3D materials printer [81], shown in Figure 8 (a). The technique is commonly referred to as fused deposition modelling (FDM). The technique is a rapid prototyping method where three-dimensional objects are created directly from 3D CAD data. The FDM process starts with importing an STL file of a model into a machine supplied pre-processing software (Catalyst). In this software the model is oriented and mathematically sliced into horizontal layers.

In use the materials printer extrudes two thermoplastic materials both a positive and negative layers (schematic of extrusion head shown in Figure 10 (b)). Both materials are ABS composites but when a support structure is needed, it is printed in the negative material which can be dissolved out in an acid bath afterwards. After reviewing the path data and generating the tool paths, the data are downloaded to the machine so that printing can begin. The temperature controlled extrusion head is fed with the thermoplastic modelling material and it is heated to a semi-liquid state. The head extrudes and directs the material onto a base. The resultant, material laminates to the preceding layer and the 3D component is realised. Once the part is completed, the support columns are removed and the surface can be finished.

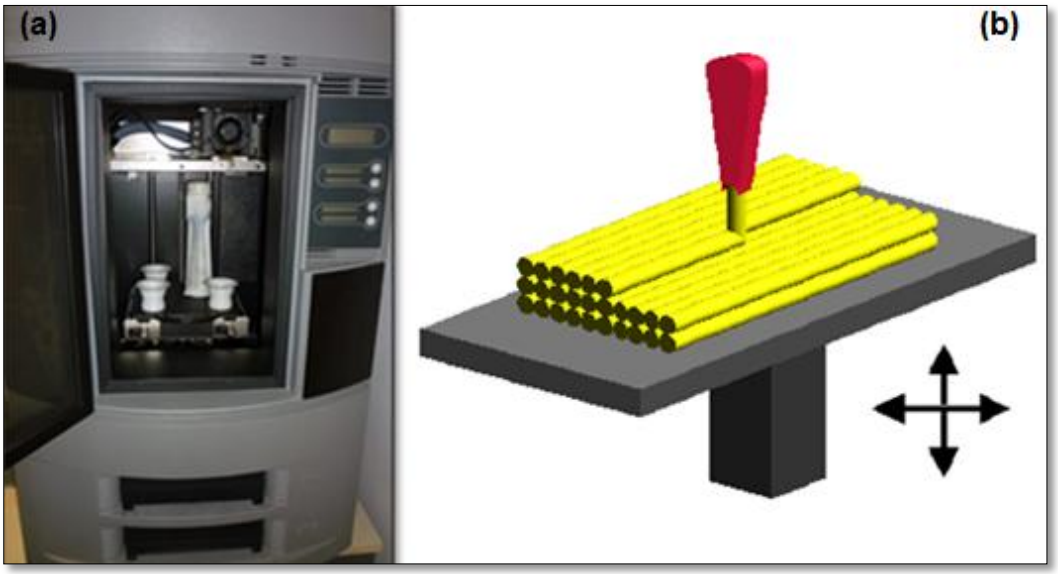

Figure 8: (a) the Dimension sst 768 used in this build (b) graphical representation of the build area and the method of deposition

Once the test rig was manufactured, it was fitted with the necessary electronics as seen in Figure 9. This included a Crossbow Mica2 mote capable of wirelessly transmitting sensed ADC (analogue to digital converted) values (1), a switch (2), two banana sockets (3) which allowed the device to be attached to a power supply for bench top testing or a battery pack for total wireless functionality. Also visible are the twisted pair wiring (4) (in order to reduce interference noise) to the surface mount LEDs (5) and the two M3 nuts (6) which were recess fitted and glued into the bottom section. This allowed the two components to be secured together tightly.

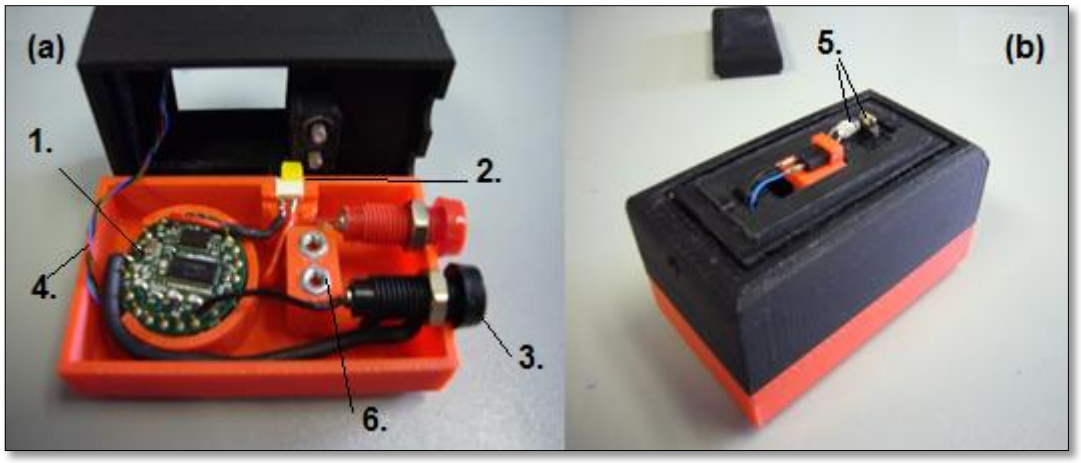

Figure 9: (a) inside of the test rig (b) the assembled test unit

The final test rig met all the design requirements, and functioned well. It allowed us to understand where the coating slide should be located in the final design and to systematically vary the distances between the LEDs to identify the optimum separation distance.

3.3. Design of the Final Flowcell

Table 2: Table of design objectives for the final sensor

Objectives	
Design a gas sensor	Firstly, the designed sensor has to be able to take pH readings from gas samples autonomously.
Reproducibility	The new sensor must be reproducible in its reading and setup. The distances between the LEDs and the slides were constrained to the point where they could only be set up in the one manner, in order to promote high reproducibility in the readings. Secondly the design accommodates the use of a coating slide, by immobilizing the coating on an optically transparent substrate. This opens up the potential of using more reproducible deposition techniques in creating the colorimetric coatings.
Low LOD	Again the introduction of the coating slide was done to drive down the LOD. Using a substrate to immobilize the colorimetric coatings allows both sides of a slide to be coated, thereby doubling the contaminant to colorimetric coating interaction surface, and potentially driving down the LOD of the device.
Sensitive	A switch was made from the proof of concept design, where surface mount LEDs were utilized, to 5mm bulb LEDs. The larger LED had a greater junction capacitance and so a greater charge/discharge current can be generated. It was hoped that this would contribute to a reduction in the sensor LOD.
Potential for development as a standalone device	The flowcell design allowed for the system to be easily coupled with a grab sampler. This ensures gas flow inside the device at all times. The proof of concept setup relied on plumes of contaminant blowing onto the sensing chemistry. The flowcell design also served to protect the slide from harsh environmental conditions and interfering light sources. Tough environmental weathering from wind and rain and changing humidity and photo bleaching could possibly lead to the degradation of the chemically sensitive slide

In the proof of concept design, a number of system or performance variables were being very loosely controlled or often not being controlled at all. It was decided that in the redesign of the sensor housing would be used to more effectively control these experimental variables, which were affecting system readings and inhibiting good repeatability in use. These variables included; the distance between LEDs (optimized to achieve maximum light coupling), alignment of LEDs, position of coating slide etc.

After being modelled in the CAD software package Pro Engineer Wildfire 4.0 ®. (Drawings included in the Appendix section as Appendix A), the flowcell was CNC milled in two sections from polytetrafluoroethylene (PTFE) which is commonly known as Teflon. PTFE is commonly used in applications where its surfaces will come into direct contact with chemicals. The material is highly chemically resistant [82] this is due to its extreme hydrophilic properties. It is also highly non-reactive and possesses an extremely low coefficient of friction, making it a good material to use for this application.

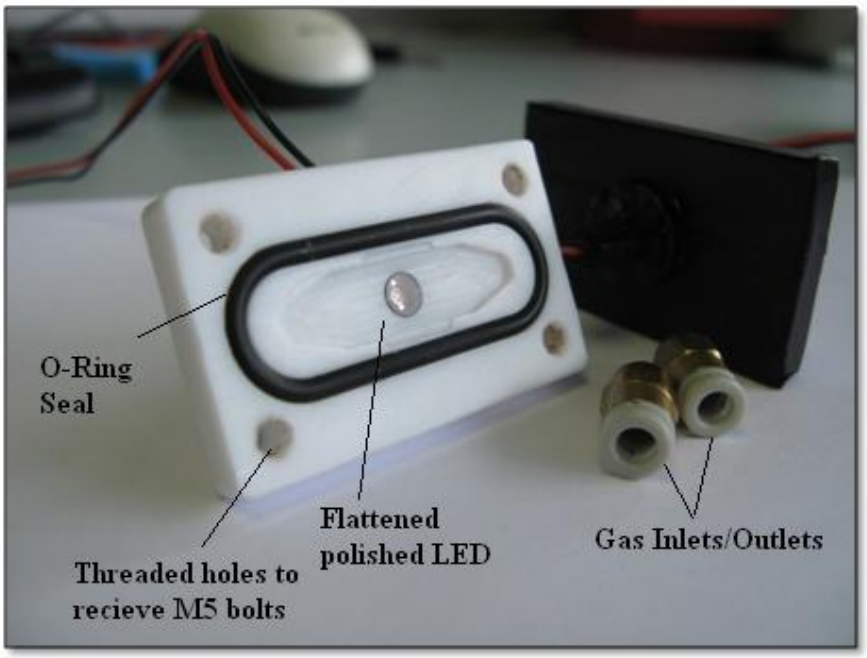

Figure 10: Annotated flowcell slide diagram

The housing accepted two LEDs, a rubber gas seal, four locking screws, the coating slide and two M5 pneumatic gas fittings (Figure 10) which acted as the gas inlet and outlet. The two LEDs were aligned on the same axis facing each other on opposite sides of the coated slide and acted as the optical detection system. The emitter LED pulses light on one side of the slide and the light intensity reaching the detector LED is modulated by the colour change of the colorimetric film, indicating the presence and concentration of our target species (acetic acid in this case).

Both sections are more clearly visible in Figure 11, the exploded view. The backside of the housing was designed to hold the slide securely in place. It also includes the recess for the slide (10 mm x 10 mm) and the slide size was chosen to be large enough to ensure that it will completely cover the 5mm LEDs on either side of it. It is also important to note that although the slide is constrained by its outside edges falling into the recesses, that it will become clamped in place as the device is secured on both its top and bottom edge. The design allowed for gases to flow over both sides of the slide surface. This facilitated the testing of slides with both sides coated. The render of the assembled unit can be seen in Figure 11. In this render the gas fittings and the rubber seal around the gas path are hidden in order to increase visibility through the component.

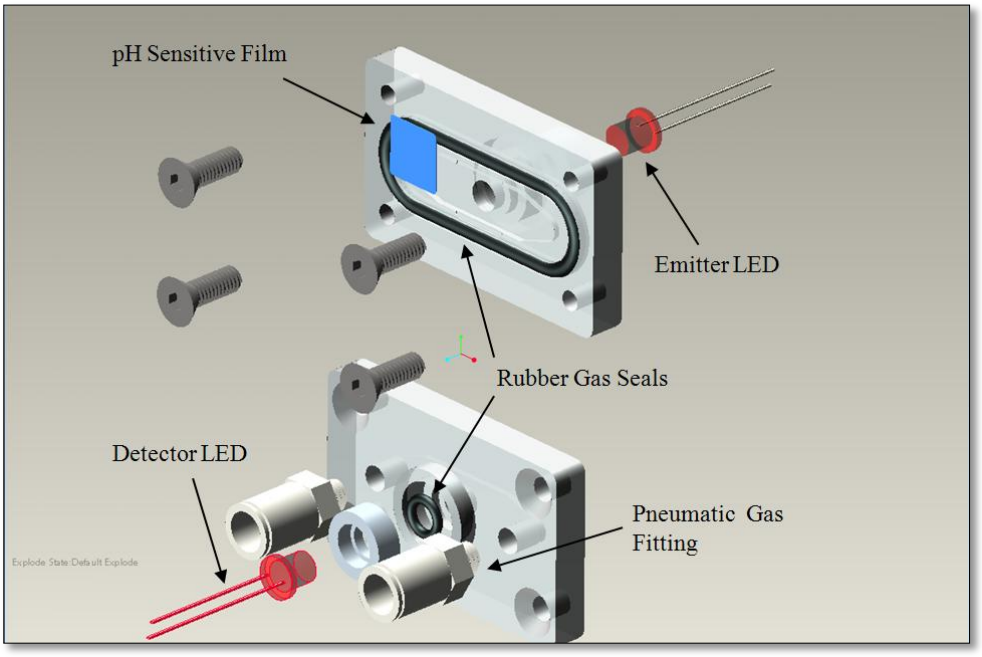

Figure 11: Exploded view of the sensor and all its components

3.4. Development of the Test Chamber

A purpose built test chamber was used for the gas sensing experiments within the study. The chamber was equipped with an injection port and septum, through which acetic acid was manually injected, using a syringe. The base of the enclosure housed two purge points which could be opened or closed. With both open, one side was attached to a vacuum line and the other to ambient air to purge the test chamber. Inside the chamber a 9 V suction pump (SKC Model No. 222-2301) was connected to the sensor housing to draw gas samples from the chamber directly into the flowcell. This ensured rapid delivery of gas samples to the device to promote a quick response time. The injected acetic acid was dispersed throughout the enclosure by a 9 V fan. The fan served to render the chamber environment homogenous and ensured a quick change in the acetic acid level through the chamber when a sample was introduced. Acetic acid was used as the target acidic species for the duration of the experimentation. It was chosen because it promoted a strong colour change was non-toxic, cheap and easily available.

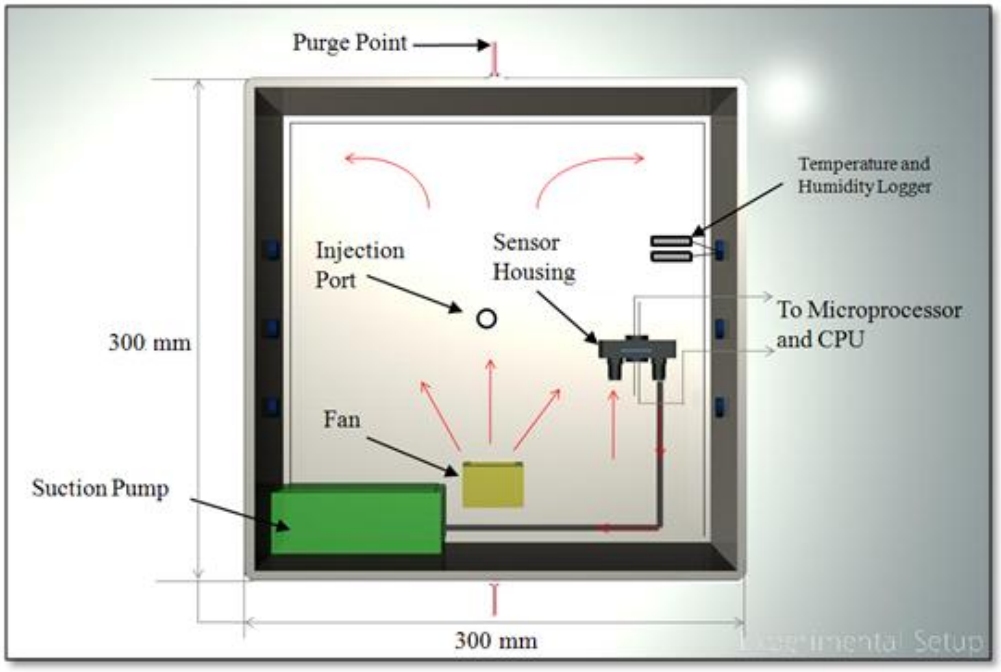

Figure 12: Annotated schematic of the experimental setup

The sensor housing was wired to the microcontroller through the side of the housing where it fed back sensor readings to a CPU connected serially by an RS232 cable via a MATLAB® designed control program. There was also a temperature and humidity sensor fixed to the side of the housing which relayed values to a CPU via a control program designed in LabVIEW ™ Further detail of the development of both collection programs can be found in sections 3.6 and 3.7.

3.5. Electronics Experimental Setup

In order to control the LEDs, a microcontroller board (Figure 13) was harvested from another research project. It was based on a MSP430 F449 chip which was programmable in C to switch I/Os as required. The board also had a power switch and a serial connection which served to relay sensor values back to the CPU. The control board was inserted into a breadboard via header pins soldered onto the I/Os. It was from these I/Os that the simple circuitry for the emitter and detector LED was developed as shown in the schematic in Figure 14.

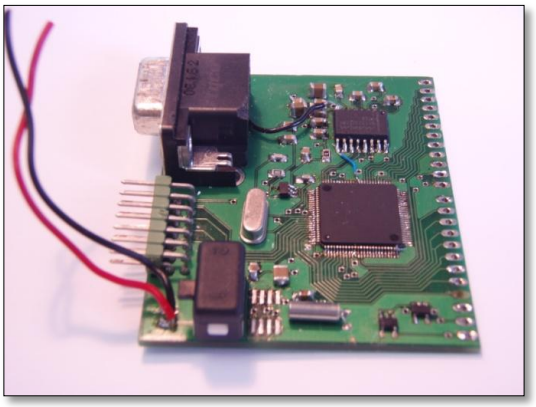

Figure 13: Developmental microcontroller PCB

The detector LED was operated by first charging its internal capacitance and then discharging it [47]. In the experimental setup, the discharge rate was proportional to the amount of light falling on it. So the logic state of the detector LED was checked over a fixed amount of processor counts (i.e., 14000) and from this check it analysed how long it took the capacitance to decay and hence how much light was falling on it. When coupled with a colorimetric slide to modulate the penetrating light, a simple chemical sensor was realised. This charge and discharge was carried out at a frequency of 50 Hz**.**

The intention in this study was to have the sampling rate set at an optimum level, because at low sampling rates, it's possible to miss key events. However, when the sampling rate is too high it can quickly saturate the input buffer of the collection software (MATLAB® in this case). It was found that at maximum sampling frequency, even when the buffer size was set to a maximum value still saturated over the duration of long tests. As a result, the sampling rate was lowered enough to prevent saturation while still collecting a rate of data at which key events would not be missed.

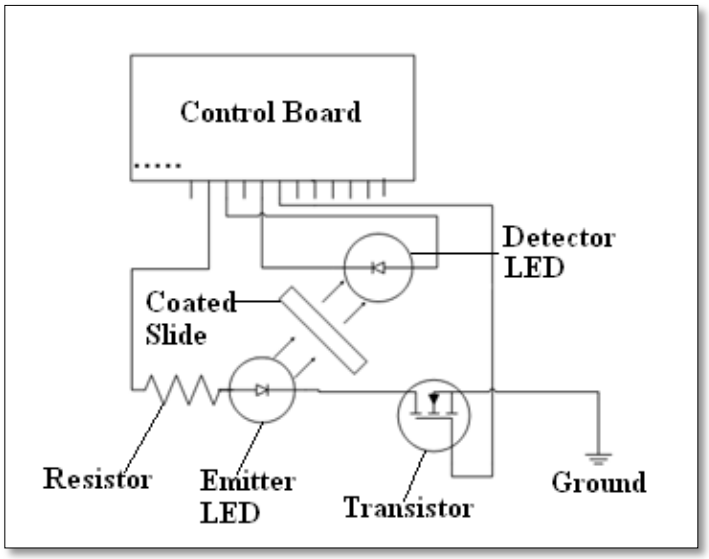

Figure 14: LED controlling circuitry

The emitter LED used in this experimental setup was a 5 mm green LED with a λmax at 565 nm (Kingbright, Radionics Ireland Part No. 451-6537), and the detector LED used in this study was a 5 mm red LED with a max at 660 nm (Digi-Key, Ireland Part No. 67-1612-ND).

These wavelengths were chosen to achieve good sensitivity by overlapping the absorbance spectra of the bromophenol blue dye which can be seen in Figure 15, with the emission spectra of the emitter led which has its peak at 565 nm. As the sensing film changes from its deprotonated blue alkaline state to its yellow protonated alkaline state, the absorbance peak of the dye at 600 nm diminishes and a new absorbance peak appears at 430 nm. Conversely, as the polymer sensing film recovers, the strong absorbance band associated with this indicator reappears so that

a significant portion of light from the emitter LED is filtered out. It is this colour change that modulates our penetrating light from the emitter to the detector LED and it is this colour change that provides us with an indirect chemical measurement. This method of light capture utilizing two LEDs was described previously by Lau *et al.* in DCU [3].

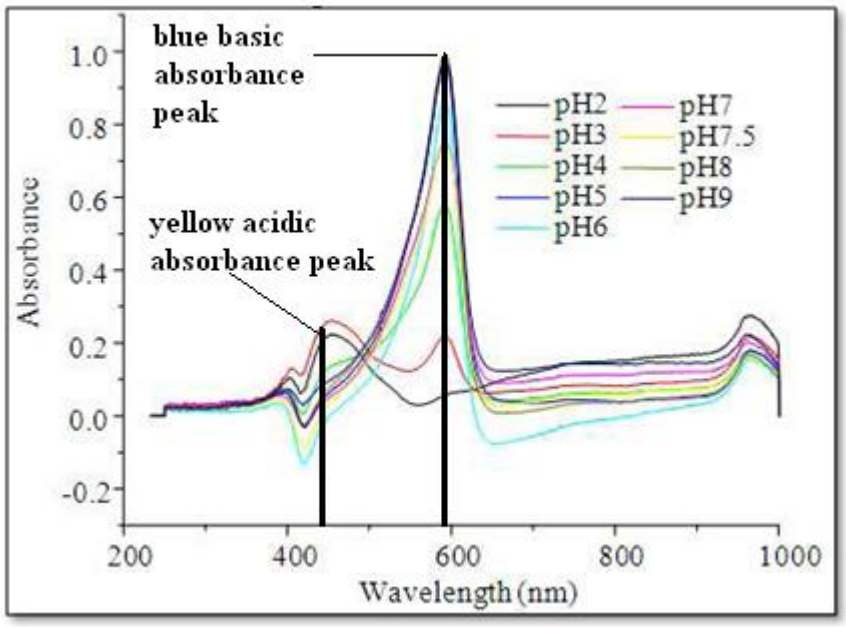

Figure 15: Absorbance spectra of bromophenol blue at a pH range between 2 and 9 adapted from [58]

The emitter in this setup was powered via a 3.3 V regulator (National Semiconductor LM1068 series CT-3.3), and smoothed using 3 capacitors in parallel (10 μF, 100 nF, 100 nF). A variable resistor was then placed in series to optimise and control the light intensity.

3.6. Development of a MATLAB® collection program

Communication between the CPU and the LEDs through the microprocessor had been traditionally accomplished using HyperTerminal. With HyperTerminal the user can input commands and read out the ADC values being returned through the microprocessor. These values were then logged to a .txt file and time stamped. From this text file an Excel plot could be generated. For the purpose of this study this setting up and reading out of sensor values was automated using MATLAB®. The program was designed to execute all the commands which had been manually

inputted using HyperTerminal to start the recording of sensor values. The reading would then terminate after a set time had been reached and an adaptive plot was generated of Sensor Value (Processor Counts) v Time (s).

The MATLAB® program began by setting up and defining the serial object. Although it was connected using USB port, a simple serial to USB driver allowed an RS23. The serial object parameters were defined, the crucial ones being a baud rate of 57600, without the use of flow control. The terminator for the end of each line was then defined as a return key, in order for it to read a single value into each virtual cell. Finally, a series of predefined functions were printed to the serial device, which turned on the emitter LED, and started the detector LED recording values at a specified rate. The sampling rate was adjustable through a "pause" code.

While running, the MSP430 begins to populate the input buffer within MATLAB®. At this point a conditional loop was specified to run in MATLAB® where each sensor value was read into a time stamped array provided the stop time had not been reached. A real time adaptive plot was also setup. Real time plotting was a big improvement, in contrast to the older method of using HyperTerminal and plotting graphs post experimentation, especially in cases of experimental break down, where long periods of time are wasted collecting data from a test which has failed. When the time stop is reached, the program exits the loop, the serial object is closed and both the input and output buffers are flushed. A copy of the MATLAB® code is included in Appendix B.

3.7. Development of a LabVIEW ™ Program

Just as the MATLAB® program was designed to robustly collect the sensor output, a LabVIEW™ program was designed to autonomously control and collect temperature and humidity data. Both the humidity sensor (Honeywell HIH 4000-001) and the temperature sensor (Therometrics DKF103N5 thermistor) were wired through a LabVIEW™ card supplying a specified voltage to them, and also collecting their output voltage. Sensor output voltage was converted to measurement units using a transformation equation which specified by the manufacturer, output temperature in ºC or output humidity in % humidity, as well as logging and time stamping the data. The program setup can be seen below in Figure 16.

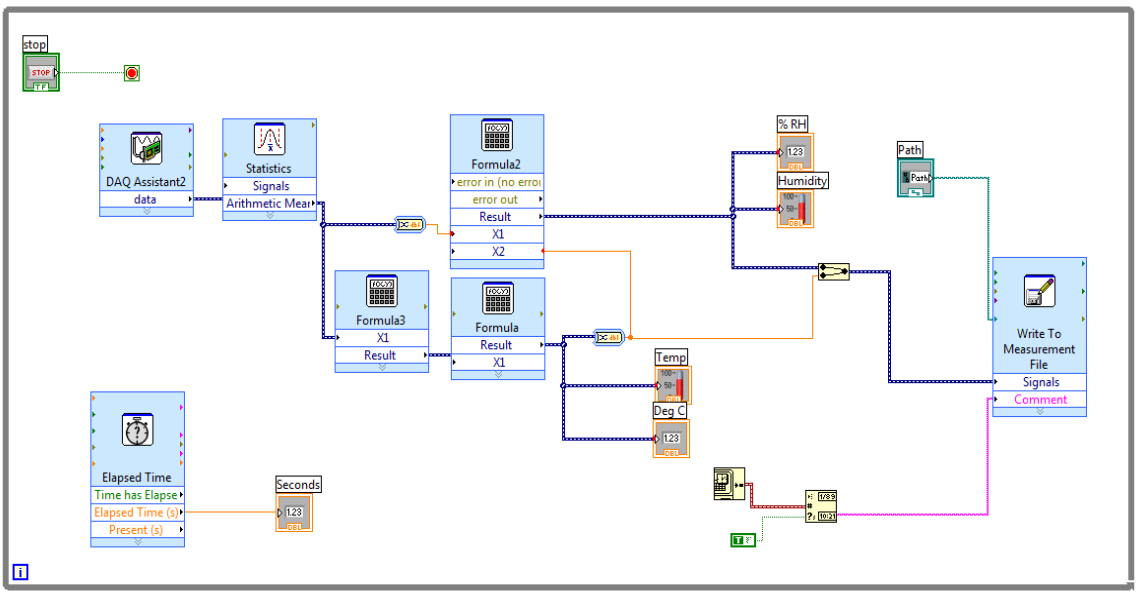

Figure 16: Temperature and humidity collection Program in LabVIEW

The sensor data was displayed in real-time via the Lab VIEW™ print panel, and also time stamped and logged into an ".xsl" format spreadsheet. . The live display can be seen in Figure 17 under typical operating conditions. The GUI as well as giving real time outputs also allowed the user to control the sensors operation. For example it was also possible for the user to start or stop the logging of data and to change the file where the data is stored. At this point having fully prepared the electronic components of the study, the next task was to optimise the sensor formulation.

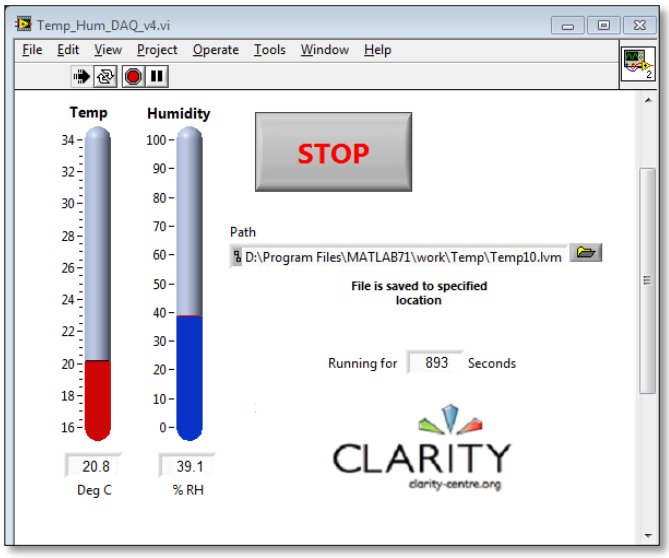

Figure 17: Real time view of temperature and humidity collection program

3.8. Optimisation of Sensor Formulation

The optimisation of the dye or ink started with the previously published sensor formulation seen in Table 3 [3,83].

Table 3: Original sensor formulation

0.5 g	Ethyl Cellulose
15 mg	Bromophenol Blue
30 mg	Tetrahexyl ammonium Bromide
20 ml	Ethanol

The colorimetric sensing polymer was prepared by dissolving the pH indicator bromophenol blue (BPB) into a solution of ethyl cellulose in ethanol. In order to prepare an acidic responsive sensing polymer, it was necessary to stabilise the BPB in the blue base form. This was achieved by adding the salt tetraoctyammonium bromide (THABr), which acts as a solid state pH buffer, to the polymer formulation. As part of the study these components were varied with a view to improving the dye for deposition onto a substrate. The requirements for the substrate to carry the sensor formulation; one it had to be optically transparent and two optically neutral neither reflecting nor refracting light. Three potential materials were chosen and tests were carried out drop casting various sensor formulations onto them in order to optimise the formulation components for a certain substrate. These were PMMA, PET and Glass.

3.8.1. Study 1: Selection of Solutions

Firstly ethanol was deemed unsuitable for inkjet printing as its boiling point is relatively low, 78 ºC and it would evaporate out of solution too quickly. This could potentially lead to the blocking of expensive cartridge heads. Other solvents were chosen which possessed higher boiling points, both propan-1-ol which has a boiling point of 97.1 ºC and *n*-butanol which has a boiling point of 118 ºC [84].

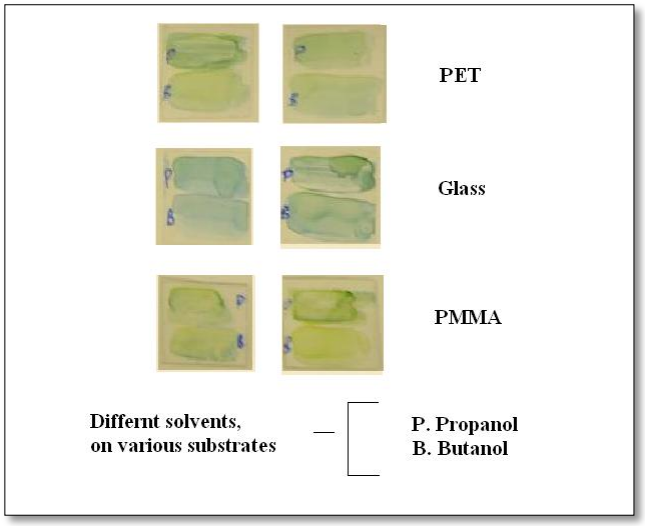

Figure 18: Dropcast films of propanol and butanol based formulations on the three substrates

It can be seen from Figure 18 that the formulation exhibits its more alkaline form (blue) colour on the glass slide, and a slightly yellow acidic colour on the PMMA slide. The formulation is in the most desirable pH neutral state on the PET slide. It can also be seen from Figure 18 that the butanol based formulation dries in a more even or homogenous fashion on all three substrates. Therefore butanol was chosen as the most suitable solvent.

3.8.2. Study 2: Selection of Stabilising Salts

The next series of drop casting experiments involved the varying of the stabilising salt, in order to see if the film quality could be further improved. At this stage the film quality was judged on the film colour and topography. It is obvious from the PET slide in Figure 19 that the tetrahexyl ammonium bromide film (1) exhibits the desired alkaline colour (blue), and the tetrabutyl ammonium bromide (2) creates a more neutral pH colour than the tetraoctyl film (3).

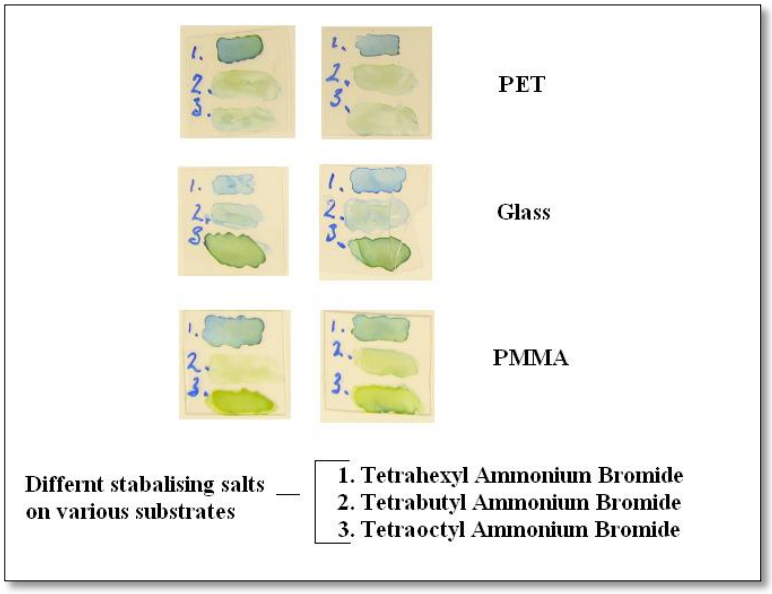

Figure 19: Drop casting of formulations based on different salts on various substrates

Once the colorimetric dye had been formulated (as in Table 4), its viscosity was measured using a rotational viscometer. A viscometer was used to determine the viscosity formulations. The viscosity is the measure of the internal friction of a fluid which only becomes apparent when a layer of the fluid is made to move in relation to another layer. The measurement is taken in centipoise (cP) which is equal to a kilopascal second (kPas) and the temperature is also taken as viscosity is dependant on temperature. All measurements need to be taken at the same temperature to get reproducible and comparable data. The formulations are compared by their viscosities which for optimal inkjet printing should be in the 10 – 15 cp range although printers can be designed to handle liquids up to 100 cP [78]. The optimised dye was measured 10 times and averaged to produce a reading of ≈ 13 cP (Data available in Appendix C).

Table 4: Optimised formulation for inkjet printing

0.5 g	Ethyl Cellulose
15 mg	Bromophenol Blue
30 mg	Tetraoctylammonium Bromide
20 ml	Butanol

3.9. Inkjet Printing of the Sensor Film

The inkjet printer used in this study was the Fujifilm Dimatix dmp (Dimatix Materials Printer) 2800. After the dye was formulated it had to be filtered. The filtering process was carried out filtering the solution through a syringe4 filter and into an empty vial by means of a peristaltic pump. The filter used was a 0.45 µm PVDF syringe filter (Acrosdisc LC). The tubing employed was silicone based Tygon® tubing. A peristaltic pump (Gilson, type Minipuls 3 M312) was chosen to drive the filtration because it was noncontact and offered a slow steady flow rate ideal for filtration. Examples of the filter type and the pump type can be seen in Figure 24.

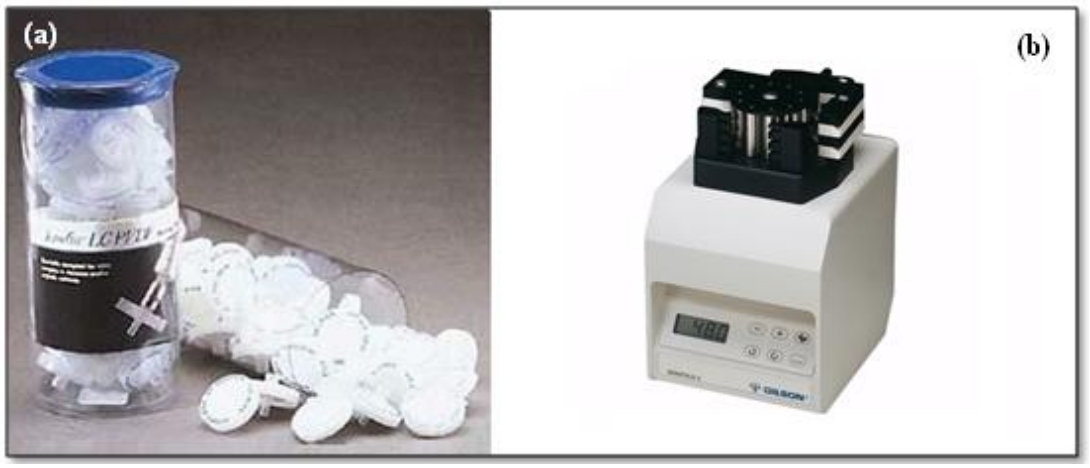

Figure 20: (a) typical PVDF syringe filters (b) peristaltic pump used to drive the filtration

At this point, the filtrate was transferred to the printing cartridge. This was carried out by means of a disposable unbevelled blunt-tip needled syringe. Roughly 1.5 ml of the solution was delivered to the bladder within the inkjet cartridge. Once the cartridge reservoir was filled, the second part of the cartridge, the cartridge head could be attached. The print head contained sixteen piezoelectrically controlled nozzles. By placing electrodes on the surface of the piezoelectric material a section of the material can be made to move without affecting the surrounding material. The voltage coupled with a communicating pumping chamber, results in ink drops being formed and excited. The replaceable print heads are available in both 1 pL and 10 pL drop volumes, however, 10 pL cartridges were chosen to complete this study as thicker films were required for the sensors.

Once the cartridge had been filled with the filtered ink and assembled, the user printing began. A typical printing routine began with a cleaning cycle to unblock and clear the printer heads, followed by inspection of the jets firing using the "dropwatcher" camera. Once satisfactory drops and a large number of the jets were firing in a vertical and reproducible fashion deposition begins. The optimised variables used for the printing of the slides used in the study were substrate and printhead temperature, drop spacing, and excitation voltage.

Having redeveloped the sensor into a new optimised configuration, and developing collection programs for sensor reading temperature and humidity, and having optimised the sensor formulation a series of experiments were carried out to characterise the sensor these experiments are outlined in Chapter 4.

4

4.1. Noise Investigation

When the sensor was originally assembled and tested, a large amount of unwanted noise was visible in the signal. It was not immediately obvious if the noise in the signal seen was something being generated by the setup or not. Therefore, it was decided to investigate the noise phenomenon, in the hope of deducing where it was coming from and possibly reducing or eradicating it. It was hypothesised, due to the sensitive nature of the electronics being used, that the signal was being affected by pick up or hum (the effect of noise being generated from AC power circuits).

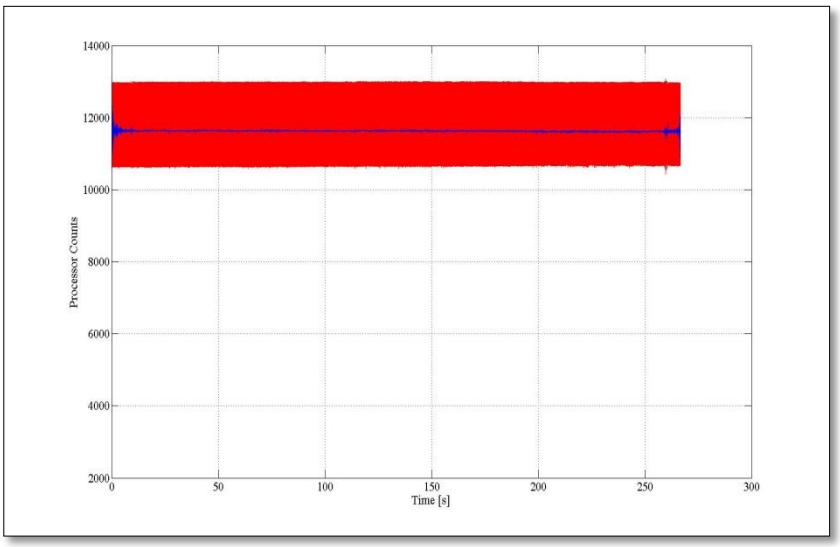

Figure 21: Stability test showing unacceptable noise generated with the sensor setup and no coated slide

In order to investigate this high level of noise the straight-line plot visible in Figure 21 was transferred to the frequency domain using MATLAB®. In order to validate the hypothesis of electrical noise, a signal operating around 60 Hz would need to be identified. However, a sampling speed close to 120 Hz or double the frequency

would be required to see such a signal in the frequency plot. However, it was possible to use the current 10 Hz sampling frequency to acquire a straight line plot (Figure 21) and to convert that to the frequency domain (Figure 22). Despite the obvious aliasing of the noise frequency it is still possible to distinctly see the noise spikes generated at about 14 Hz and what appears to be a harmonic of this signal at 27 Hz. Although, these are not accurate in terms of frequency they still represent a band of noise and serve as a point to filter from.

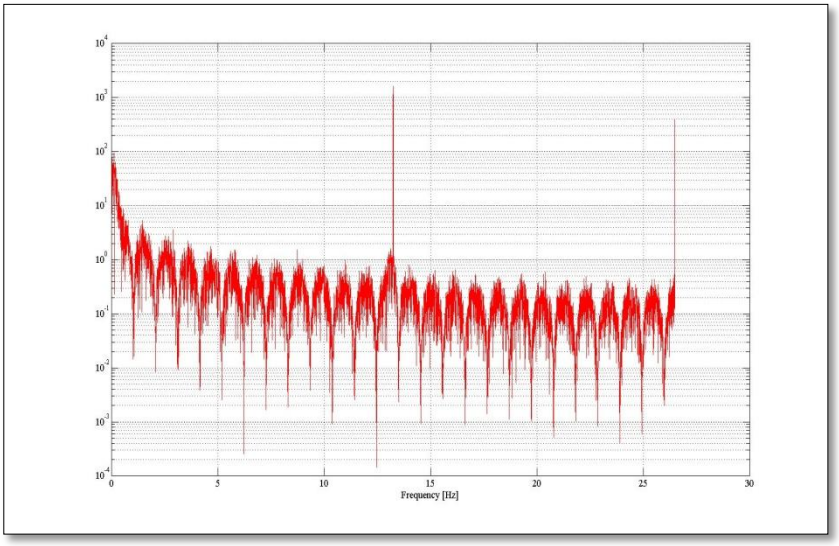

Figure 22: The Fourier Transform of the time series seen in Figure 24

From the data shown in Figure 22, a band pass filter was applied at the spike frequencies to generate Figure 23, and from this filtered plot a time series was then regenerated producing Figure 24.

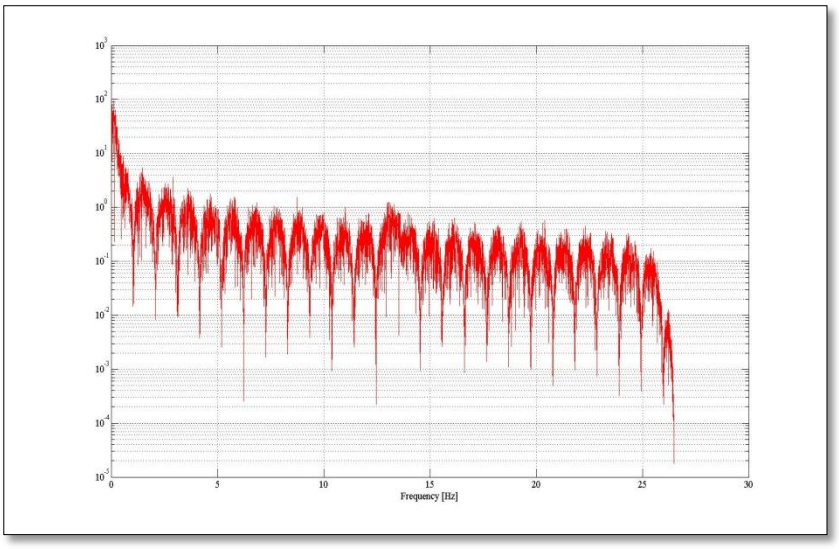

Figure 23: Adapted from Figure 22 after the introduction of a bandpass filter.

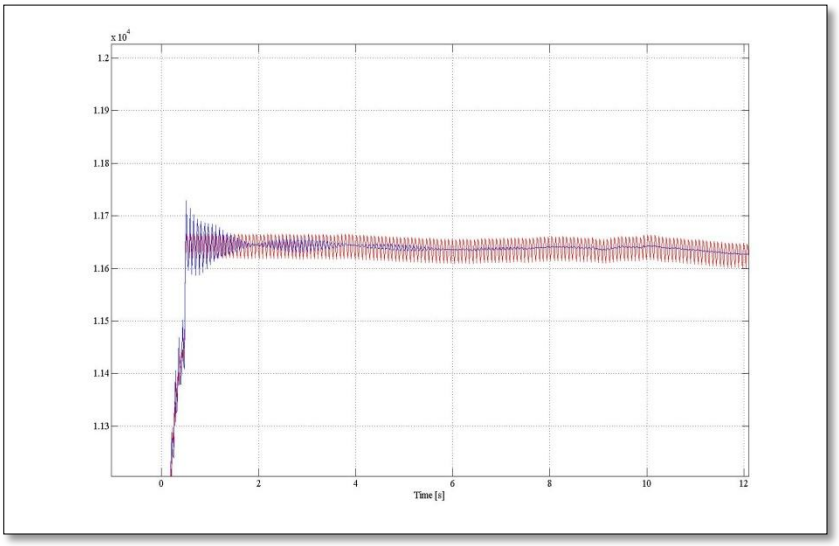

Figure 24: The time plot from Figure 22 after use of the bandpass filter in the Fourier domain

It is obvious from the increased signal-to-noise ratio (SNR) that these spikes are responsible for the noise seen in the sensor signal. However, it cannot be verified at this point that the noise is indeed electrical noise. It could also be noise generated from within the microprocessor board. In order to verify that the noise was pickup noise as hypothesised, a test was setup. The device and electronics were setup within a Faraday cage in order to repeat the test that generated Figure 24. This time, without any filtering Figure 25 was generated, proving that the noise in the signal was pickup influencing the sensor reading. At this point the cause of the noise has been verified as coming from external electrical devices. Filtering is an acceptable technique for negating the effect and filters will be applied to all future plots generated.

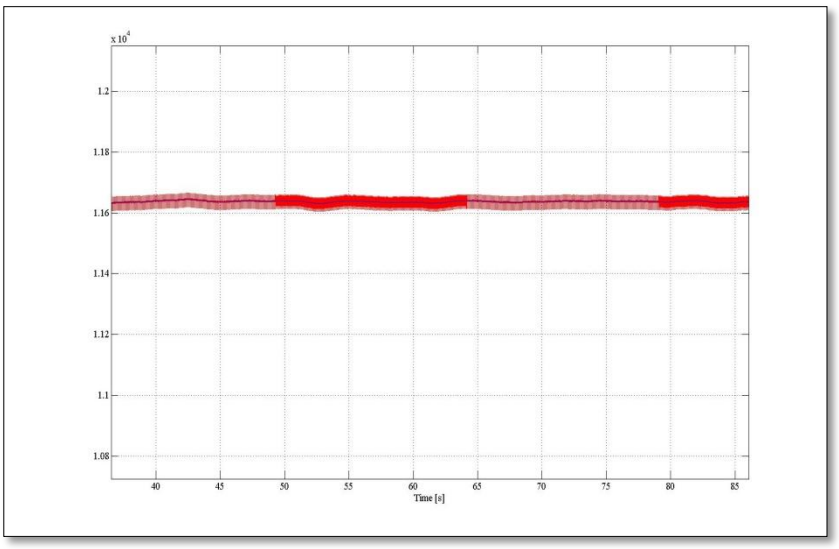

Figure 25: A control test, with the addition of a Faraday cage

4.2. Testing with Dropcast Sensor Films

Once the colorimetric sensor formulation had been optimised for printing and the signal to noise ratio had been satisfactorily increased, testing began by drop casting the formulation. The optimised dye was used and PET was used as the substrate since it performed best in the earlier test, being the most pH neutral substrate while still being flexible enough to be compatible with both inkjet printing and use in the designed flowcell.

These tests were carried out with the drop cast slides in order to make sure that the formulation still behaved as the original proof of concept (POC) formulation did. This confirmed the functioning of the different collection programs, and gave a benchmark which the inkjet printed slides could be compared against in terms of performance. It immediately became clear that although the collection programs for both the sensor and the temperature and humidity data worked as expected, the collected plots exhibited significant drift in response. A typical sensor plot using the optimised formulation can be seen in Figure 26. The baseline is clearly not stable as the 7 µl acetic acid injection is delivered to the 13 litre chamber. Despite having over 30 minutes to stabilise after the injection, the sensor never fully stabilised.

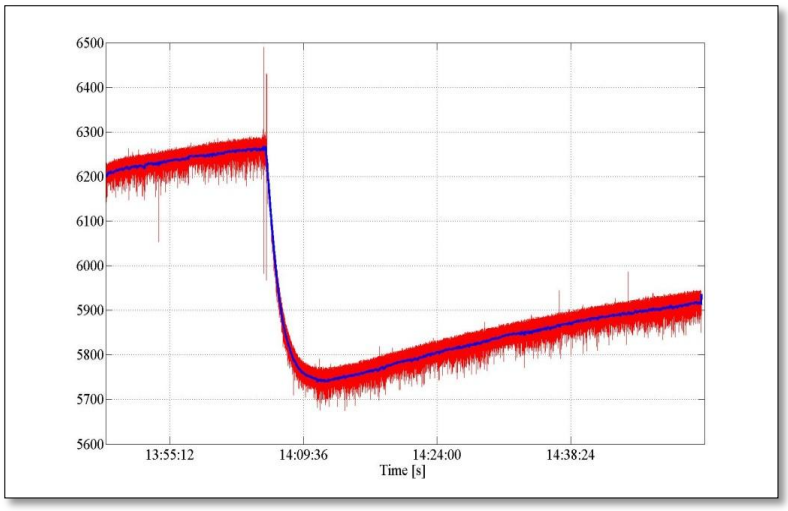

Figure 26: A sensor plot from a 15 minute baseline and 30 minute exposure to a 7 µl of acetic acid

After this test a number of stability tests were carried out. A test was run where the acetic acid injection was delivered to the chamber where the sensor flowcell and the optical detection unit operated without the chemically responsive coated slide. The system remained stable throughout, and demonstrated that the drift was a direct result of varying the sensor formulation and not the electronics. Similarly, leak tests were carried out. However, again the tests pointed towards a problem with the sensor formulation. To test this hypothesis a third formulation was made up and deposited onto films for testing. The formulation was a variation on the POC formulation utilizing butanol as the solvent. The formulation is shown in Table 5.

Table 5: A variation on the original formulation using butanol as the solvent

0.5 g	Ethyl Cellulose
15 mg	Bromophenol Blue
30 mg	Tetrahexyl ammonium Bromide
20 ml	Butanol

This altering of the sensor dye formulation resulted in the return of steady baselines, and clearly defined responses to acetic species without any noticeable drift. It is believed that the altering of the film to the teraoctly ammonium bromide salt would have increased the solubility of the film permitting the ions to transfer quicker in and out of the film.

The next test was carried out to investigate the effect of humidity on the sensor. In gas sensors, cross-response to humidity is a common issue. In these particular sensors, the response mechanism depends on proton transfer between the sample molecules and the dye. This transfer is effectively modulated by water; therefore the effect of humidity on the sensor response was investigated while the temperature was regulated at room temperature (ca. 20^{o}C).

Testing began with a 10 minute purge to establish a baseline prior to injection of 7 µl of water delivered to the test chamber. 7 µl was chosen to attempt to validate any further 7 µl acetic acid injections as a response to the pH change and not the induced humidity change. After 10 minutes the chamber was purged with ambient air. This resulted in a change in the humidity of the chamber with the humidity rising from 47.2 % up to 48.8 % before returning to 47.2 % after the purge (Figure 27 (b)). This change did not manifest itself as a recognizable effect on our sensor response and the device continues to stay at a steady state throughout the injection (Figure 27 (a)). This validated our responses in normally testing with acetic acid as a response to the pH change and not the humidity change.

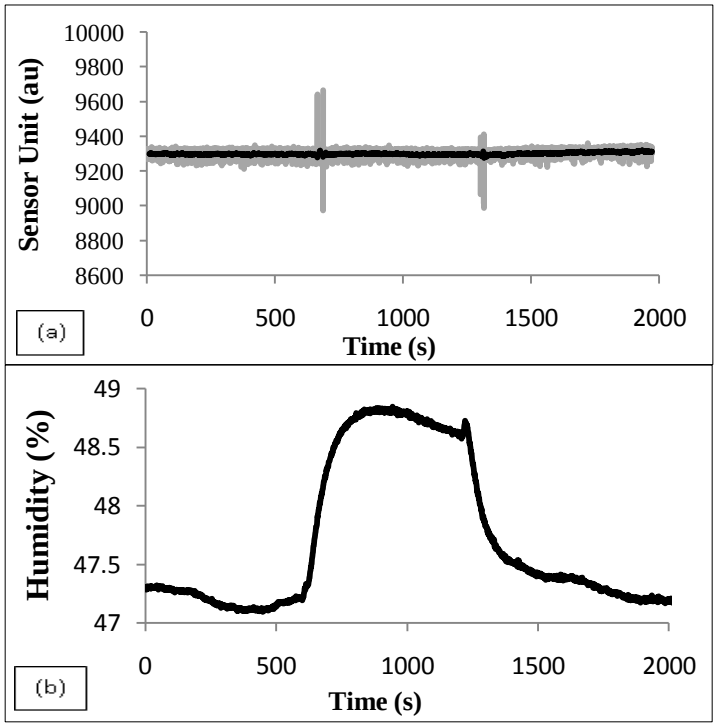

Figure 27: The simultaneous plotting of sensor output and humidity over the duration of a water injection

At this stage, it has been proved that the sensor exhibited a positive response to acetic acid, and remained unaffected by the humidity change induced in the last experiment. At this point, a large drop cast pool was made of the new formulation and multiple sensor slides were extracted from it for experimentation. These sensor slides were carefully setup within the flowcell between the detector and emitter LEDs, sitting in the middle of the gas flow path.

In this experiment the sensor was set into operation and an initial "baseline" was developed. The baseline serves as a control, since it has been developed without any contaminant being in the test chamber or flowcell and serves as a point of comparison for subsequent points.

In this first test the baseline was left to develop for 5 minutes before the first injection of liquid acetic acid. The 99 % acetic acid was syringe injected through the injection septum on the roof of the test chamber. Once inside, the acetic acid was blown throughout the test chamber by a small axial fan (Sunon 2082HBL.GN), ensuring the acetic acid remained in a gaseous state and the chamber environment became homogenous throughout. This setting time was used in order to ensure homogeneity in the chamber environment and also to ensure a maximum response from the sensor for the injected quantity of acetic acid.

Five minutes were left elapse after the injection. Once the 5 minutes had elapsed, it is visible from the plot that the sensor was beginning to exhibit a steady or straight line response. When the second 5 minute exposure period had elapsed the chamber was purged with ambient air. This was achieved by connecting one purge line to a vacuum pump and the other to atmosphere, which served to draw ambient air throughout the chamber whilst removing all contaminant. The effectiveness of the method can be seen by the return of the sensor to the original baseline state (Figure 28). This process of delivering acetic acid, 5 minute wait, purge, 5 minute wait was repeated until a plot was collected with the desired number of exposures.

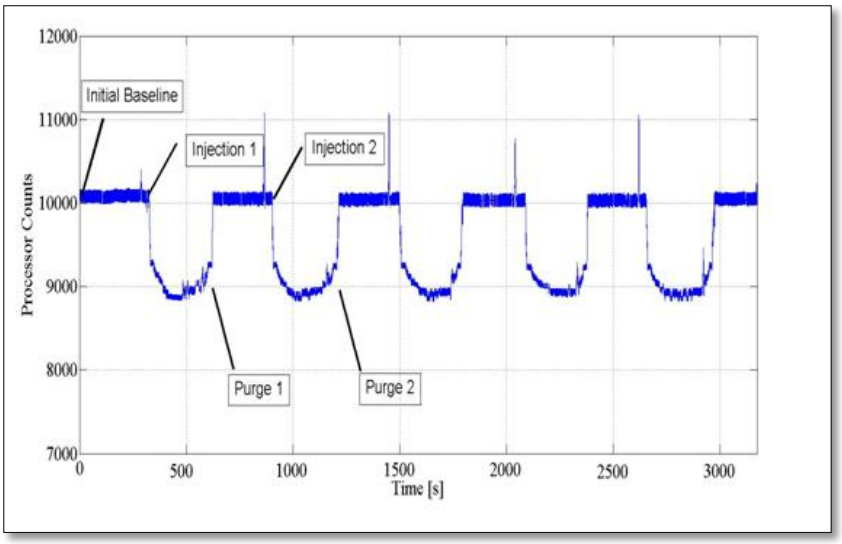

Figure 28: Repeated sensor response to 5 minute acetic acid exposures and ambient air purges

Based on Figure 28, the sensor response appears to be relatively rapid (stabilizing in 2-3 minutes; compared to most bulk membrane colorimetric sensors which can be 10's of minutes), this is however, a feature dependant on the thickness of the membrane/film. The response and recovery is almost symmetrical; usually the recovery is slower due to diffusion issues in the membrane.

As well as tracking the sensor output over this study, humidity and temperate data were also collected. It has been hypothesised that with a change in temperature, the internal resistance within the LEDs will also change. When this is coupled with the low current nature of the device it seems logical that a change in temperature will affect the sensor output. However, for the basis of this study, the effect of changing temperature will be ignored. This is because all of the experiments were carried out at room temperature and it was shown that over the duration of an experiment such as this that the temperature changes very little (i.e., ± 1 ºC).

The collected humidity data for the test is shown in Figure 29. It demonstrates that there is a significant change in humidity for the duration of the experiment. However, we have already shown from the plot in Figure 27 that the response seen by the sensor is a response to the acidic species, but we also must remember that a certainly humidity is required to facilitate the ion exchange required. This relationship should be explored more fully and is included in the future work chapter in Chapter 5 section 5.1.

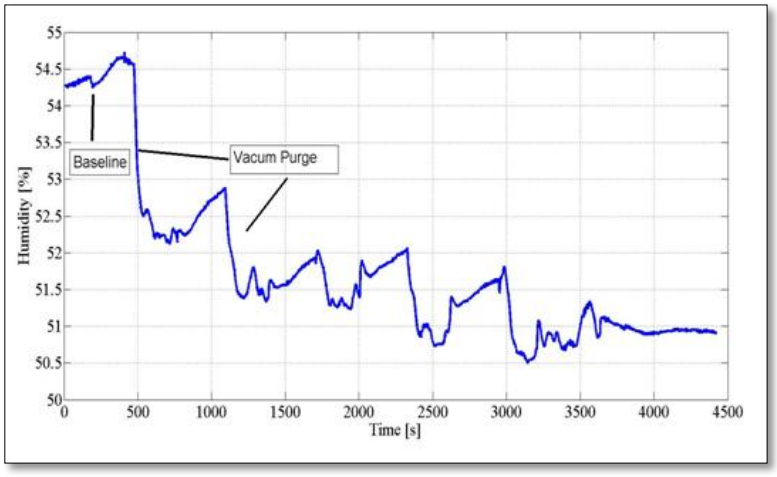

Figure 29: Percentage humidity over the duration of the experiment

At this point, performances of the drop cast sensor films were benchmarked. Since a large sensor redesign had taken place quantifying the improvements made in terms of the sensor performance was important. Figure 30 was developed in a similar manner to Figure 28. However, in this instance, after the initial baseline was generated just three exposure/purge cycles were carried out. The raw data are shown in grey, with a floating average in black. The drop cast films where thicker than the slides used to generate Figure 28 and this can be seen in the performance of the device (i.e., the response time is slower than that of a thinner film, and the recovery time is slower than the response times as its harder for the molecules to easily escape the film.)

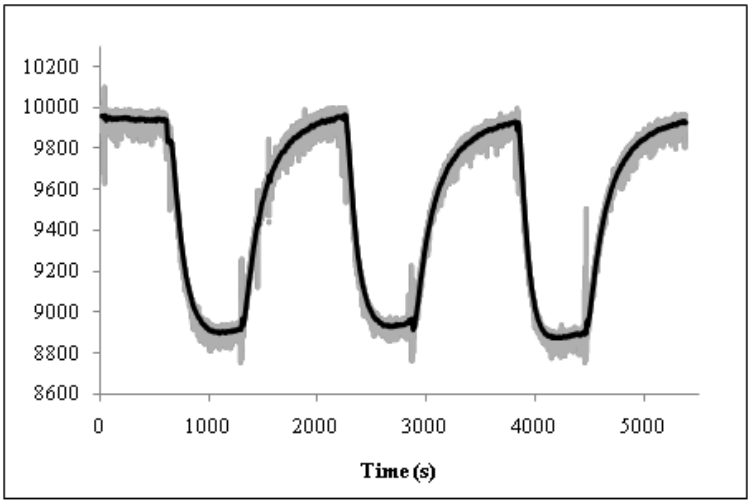

Figure 30: Sensor raw data (grey background) and smoothed data plot (black foreground)

In order to generate Figure 30 the test began with the test chamber being purged with ambient air. This was done for 10 minutes to establish a baseline. After this, the enclosure was sealed. Then 7 µL of 100 % acetic acid was injected into the chamber and dispersed by the fan, creating a concentration of 0.56 mg/L acetic acid in air. (The method used for calculating the acetic acid concentration in mg/L is explained in Appendix D). Once the sensor had been exposed to the acetic acid for 10 minutes it was purged for 15 minutes by drawing ambient air through the chamber. This purge and injection sequence was repeated three times in total. It can be seen from Figure 30 that the procedure generated a clear positive response, which exhibited a maximum relative standard deviation between exposures of 0.8% RSD, exhibiting a well defined repeatable response (this calculation can be seen in Table 6 below). The residual standard deviation is a good measurement for the repeatability within a process or event and is calculated as $\left(\frac{Stdev\ of\ array\ X}{Average\ of\ array\ X}\right)\ x\ \frac{100}{1} = RSD\%$.

Table 6: RSD Calculation based on Figure 30

	Start Point	Finish Point	Total Response
Injection 1	9931.06	8907.9	1023.16
Injection 2	9948.7	8925.7	1023
Injection 3	9917.44	8880.34	1037.1
Average			1027.75
Stdev			8.09
%RSD			0.78

Another important parameter when characterising a sensor is the speed of the response of the sensor. In this case our sensor (the colorimetric film) is packaged within the flowcell, and samples are routed to the flowcell by the grab sampler. Therefore, the response time of the entire sensing setup was first calculated from the time it took the sensor film to reach 95 % of its steady-state response from within the flowcell. This time includes dispersion of the acetic acid throughout the chamber, establishment of equilibrium between the chamber and the sensor, the movement of the gas through the testing flowcell, and the diffusion of the sample into the sensor film. From the test shown in Figure 30 the speed of response of the sensing setup was evaluated over the three exposures to be 5 minutes 24 seconds ± 27s. The calculation of this value is shown in Table 7.

Table 7: Speed of system response calculation

	Time of Injection	Sensor baseline	End Sensor Value	Total Value Change	95% of Response	Time at 95% point	Time taken for the 95% response
Run 1	9m 31s	9936.38	8904.58	1031.8	980.21	15m 18s	5m 42s
Run 2	36m 48s	9950.1	8929.08	1021.02	969.96	41m 48s	5m 0 s
Run 3	63m 20s	9921.88	8873.5	1048.38	995.96	68m 51s	5m 31 s

This response time is the response time of the entire system, the speed of response of the colorimetric film was evaluated separately by injecting acetic acid into a custom miniaturized flowcell shown in Figure 31.

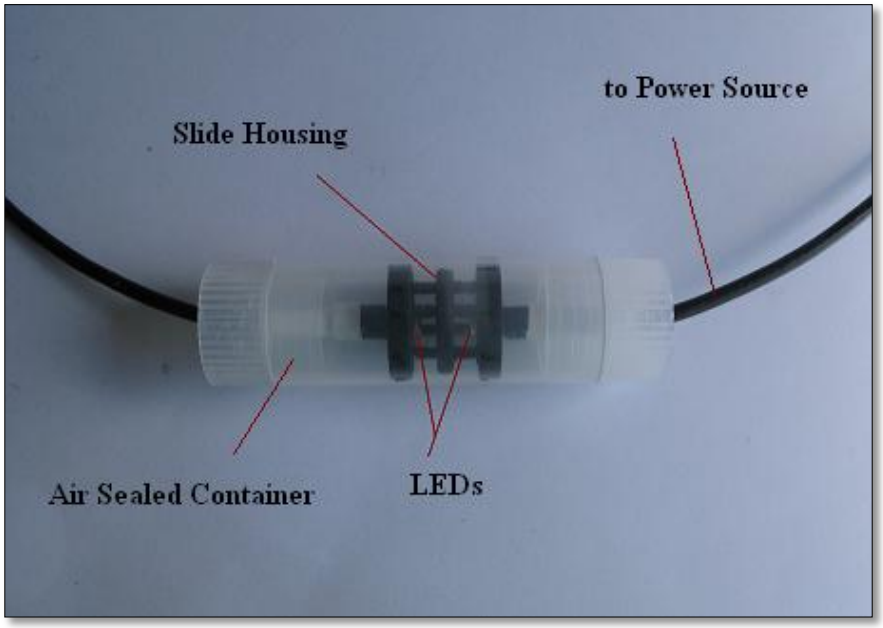

Figure 31: Test flowcell designed to saturate coated slide

The flowcell's small internal volume and the direct injection ensured that the sensing film was immediately exposed to the acetic acid vapour. The speed of response of the coated slide was calculated from the time it took the slide to reach a 95 % response to a 7 µl 100 % acetic acid injection which equated to a concentration of 268.81 mg/L acetic acid in air. The evaluated time response value was 25 ± 2.6 seconds and was calculated from three runs as shown in Table 7.

Table 8: Table for sensor speed of response calculation

	Time taken for full response (s)	Time taken for 95% of response (s)	Stdev
	23.42	22.24	2.6
	27.87	26.476	
	28.41	26.98	
Average	26.56 s	25.23 s	

4.2.1. Calibration of Sensor

A ten point calibration was carried out using acetic acid and repeated a total of three times with three separate sensor slides. It was carried out by increasing the sample concentration in 0.1 mg/L steps up to 1 mg/L. An initial 10 minute baseline was established, followed by 10 sequential injections of 0.1 mg/L of acetic acid. After each injection, a 10 minute period was allowed for the sensor to reach a steady state response (Figure 32). From this plot the LOD was calculated from three times the standard deviation in the baseline as 21 ppb. This limit of detection calculation can be found in Appendix E.

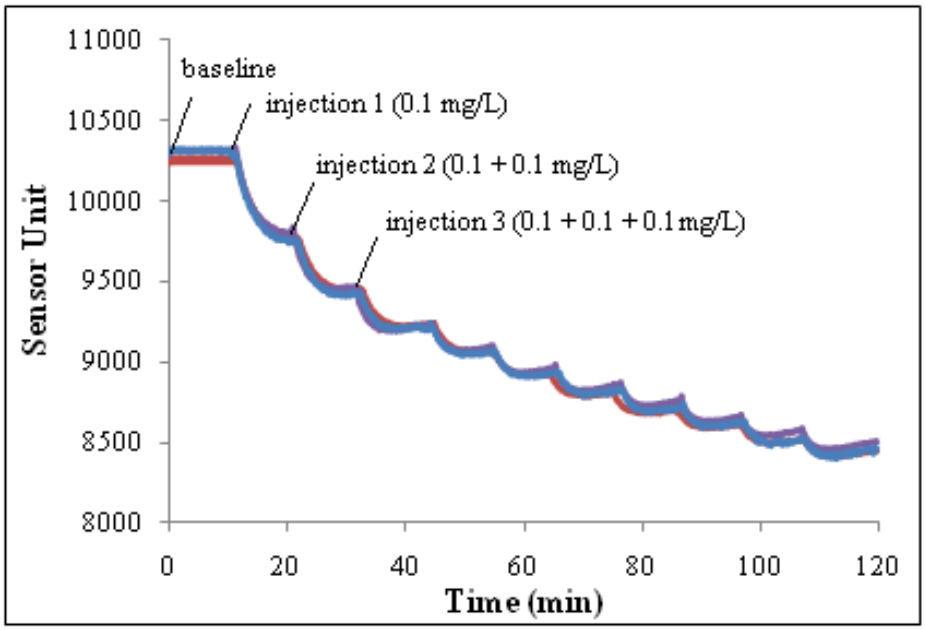

Figure 32: Ten cumulative 0.1 mg/L injections, results from three different slides shown

From this data a calibration curve was generated by using the averaged linear section of each response. The calibration curve can be seen below in Figure 33, where the error bars represent the standard deviation in each response. The source data can be seen in Table 9. From analysis of the calibration plot in Figure 33, we can see that the 0.1 mg/L steps are clearly defined at under 0.3 mg/L, and that the sensor response appears linear over the 0 - 0.2 mg/L acetic acid range. It is from this linear section that the sensitivity of the sensor can be deduced. The clarity of definition is reduced above this level a more curved section of the graph can be seen. It is also worth noting that at higher concentrations of acetic acid the signal to noise ratio is decreased which causes a slight distortion of the readings. This bimodular nature of the graph is hypothesised to be due to the two different types of absorption present the quick surface ion exchange, and the slower diffusion and exchange of ions deeper into the film. From the calibration curve plot the devices sensitivity has been calculated from the slope of the linear section of the calibration curve as 44 units / mgL^{-1}. This calculation exhibits how much deviation there is on the y scale over the range of 1 mg/L acetic acid in air on the x axis.

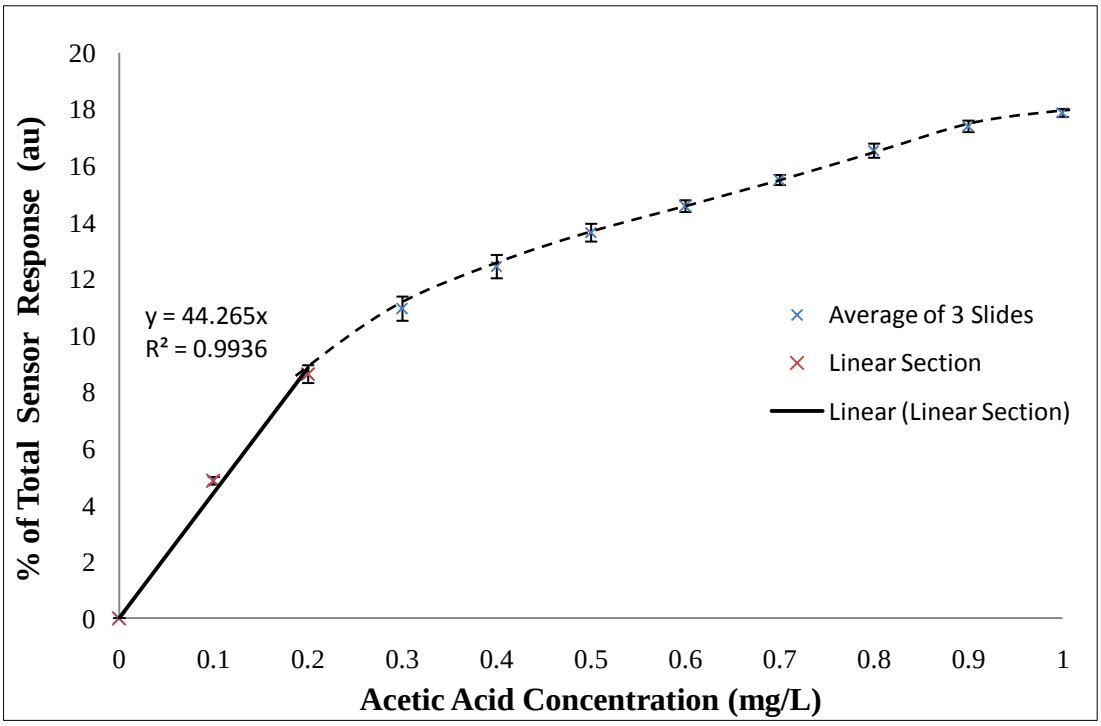

Figure 33: Calibration curve generated from the three calibrated drop cast sensor films, error bars equate to stdev

From these graphs many of the performance characteristics of the sensing platform can be effectively deduced. The maximum RSD% over the calibration range between the three slides on any one exposure was calculated to be 7.82 %.

Table 9: Calculation of the %RSD between the 3 calibrations

mg/L	Cal 1	Cal 2	Cal 3	Stdev	Average	RSD%
0	0	0	0	0	0	0
0.1	4.89	4.58	5.12	0.27	4.86	5.59
0.2	8.46	8.10	9.32	0.62	8.63	7.27
0.3	10.53	10.37	11.93	0.85	10.94	7.81
0.4	12.04	11.87	13.38	0.82	12.43	6.63
0.5	13.39	13.16	14.34	0.62	13.63	4.61
0.6	14.42	14.25	15.04	0.41	14.57	2.84
0.7	15.36	15.22	15.90	0.35	15.49	2.29
0.8	16.40	16.11	17.08	0.49	16.53	3.02
0.9	17.34	17.01	17.82	0.40	17.39	2.33
1	18.14	17.71	17.69	0.28	17.86	1.56

A maximum RSD of 8% over an entire calibration range demonstrates a certain level of reproducibility, which has been attained though drop casting of large pool regions, where multiple similar smaller sensor slides can be cut from. The RSD value in fact is not that dissimilar to the inkjet printing work of O' Toole *et al*. [4] where similar colorimetric sensors where fabricated which exhibited RSD% values as high as 8.4% for just two printed layers of deposited material. Further improvements could be made in terms of sensor reproducibility through use of different fabrication techniques. Ones which possess extremely low position repeatability and low drop volume resolution could potentially be used to drop the RSD% values further.

As well as showing favourable performance characteristics, the newly designed flowcell displays other useful characteristics. The flowcell shrouds the sensor and detector LEDs from environmental light, a cause of noisy sensor signals in previous work [5, 81] and could potentially protect the slide from harsh external conditions, which fufills two of our design requirements set out in the design phase of the study. Similarly, the sensor has shown good reproducibility in its setup showing a reproducibility of > 99 % with three exposures. The chosen design has also met our design requirements in terms of being sensitive and having an ultra low LOD.

4.3. Depositing and Testing Inkjet Printed Sensors

The printed formulation comprised bromophenol blue, ethyl cellulose, tetrahexyl ammonium bromide and butanol as outlined in section 3.7. With the printing of a new dye a large amount of experimentation with the printer was required. The inkjet printing process requires delicate control of its variables in order to create homogenous films. In this study the home made sensor formulation presented challenges in effective printing. A series of experiments were carried out in order to find the optimum deposition settings. The printer used in this study was a Diamatix Materials Printer DMP-2800 as shown in Figure 34. Inkjet printing was trialled as a deposition method because it's widely known as a cost-effective, easy-to-use precise materials deposition system [85].

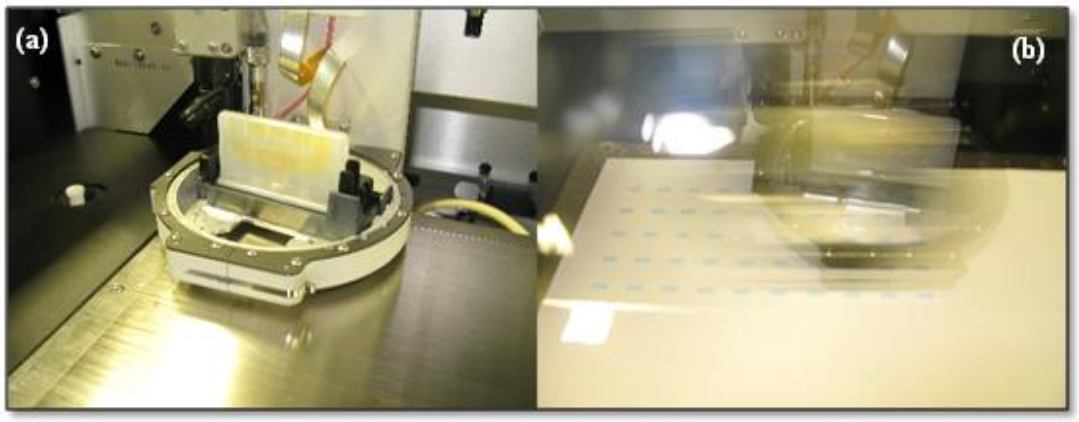

Figure 34: (a) a loaded cartridge before printing (b) the printer in use printing on paper

Firstly, the viscosity of the ink was adjusted to fall within the correct viscous range (10- 20 cP) 13 cP in this case; this was achieved by varying the amount of the ethyl cellulose polymer. Then the ink was substrate matched, in order to produce a pH neutral film (PET). The optimum printing parameters were found through varying the stage temperature, cartridge temperature, excitation voltage and drop spacing. The following image sequence illustrates the print optimisation, and how the film topography and pH can change dramatically with just a small change in any deposition variable.

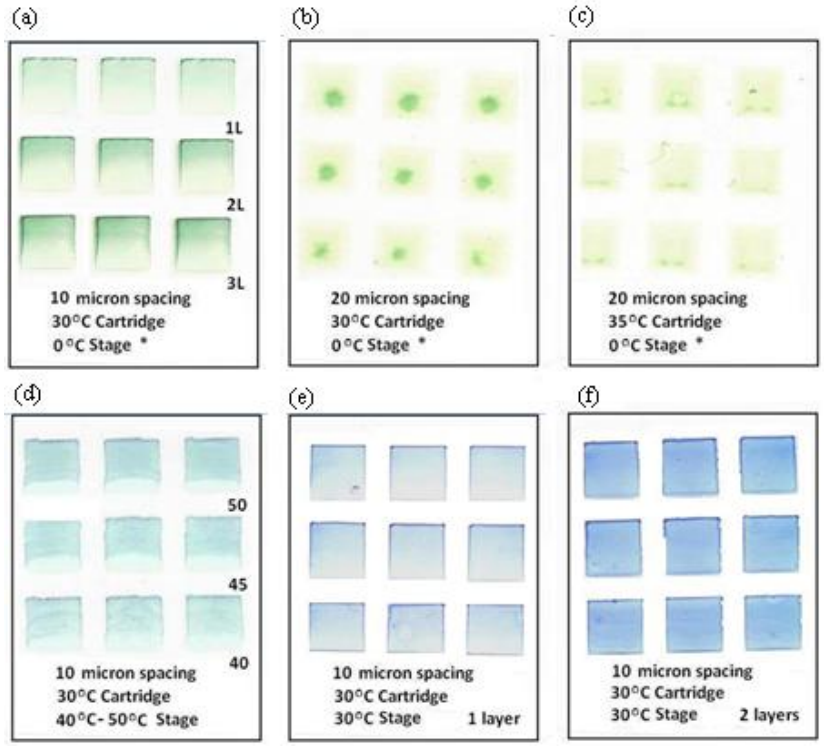

Figure 35: An array of printed slides, demonstrating the sensitivity to parameter change

From this array of printed slides shown in Figure 35 a number of things can be deduced. Firstly, looking at print (a), it shows the printing of three layers. It is visible that each subsequent layer deposited amplifies the evaporation effect (where material is drawn to the top of the slide in order to replace the already evaporated solvent). It was thought that reducing the stage temperature, would help to alleviate this effect, but the stage was in fact at room temperature (denoted by 0 ºC* in Figure 35). It was decided at this point that the sensors would be best manufactured in one layer, in order to minimize this effect. With this in mind it was important to deposit as much material as possible in a single layer. In order to do this the minimum drop spacing (10 micron drop spacing) was used. After printing, if the slides are too optically transparent they will not function well as sensors because the colour change from the alkaline blue state to the yellow acetic state will not result in a sufficient modulation of the light passing from the emitter to the detector LED. So evaluation of prints (b) and (c) visible in Figure 35 highlights faint images of the sensors fabricated. This resulted when the drop spacing was increased from the lowest setting of 10 microns up to 20 microns, and where enough material was not deposited to create a homogenous film. Image (e) is an example of the optimised print settings.

The gradient was found to be ≈ 2 µm across 10 x 10 mm films which measured 5 µm in thickness at their thickest point. Measurements were carried out using a Datek stylus profilometer. From the measurements, it became clear that the gradient was large when compared with the total film thickness (a graphical representation of the printed gradient can be seen in Appendix F as well as the measured thickness values). In order to overcome this effect, printing was carried out on both sides of the substrate.

However, printing on both sides of the substrate, also served to double the film thickness providing a larger colour change range and hence improving the sensing resolution. Printing on both sides of the substrate also served to double the surface interaction between the sensor film and the contaminant which should improve the speed of response of the film, a double sided printed film array can be seen in Figure 36.

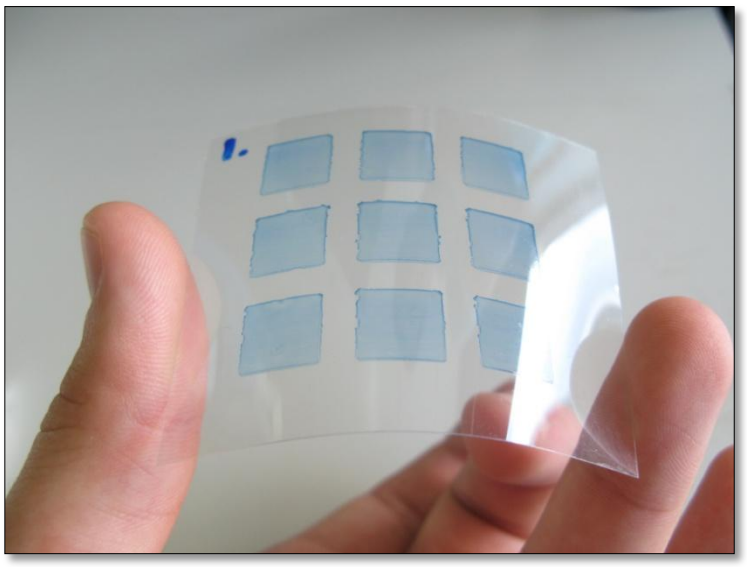

Figure 36: Final optimised double-sided printed array of sensors

4.4. Characterising the Inkjet Printed Slides

A number of analytical techniques were used to characterise the inkjet printed films. Firstly, as already mentioned, the thicknesses of the films were measured using a Detak 8 Surface Profiler (Figure 37 (a)). Within this technique the machine offers up the stylus to the film being measured. Once contact has been made the stylus is moved with an ultra low force across the sample in a straight line of a length specified by the user. The vertical position of the stylus generates an analogue signal which is converted into a digital signal, stored, analysed and displayed.

Figure 37: (a) the Veeco Detak 8 Profiler, (b) the Veeco NT9080™ Surface Metrology System

In order to capture thickness data, scans were continually made, dragging the stylus horizontally across the substrate from an area free of printing to an area where a slide had been printed. It became clear after a number of measurements with this device, that there was a split in the data. It was clear that the films had a gradient across them. Where they were thicker on the side of the slide printed first and thinner on the bottom slide of the side, the side deposited last. At the thin edge, films were measured to be within the range 2.8 - 3.3 µm, and on the thicker side the films ranged from 6.8 - 7.5 µm thick. The measured profilometery data set can be found in Appendix F as well as a graphical representation of how the gradient appeared.

At this stage it also became obvious that the technique used for measuring the films was not satisfactory since they possessed arenas of different heights and also during measurements occasionally the stylus head penetrated the surface of the film. A noncontact method of measurement would better suit measurement of the films. Ideally, one where the entire film topography, or thickness could be recorded.

The Veeco NT9080™ Surface Metrology System (Figure 37 (b)) is a type of optical profiler which use on light interferometry. It was employed to verify the stylus data in this study. The technique operates by emitting two separate wave bands of light. The interference within the reflected rays are used to plot the 3D profiles of the items being measured. However, the printed sensor films are optically transparent which makes the technique incompatible. To measure them, the films were first sputter coated with a thin layer of gold, seen in Figure 38 (a). The sputter coating is even, so the height difference between the film and the PET substrate should remain unchanged.

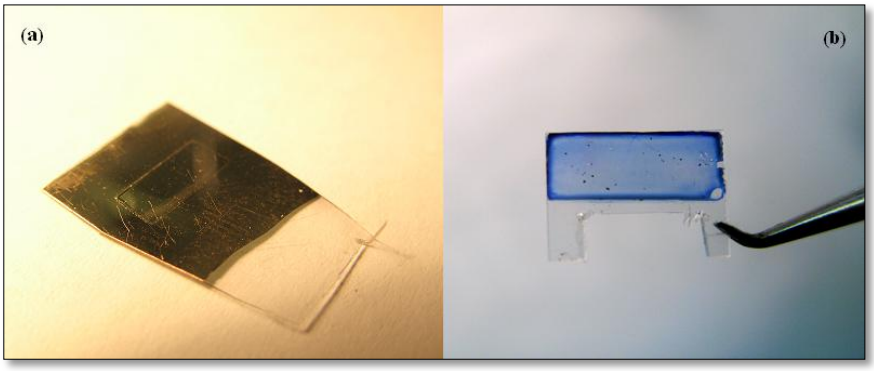

Figure 38: (a) a gold sputter coated printed film (b) a printed film with the "coffee ring effect"

The interferometry results verified the thickness results collected using the stylus profilometer, showing films possessing a gradient across them. The results also showed that some inkjet printed slides exhibited what's known as a "coffee ring effect" where the outermost band of deposited material forms a thicker ring around the outer edge of the film (see Figure 38 (b), and measured in Figure 39). Although this effect is clearly visible, it does not necessarily affect the operation of the sensor, as long as it is outside the operating zone of the film. In this case, the slide is 10 mm x 10 mm in size and the LED is a 5 mm bulb LED, ensuring the illuminated zone of the sensor film lies well within the homogenous central zone.

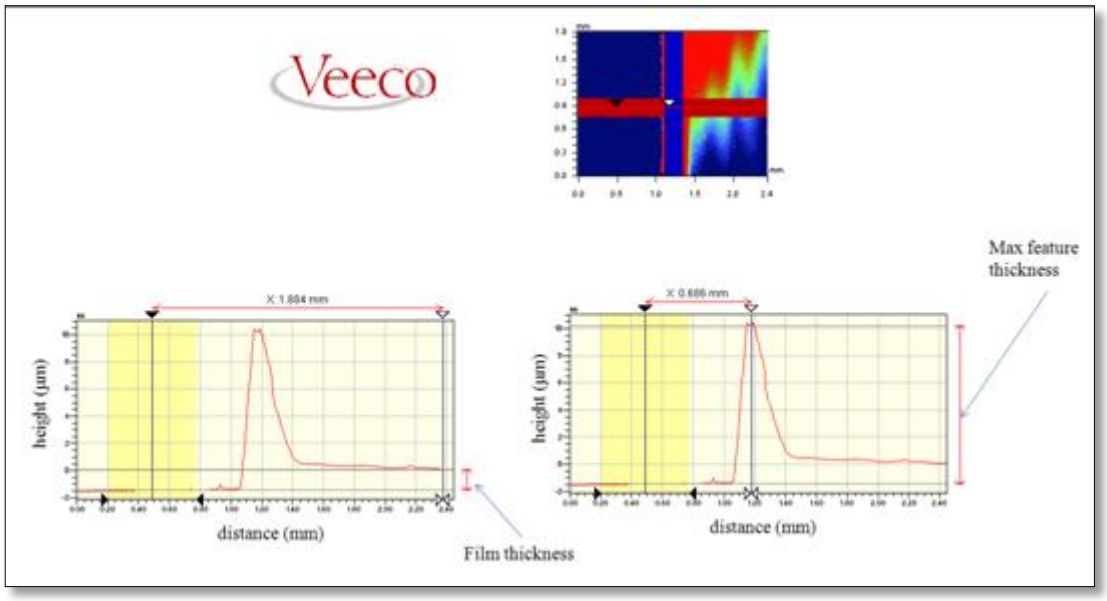

Figure 39: Y thickness profile across the edge of a drop cast sensor with the "coffee ring effect"

4.5. Atomic Force Microscopy

Using both the stylus and optical profilometer the gradient effect across the slides was observed. However, printing in two opposing directions on both sides of the substrate should mean that the slides should operate normally as optical sensors. As well as being homogenous, for films to operate effectively as optical sensors they should be smooth and devoid of any bumps or troughs. Atomic force microscopy (AFM) scans were used in order to characterise the roughness of the films.

AFM works by scanning a silicon cantilever beam over a sample. The technique can be used in a couple of different modes. For example; contact, non-contact and in tapping mode. In this study the AFM images were recorded in tapping mode on a Veeco Dimension 3100 instrument (Figure 40). In tapping mode, the cantilever tip is driven to oscillate up and down by a small piezoelectric element mounted in the AFM tip. Due to the interaction of forces acting on the cantilever when the tip comes close to the surface, (i.e. Van der Waals force, electrostatic forces, dipole-dipole interaction) it causes the amplitude of this oscillation to decrease as the tip gets closer to the sample. An electronic servo uses the piezoelectric actuator to control the height of the cantilever above the sample. The servo adjusts the height to maintain a set cantilever oscillation amplitude as the cantilever is scanned over the sample. A tapping AFM image is, therefore, produced by imaging the force of the intermittent

contacts of the tip with the sample surface. This method of 'tapping' is less destructive to the surface of the sample than contact AFM. Tapping mode is gentle enough even for the visualization of supported lipid bilayers or, in this case, the polymer based films used in this study. AFM images were analysed and processed using WSxM software for approximating surface roughness and visualizing data in 3D.

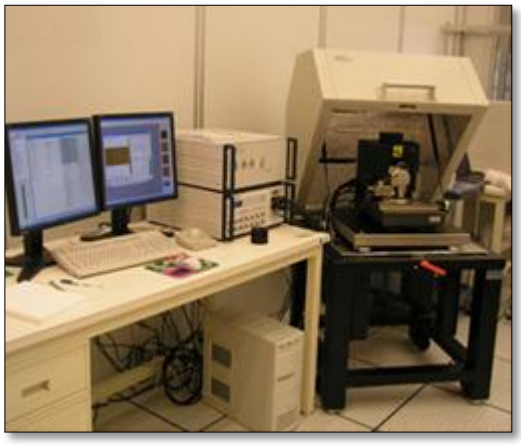

Figure 40: The Veeco Dimension 3100 AFM instrument

AFM scans were carried out across a sample of 6 printed slides. From the scans, surface roughness was quantified by the software in terms of root mean square roughness. It is logical to assume that the smoother the film the greater the optical clarity of the slide and hence the more desirable the deposition process for sensor creation. The complete results from the AFM scans can be seen in Appendix G. The first three scans completed RMS values of 7.75, 11.83 and 11.53 respectively. Giving an average recorded RMS value of 10.37. The delicacy of the process was perfectly displayed in the other scans. The silicone tapping probe can easy be damaged irreparably if it is at any time brought in too close to the substrate. This is what happened on the 4^{th} AFM scan, and after this point the topography plots support the belief that the tip was not replaced in a satisfactory fashion leading to the appearance of low magnitude noise across the sample. It is also possible that this is silicone dust from the crashed tip that contaminated the samples. A successful afm scan can be seen in Figure 41 (a), a poor quality afm scan can be seen in Figure 41 (b) where low magnitude noise dominates the topography.

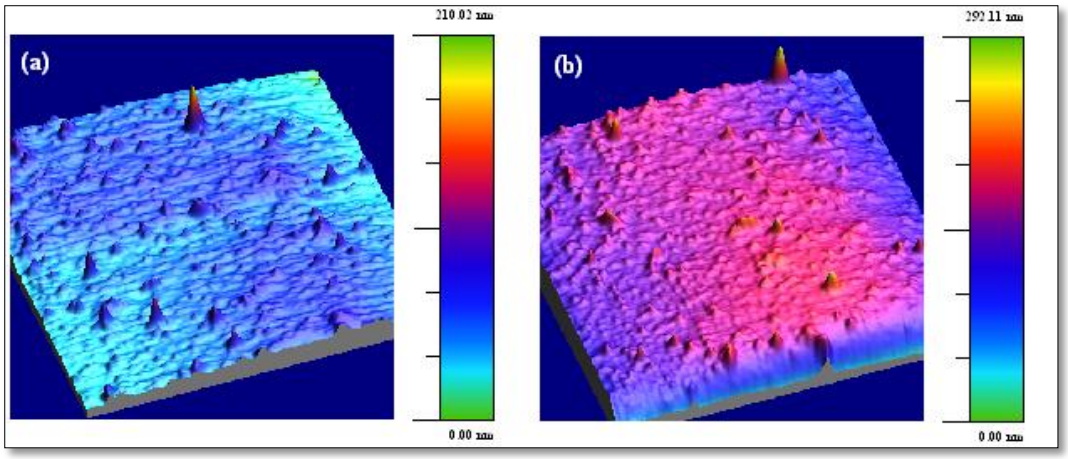

Figure 41: (a) 80 µm x 80 µm sensor film AFM scan, (b) similar scan with a badly replaced tip

Having recorded an average AFM value of ≈ 10 nm, it's important to give some relevance to this value, a "super smooth" mirror exhibited an RMS roughness value of 0.55 nm, when measured by Wyant and Creath [86]. Similarly, in the surface roughness study carried out by Bennett [87], fused quartz exhibited a RMS roughness of 11.0 nm, BK-7 Glass was measured as 19.3 nm, and machined copper was measured as 22.5 nm. It can be deduced, when compared against these values, that the inkjet printed polymer films exhibits very low roughness values, similar to glass, which suits the application of optical modulation well.

4.6. Testing the Inkjet Printed Sensors

Although thickness and surface roughness measurements build up a nice picture of the deposited films from the inkjet process, thickness measurements aren't critical performance measurements. An original aim of the study was to provide proof of concept that if sensors are created in a reproducible enough fashion, they could be potentially calibrated in batches, a technique known in industry as machine calibration. In order to investigate this the printed sensors were tested within the flowcell, and analysed against each other.

In order to test the reproducibility between the printed sensors, a repeat of the calibration carried out on the drop cast sensors was once again carried out. This test was setup exposing the sensor to ten cumulative exposures in 0.1 mg/L steps over the range from 0 – 1 mg/L acetic acid in air. The resulting calibrations can be seen in Figure 42.

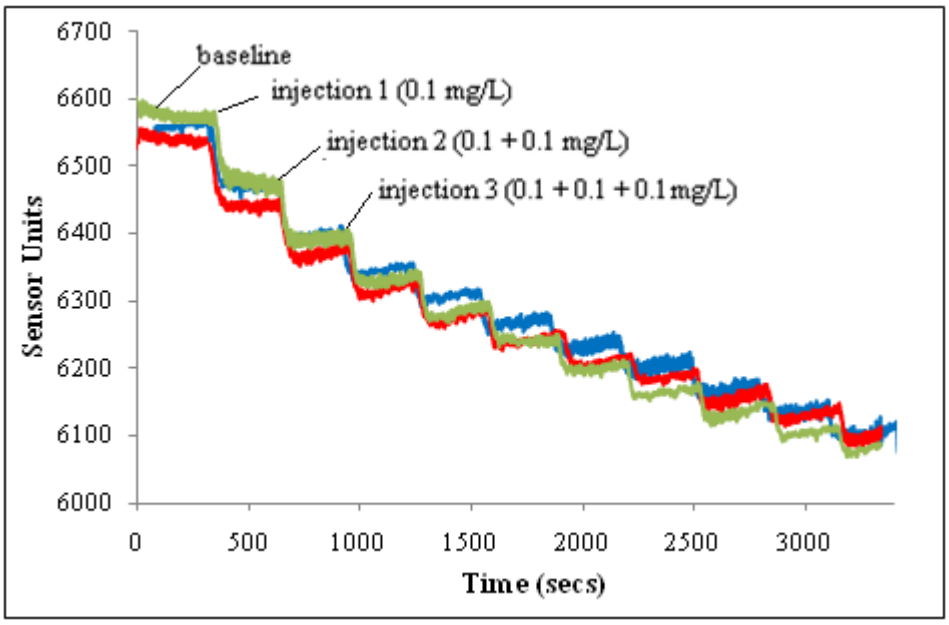

Figure 42: Raw sensor data from the 3 different slides over the calibration range

The data generated from the inkjet printed slide calibrations (Figure 42) displays a very similar response trend to that of the drop cast sensors in Figure 32. In fact, the data from all the slides are hard to see because they are so closely stacked. In contrast to the calibration carried out on the drop cast sensors the range of ADC

points covered by the total response is far less. This is due to the thickness of the slides and the fact that they are thinner than the drop cast sensors resulting in a more optically transparent film. In addition to this the total response takes much less time to stabilise at a final value. The raw data similar to the drop cast sensor calibration was then averaged for each response and plotted as points against the acetic acid concentration. The generated plot is shown in Figure 42, where error bars represent the standard deviation in each response (The souse data is visible in Table 10).

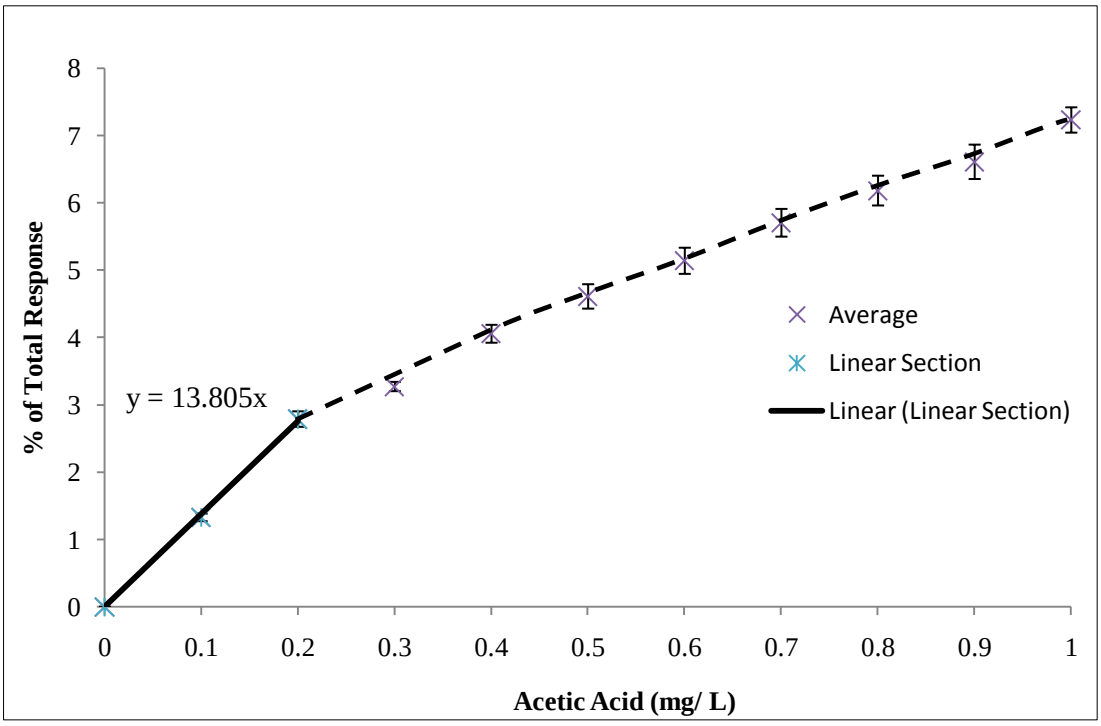

Figure 43: Average of each response over the calibration range, error bars equate to Stdev

Table 10: Calibration data from three inkjet printed slides, and the calculated RSD%.

	Cal 1	Cal 2	Cal 3	Average	Stdev	RSD%
0	0	0	0	0	0	0
0.1	1.22	1.31	1.44	1.32	0.11	0.05
0.2	2.82	2.54	2.99	2.78	0.23	0.11
0.3	3.15	3.23	3.42	3.27	0.13	0.06
0.4	3.96	3.84	4.35	4.05	0.26	0.13
0.5	4.34	4.45	5.01	4.60	0.36	0.18
0.6	4.91	4.91	5.58	5.13	0.38	0.19
0.7	5.56	5.37	6.16	5.70	0.41	0.20
0.8	6.07	5.80	6.66	6.18	0.44	0.22
0.9	6.48	6.17	7.16	6.60	0.51	0.25
1	7.13	6.90	7.64	7.22	0.37	0.18

The maximum RSD % over the calibration range at any point was calculated to be 0.25 %. This shows a significant reduction on the 8 % RSD calculated over the similar drop cast slide calibration. The speed of response of the films (i.e., the time taken to reach 95 % of a total response) was calculated from 95% the time taken for a full response over the first three responses of the red data set in Figure 42. The speed of response was calculated to be 1 minute 14 seconds ± 2 seconds; the calculations can be seen in Table 11.

Table 11: Speed of response calculation

	Start Pt	End Pt	100% Response	95% Response	95% Response Point	Time taken to reach this point since last injection (s)
Response 1	6530	6441	88.53	84.1035	6445.896	73.4
Response 2	6456	6377	78.69	74.7555	6381.244	76.8
Response 3	6382	6314	68.06	64.657	6317.343	72.8
					Average	74.3
					Stdev	2.15

As with the testing of the drop cast slides, this time response is the time it takes the whole system to respond to the contaminant and not the response time of the colorimetric film which has been shown to be much faster. The limit of detection of the film was calculated from three times the standard deviation of the base line and was found to be 0.15 mg/L or .15 ppm or 150 ppb.

This LOD is far higher than that of the drop cast films. However, the LOD is merely a function of slide thickness, increasing the thickness of printed layers would enable the reduction of the LOD. Lastly, the sensitivity of the film was measured from the linear section of the calibration curve to be 14 units / mgL^{-1}. The sensitivity reduction and the LOD increase is a direct result of the shift to a thinner thickness film. The total shift of the sensor points over the duration of the experiment is lower as the film can't modulate the light to the extent a thicker film would be capable of. Thin films suit applications where quick response times are more desirable than high sensitivities for example in the area of leak or process monitoring.

At this point in the study a number of key aims have been achieved. A full system redesign was carried out reducing the effect of unwanted system variables and hence reducing noise. The shift to the flowcell design, the 5 mm LEDs and the coated slide have all translated to improved sensor performance. Similarly, the goal of immobilising the coating onto a substrate has meant that the device can be potentially used in conjunction with other coatings for different targets. Another aim that has been met successfully is the inkjet printing of the chemical coating. The high reproducibility achieved between films suggests the technology could be suitable for creating these films in a commercial capacity.

5

Within this project a low cost low power chemical gas sensor was improved upon from a previous proof of concept project. Its performance characteristics have been significantly improved, key developments and improvements achieved during this body of work include:

1. The redesign of the sensor has seen the sensor LOD drop from the ppm level to the ppb level. This is of course dependant on many factors. However, the shift to using 5 mm bulb LEDs rather than surface mount LEDs has meant a greater capacitance can be discharged each time, contributing to the improved LOD and sensitivity values. It has also been shown that thicker sensor films will exhibit greater levels of sensitivity and lower LODs.

2. The introduction of a coating slide resulted in significant advantages. Typically the surface mount LEDs have a glass or silicone like lens. These materials are hydrophilic, making it difficult to print on them. The introduction of the coating slide allowed another of the original study aims to be achieved. Batches of colorimetric sensors were inkjet printed and tested resulting in high levels of reproducibility within the prints.

3. The introduction of a substrate for printing onto has also meant that, gases and other contaminants can flow over both sides of the slide. This has effectively doubled the interaction surface area between the sensor film and the contaminant, which translates to a reduction in the response time of the system and a sensitivity increase.

4. The incorporation of the sensor into a flowcell device has brought with it many benefits. Firstly, it serves to shroud and protect the coated sensor slide, from external environmental light and possible weathering. It also highlights the potential of the device for development as a standalone device. It now operates in conjunction with the grab sampler and is capable of servicing itself with samples continuously, offering potential for standalone field deployment.

5. The coupling of the device with its own grab sampler also has advantages over previous experimental setup. The system is now always going to be testing fresh samples, even in areas of low circulation. In the POC project, the device was simply left deployed in an area in the hope that contaminated samples would blow directly across the coated LEDs.

6. Inkjet printing of films has been achieved in a reproducible fashion and smooth films have been created. However, they did possess a slight gradient across the slide. It's hypothesised that as the deposited film dries the butanol evaporates out of the film, wet material printed below it is then pulled into the space it once occupied. These small gradients were overcome by printing on both sides of the film in opposing directions. This is highlighted by extremely low levels of RSD in the printed sensors (>1 %).

7. The inkjet printing technique was found to be only viable for development of thinner films, with multilayered films highlighting problems with the solvent redissolving into previous layers. Thin films suit applications such as trace pH sensors, for applications such as leak detection an early warning device where the speed of response of the sensor is crucial (< 2 minutes).

8. The project also demonstrated that the idea of calibrating a number of inkjet printed slides in one calibration is possible, which achieves another of the project aims. Given that the max RSD was 0.3 %, it could be deduced that all slides are identical and could be calibrated within an accuracy of $\pm$ 0.3 %.

9. Through collection of humidity data the sensor response has been validated as a response to the acetic species and not to the induced humidity change. Secondly, printed films have been shown to operate, after a period of 3 months showing that once stored in dark dry conditions the films are very stable.

10. Finally, it is clear from the testing in this study, that the PEDD sensor setup is a very flexible sensing technique. The user can tune their device depending on their sensing requirements and applications. Films can either be cast (i.e., inkjet printed) in very thin layers, achieving extremely high levels of reproducibility >99%, with the potential to quickly sense trace levels of contaminant. Alternatively, films can be cast in thicker layers, in order to achieve an optimum sensor in terms of low detection limits (i.e., ppb), where a trade off is made in terms reaction time. This flexibility will broaden the range of potential applications.

In this final chapter, the conclusions, drawn from the work in this thesis, have been detailed. As a consequence of these conclusions, some potential areas of further research can be highlighted. Real world potential application areas include; air ventilation, landfill monitoring, environmental monitoring (ammonia), leak monitoring, process monitoring, and horticultural monitoring (acetic acid).

5.1. Suggested Future Work

Despite the conclusions found in this work, and in order, to facilitate practical real world deployments of future generations of wireless chemical sensor nodes, it will be necessary to address some issues that this research work raised.

1. Range improvement

   A device with a larger sensing range, but with a slower response time could be achieved through use of a different deposition process to create thick films. For example, screen printing of the dye might be possible, providing the polymers it was cast in were suitably porous. However, the viscosity range required for this type of printing would make tailoring the dye to the range quite difficult. Alternatively casting of the dye in a porous membrane might be possible. Trapping a dye in such a film would mean that the deployment lifetime of such a sensing film, could be greater than an inkjet printed slide.

2. Different targets

   Potential also exists for the development of an array of these PEDD sensors, where they are setup with a selection of different thin film sensors based on different indicator dyes to provide sensitivity in multiple pH ranges or for multiple species.

3. Interferents

   For the continued development of these devices, a full temperature and humidity study should take place. Ideally a test chamber could be developed where both humidity and temperature could be regulated as required.

4. External factors

   It is logical to believe that a second emitter and second detector LED could be setup without any sensor slide, and that with a simple subtraction, the effects of changing temperature or humidity could be negated. This idea of a reference LED should be explored and fully tested.

5. Communications

   If this device is going to go forward into a commercialisation project, a number of tasks should be carried out. Firstly a study should be carried out to trial available communications platform. The Xbee platform although seemingly obviously doesn't suit the sensor configuration as the I/Os cannot be programmed in the desired manner. So in order for a commercialisation project to be viable a suitable wireless transmitting package would have to be selected and tested.

6. Noise Reduction

   Once a wireless platform had been decided on to handle communications a more robust PCB could be designed where track lengths were optimised in order to reduce noise.

7. In Dept Study of Liner Response Range

   At low concentration of acetic acid, <0.2 mg/L the sensor response appears to be linear, this has been explained within the text but it would be beneficial to extend the testing within this range to include more data points and further develop understanding of the relationship that exists.

It is hoped that the work described in this thesis and the resultant publications, in peer reviewed journals will motivate and inspire further research into this innovative, developing research area.

References

[1.] Li, J., Vanysejk, P., Brown, R., el al. (2009), "Carbon Nanotube Based Chemical Sensors for Space and Terrestrial Applications" 35 Years of Chemical Sensors - An Honorary Symposium Celebration, Vol 19 (6), NASA Ames Research Center, Moffett Field, CA 94035, USA

[2.] McDonagh, C., Burke, C.S. (2008), "Optical Chemical Sensors", Chemical Society Reviews, Vol 108, pp 400-422

[3.] Lau, K.T., Baldwin, S., Sheppard, R.L., et al. (2004), "Novel Fused-LEDs Devices as Optical Sensors for Colorimetric Analysis", Talanta, Vol 63, pp 167 - 173

[4.] O' Toole, M., Shepherd, R.L., Wallace, G.G., Diamond, D. (2009), "Inkjet printed LED based pH chemical sensor for gas sensing", Analytica Chimica Acta, Vol 652 (1-2), pp 308 - 314

[5.] Beirne, S, Corcoran, B., Lau, K.T., Diamond, D. (2008), "Chemical event tracking using a low-cost wireless chemical sensing network", IEEE Sensors, pp 1615 - 1618

[6.] Jung, Y., Kim, S., Lee, D., Oh, K. (2006), "Compact three segmented multimode fibre modal interferometer for high sensitivity refractive-index measurement", Meas. Sci. Technology, Vol 17, pp 1129 - 1133

[7.] Zhang, L., Kangmuir, M.E, Bai, M., Seitz, W.R. (1997), "A sensor for pH based on an optical reflective device coupled to the swelling of an aminated polystyrene membrane", Talanta, Vol 44 (9), pp 1691-1698

[8.] Shusterman, A., Lecture Notes: Organic Chemistry Online. Reed University, Portland, Oregan, Department of Chemistry, [online] http://academic.reed.edu/chemistry/alan/201_202/lab_manual/Expt_pKa/index.html (Accessed 28th July 2010)

[9.] Stankovic, J.A., (2006), "Wireless Sensor Networks", Department of Computer Science University of Virginia, Charlottesville, Virginia, [online], http://www.cs.virginia.edu/~stankovic/psfiles/wsn.pdf (Accessed 01 November 2010)

[10.] Estrin, D., Culler, D., Pister, K., Sukhatme, G. (2002) "Connecting the physical world with pervasive networks ", IEEE Pervasive Computing, pp 59 - 69

[11.] Mobile Networking Laboratory, Computer Science and Engineering, Pohang University of Science and Technology, [online], http://monet.postech.ac.kr/research.html (Accessed 28th July 2010)

[11.] Wang, N., Zhang, N., Wang, M. (2007), "Wireless sensors in agriculture and food industry-Recent development and future perspective", Comput. Electron. Agr., Vol 50, pp 1-14

[12.] Horan, B., Bush, B., Nolan, J., Cleal, D. (2007), "A Platform for Wireless Networked Transducers" Sun Microsystems, Inc., Mountain View, CA, USA

[13.] Morrin, A., Ngamna**,** O., O'Malley, E. *et al.* (2008), "The fabrication and characterization of inkjet-printed polyaniline nanoparticle films", Electrochimica Acta, Vol 53 (16), pp 5092 - 5099

[14.] Loffredo, *F.,* Burrasca, G., Quercia, L., Della Sala, D. (2007), "Gas Sensor Devices Obtained by Ink-jet Printing of Polyaniline Suspensions*"*, Macromolecular Symposia, Vol 247 (1)**,** pp 357 - 363

[15.] Moulton, S.E., Smyth, M.R., Wallace, G.G., *et al*. (2007), "Inkjet Printable Polyaniline Nanoformulations", Langmuir, Vol 23(16), pp 8569 – 8574

[16.] Song, J.W., Kim, J., Yoon, Y.H., *et al.* (2008), "Inkjet printing of single-walled carbon nanotubes and electrical characterization of the line pattern", Nanotechnology, Vol 19 (9).

[17.] Lok, B.K., Ng, Y.M., Liang, Y.N., Hu, X. (2010), "Inkjet Printing of Multi-Walled Carbon Nanotube/Polymer Composite Thin Film for Interconnection", Journal of Nanoscience and Nanotechnology**,** Vol 10 (7), pp 4711 – 4715

[18.] Renewable Energy, Inhabitat – Green Energy will save the world, [online] http://www.inhabitat.com/wp-content/uploads/nanosys_solar.jpg, (Accessed 17th August 2010)

[19.] Engineering Information Portal: All the Information of Engineering, [online] http://www.4engr.com/images/press/e1a433f2d564cf721a379e85ed5d3c42.jpg, (Accessed 17th August 2010)

[20.] Nash III, T.H., (1996), "Lichen Biology", Cambridge University Press, Cambridge, pp 303

[21.] Ngai, E., Zhou, Y., Lyu, M.R., Liu, J. (2010), "A delay-aware reliable event reporting framework for wireless sensor-actuator networks", Ad Hoc Networks, Vol 8 (7), pp 694 – 707

[22.] López Riquelme, J.A., Soto, F., Suardiaz, J. *et al.,* (2009), "Wireless Sensor Networks for precision horticulture in Southern Spain", Computers and Electronics in Agriculture, Vol. 68, pp 25 – 35

[23.] Bogue, R. (2007), "Optical chemical sensors for industrial applications", Sensor Review, Vol. 27 (2), pp 86-90

[24.] "The American Heritage Stedman's Medical Dictionary", (1995), Version 7.0.7, Houghton Mifflin Harcourt Publishers, Boston

[25.] McNair, H.M., & Miller, J.M., (1997), "Basic Gas Chromotography", Wiley Interscience, New York, 1997, pp 153 - 166

[26.] de Hoffman, E., & Stoobant, V. (2001), "Mass Spectrometry Chromatography Coupling", Mass Spectrometry Principles and Applications, Wiley, Chichester, pp 157 - 180

[27.] LabX. The Scientific Equipment Marketplace, [online] Http://www.labx.com/v2/category_main.cfm?MainCatID=31&CatID=433, (Accessed 18th August 2010)

[28.] Comparison of Photoionisation Detectors and Flame Ionisation Detectors, [online], Http://www.raesystems.com/~raedocs/App_Tech_Notes/App_Notes/AP-226_PID_vs_FID_Comparison.pdf, (Accessed 18th August 2010)

[29.] Saito, M., & Kikuchi, K. (1997), "Infrared Optical Fiber Sensors", Optical Review, Vol. 4 (5), pp 527-538

[30.] Anderson, G.M., & Hadden, D.M. (1999), "The Gas Monitoring Handbook", Avocet Press, New York

[31.] Paschotta, R. (2008), "Encyclopedia of Laser Physics and Technology", Willey-VCH, Weinheim, ISBN: 978-3527408283

[32.] Optical Sensor Technologies, (1996), International Technology Research Institute, Loyola College Maryland, [online], http://www.wtec.org/loyola/opto/c6_s3.htm, (Accessed 18th August 2010)

[33.] Schultz, J.S., Taylor, R.F. (1996), "Handbook of Chemical and Biological Sensors", IOP Publishing Ltd, London

[34.] Agayn, V., Walt, D.R. (1994) "Fiber-Optic Sensors Based on Degradable Polymers", ACS Symposium Series, Vol. 556 (2), pp 22 -33

[35.] Shepherd, R.L., Yerazunis, W.S., Lau, K.T., Diamond, D. (2006), "Low-Cost Surface-Mount LED Gas Sensor", IEEE Sensors Journal, Vol 6 (4), pp 861 - 866

[36.] Gunnlaugsson, T., Glynn, M., Tocci, G.M., Kruger, P.E., Pfeffer, F.M. (2006), "Anion recognition and sensing in organic and aqueous media using luminescent and colorimetric sensors", Coordination Chemistry Reviews, Vol 250 (23-24), pp 3094 - 3117

[37.] Higuchi, A., Yang,S.T., Siao, T.D., Hsieh, P.V., Fukushima, H., Chang, Y., Chen, W.Y. (2009) "Preparation of fractioned DNA aptamer-Pt complex through ultrafiltration and the colorimetric sensing of thrombin", Journal of Membrane Science, Vol 328, (1-2), pp 97 – 103

[38.] Yu, C.J., Lin,C.Y., Liu, C.H., Cheng, T.L., Tseng, W.L. (2010), "Synthesis of poly(diallyldimethylammonium chloride)-coated Fe3O4 nanoparticles for colorimetric sensing of glucose and selective extraction of thiol", Biosensors and Bioelectronics, Vol 26, (2), pp 913 - 917

[39.] Nakamura, N., & Amao, Y. (2003), "An optical sensor for CO2 using thymol blue and europium (III) complex composite film", Sensors and Actuators B: Chemical, Vol 98 (1-2), pp 98 - 101

[40.] Mills, A., Change, Q. (1994), "Colorimetric polymer film sensors for dissolved carbon dioxide", Sensors and Actuators B: Chemical, Vol 21 (2), pp 83 - 89

[41.] Eaton, K. (2002),"A novel colorimetric oxygen sensor: dye redox chemistry in a thin polymer film", Sensors and Actuators B: Chemical, Vol 85 (1-2), pp 42 – 51

[42.] Byrne, L., Lau, K.T., Diamond, D. (2004), "Monitoring of headspace total volatile basic nitrogen from selected fish species using reflectance spectroscopic measurements of pH sensitive films", The Analyst, Vol 127, pp 1338 - 1341

[43.] Dietz, P., Yerazunis, W., Leigh, D. (2003), "Very low-cost sensing and communication using bidirectional LEDs", In Proceedings UbiComp, Vol 2864, pp 175 - 191

[44.] Mims III, F.M. (1986), "Siliconnections: Coming of Age in the Electronic Era" McGraw- Hill, New York, ISBN: 978-0070424111

[45.] Mims III, F.M. (1973), "LED Circuits and Projects", Howard W. Sams and Co. Inc, New York, ISBN: 978-0672210068

[46.] O'Toole, M., Lau, K.T., Shazmann, B., Shepherd, R., Nesterenko, P.N., Paul, B., Diamond, D. (2006), "Novel integrated paired emitter-detector diode (PEDD) as a miniaturized photometric detector in HPLC", The Analyst, Vol 131, 938-943

[47.] O' Toole, M., Diamond, D (2008) "Absorbance Based Light Emitting Diode Optical Sensors and Sensing Devices", Sensors, Vol 8, 2453-2479

[48.] Shepherd, R.L., Yerazunis, W.S., Lau, K.T., Diamond, D. (2004), "Novel surface mount LED ammonia sensors",IEEE Sensors, pp 951 – 954, Vienna, Austria

[49.] Baldwin, S., Lau, K.T., Shepherd, R.L., Yerazunis, W.S., Diamond. D. (2004), "Colorimetric Detection of Iron (II) Using Novel Paired Emitter Detector Diode (PEDD) Based Optical System", Ieice Transactions on Electronics, pp 2099 - 2102

[50.] Courbat, J., Briand, D., Damon-Lacoste, J., Wollenstein, J., de Rooij, N.F. (2009), "Evaluation of pH indicator-based colorimetric films for ammonia detection using optical waveguides", Sensors and Actuators: B Chemical, Vol 143, pp 62 - 70

[51.] Sadeghi, U., Doosti, S. (2009), "Uranyl ion-selective optical test strip", Dyes and Pigments, Vol 80 (1), pp 125 - 129

[52.] Moody, A., Setford, S., Saini, S.. (2001), "Peroxidase enzyme sensor for on-line monitoring of disinfection processes in the food industry", The Analyst, Vol 126 (10), pp 1733 - 1739

[53.] Shepherd, R., Beirne, S., Lau, K.T., Corcoran, B., Diamond, D. (2007), "Monitoring chemical plumes in an environmental sensing chamber with a wireless chemical sensor network", Sensors and Actuators, B: Chemical, Vol 121 (1), pp 142 – 149

[54.] Diamond, D., Coyle, S., Scarmagnani, S., Hayes, G. (2008), "Wireless Sensor Networks and Chemo Biosensing", Chemical Reviews, Vol 108 (2), pp 652 – 679

[55.] Zeng, Y., Xiong, N., Park, J.H., Zheng, G. (2010), An Emergency-Adaptive Routing Scheme for Wireless Sensor Networks for Building Fire Hazard Monitoring", Sensors, Vol 10, pp 6128 – 6148

[56.] Garcia-Sanchez, A.J., Garcia-Sanchez, F., Losilla, F., Kulakowski, P., Garcia-Haro, J., Rodríguez, A., López-Bao, J.V., Palomares, F. (2010), "Wireless Sensor Network Deployment for Monitoring Wildlife Passages" Sensors, Vol 10, pp 7236 – 7262

[57.] Korkua, S.K., Lee, W.J. (2009), "Wireless sensor network for performance monitoring of electrical machine", IEEE North American Power Symposium, Issue 4 -6, pp 1 – 5

[58.] Seman, A., Donnelly, M.E., Mastro, S. (2007), "Wireless Systems Development for Distributed Machinery Monitoring and Control", American Society of Naval Engineers (ASNE) Intelligent Ships Symposium VII, Philadelphia, PA

[59.] Coleri, S., Cheung, S.Y., Varaiya. P. (2004), "Sensor networks for monitoring traffic", In Forty-Second Annual Allerton Conference on Communication, Control, and Computing, Allerton House, Monticello, Illinois

[60.] Yajie, M., Richards, M., Ghanem, M., Guo, Y., Hassard. J. (2008), "Air pollution monitoring and mining based on sensor grid in London", Sensors, Vol 8 (6), pp 3601 – 3623

[61.] Slater, C., Cleary, J., Lau, K.T., Snakenborg, D., Corcoran, B., Kutter, J.P., Diamond, D. (2010), "Validation of a fully autonomous phosphate analyser based on a microfluidic lab-on-a-chip", Water Science & Technology, Vol 61, pp 1811 - 1818

[62.] Henari, F.Z., Culligan, K.G. (2010), "The Influence of pH on Nonlinear Refractive Index of Bromophenol Blue", Physics International, Vol 1, pp 27 - 30

[63.] Hefeeda, M., Bagheri, M. (2007), "Wireless sensor networks for early detection of forest fires", In Proc. of International Workshop on Mobile Ad hoc and Sensor Systems for Global and Homeland Security (MASS-GHS'07), in conjunction with IEEE MASS'07, Pisa, Italy, pp. 2376 - 2380

[64.] Ruzzelli, A., Doherty, A.R. (2010), "Energy monitoring in homes", In: ESB Sustainability Week, Dublin, Ireland

[65.] Chan. E., Han, S. (2009), "Energy Efficient Residual Energy Monitoring in Wireless Sensor Networks", International Journal of Distributed Sensor Networks, Vol 5 (6), pp 748 – 770

[66.] Yu, Y., Prasanna, V.K., Krishnamachari, B. (2006), "Information processing and routing in wireless sensor networks", World Scientific Publishing, Singapore, ISBN: 978-981-277-258-9

[67.] Crossbow technology, the smart sensors technology Inc, [online], www.xbow.com, (Accessed 19th August 2010)

[68.] Polastre, J., Szewczyk, R., Culler. D., (2005) "Telos: Enabling ultra-low power, wireless research", In ACM/IEEE International Symposium on Information, Processing in Sensor Networks, (UCLA) Los Angeles, California, USA

[69.] Ember wireless sensor and control network technologies, The Ember Corporation, [online], http://www.ember.com, (Accessed 19th August 2010)

[70.] Digi, Making Wireless M2M easy, XBee-PRO® specs, [online], http://www.digi.com/products/wireless/point-multipoint/xbee-series1-module.jsp, (Accessed 19th August 2010)

[71.] Ding, F., Song, G., Yin, K., Li. J., Song, A. (2009), "A GPS-enabled wireless sensor network for monitoring radioactive materials", Sensors and Actuators A: Physical, Vol 155, pp 210 – 215

[72.] Jiang, P., Xia, H., He, Z., Wang, Z. (2009), "Design of a Water Environment Monitoring System Based on Wireless Sensor Networks", Sensor, Vol 9, pp 6411 - 6434

[73.] Becher, C., Kaul, P., Mitrovics, J., Warmer, J. (2010), "The detection of evaporating hazardous material released from moving sources using a gas sensor network", Sensors and Actuators B: Chemical, Vol. 146, pp 513–520

[74.] Choi, K.Y., Park, J.S., Park, K.B., *et al*., (2010), "Low power micro gas sensors using mixed SnO2 nanoparticles and MWCNTs to detect NO2, NH3, and xylene gases for ubiquitous sensor network applications", Sensors and Actuators B: Chemical, doi:10.1016/j.snb.2010.07.041 (article in press)

[75.] Krebs, F.C. (2009), "Fabrication and processing of polymer solar cells: A review of printing and coating techniques", Solar Energy Materials and Solar Cells, Vo 93 (4), pp 394 – 412

[76.] Van Bavel, M., Aernouts, T., (2010), Organic Solar Cells on the Path to Commercialization, Technology Trends, [online], http://www.exposolar.org/2011/eng/center/contents.asp?idx=124&page=1&search=&searchstring=&exposolar=, (Accessed 01 Novemeber 2010)

[77.] De Gans, B.J., Schubert, U.S. (2003), "Inkjet Printing of Polymer Micro-Arrays and Libraries: Instrumentation, Requirements, and Perspectives Macromolecular Rapid Communications", Vol 24, 659 - 666

[78.] Le, H.P., (1998), "Progress and trends in ink-jet printing technology*",* Journal Imaging Science Technology, Vol 42, 49 - 62.

[79.] Setti, L., Fraleoni-Morgera, A., Ballarin, B., Filippini, A., Frascaro, D., Piana, C. (2004), "An amperometric glucose biosensor prototype fabricated by thermal inkjet printing", Biosensors and Bioelectronics, Vol 20 (10), pp 2019 - 2026

[80.] Pekkanen, V., Mäntysalo, M., Kaija, K. (2010), "Utilizing inkjet printing to fabricate electrical interconnections in a system-in-package", Microelectronic Engineering, Vol 87, Issue 11, November 2010, pp 2382 - 2390

[81.] Dimension 768 Series, Product Specifications, [online], http://www.dimensionprinting.com/3d-printers/printing-productspecs768series.aspx (Accessed 18th August 2010)

[82] Cole-Parmer Technical Library, Chemical Resistance of Fluoropolymers, [online], http://www.coleparmer.com/techinfo/techinfo.asp?htmlfile=Zeus_Chem_Resistance.htm&ID=827 (Accessed 19th August 2010)

[83.] Hayes, G., Beirne, S., Kiernan, B., *et al.,* (2008), "Chemical Species Concentration Measurement via Wireless Sensors" World Academy of Science, Engineering and Technology, Vol 44, pp 158 - 162

[84.] Rankin, D.W.H. (2009), "CRC Handbook of Chemistry and Physics", CRC Press (an imprint of Taylor & Francis Group): Boca Raton, Florida

[85.] van den Berg, A.M.J., Smith, P.J., Perelaer, J., *et al.*, (2006), "Inkjet printing of polyurethane colloidal suspensions", Royal Society of Chemistry- Soft Matter, Vol 3, pp 238 – 243

[86.] Wyant, J.C., Creath, K. (1990), "Absolute Measurement of Surface Roughness", Applied Optics, Vol.29 (26), pp 3823 – 3827

[87.] Bennett, J.M., (1976) "Measurement of the rms roughness, autocovariance function and other statistical properties of optical surfaces using a FECO scanning interferometer , Optics info base, Vol 15 (11), pp 2706 – 2721.

6

Appendix - A

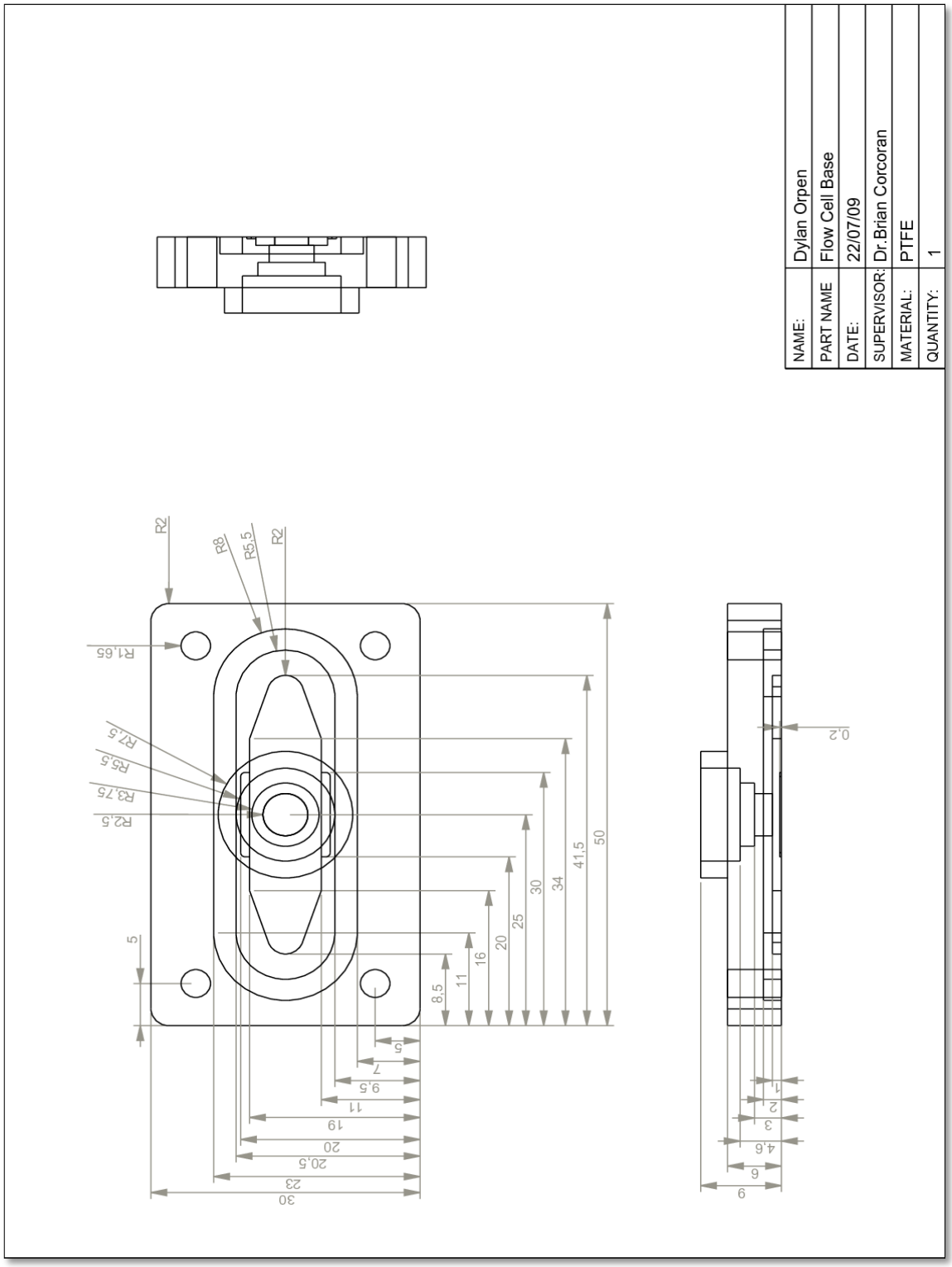
NAME: Dylan Orpen
PART NAME Flow Cell Base
DATE: 22/07/09
SUPERVISOR: Dr.Brian Corcoran
MATERIAL: PTFE
QUANTITY: 1
R2
R8
R5.5
R2
R1.65
R7.5
R5.5
R3.75
R2.5
5
8.5
11
16
20
25
30
34
41.5
50
5
7
9.5
11
19
20
20.5
23
30
0.2
1
2
3
4.6
6
9

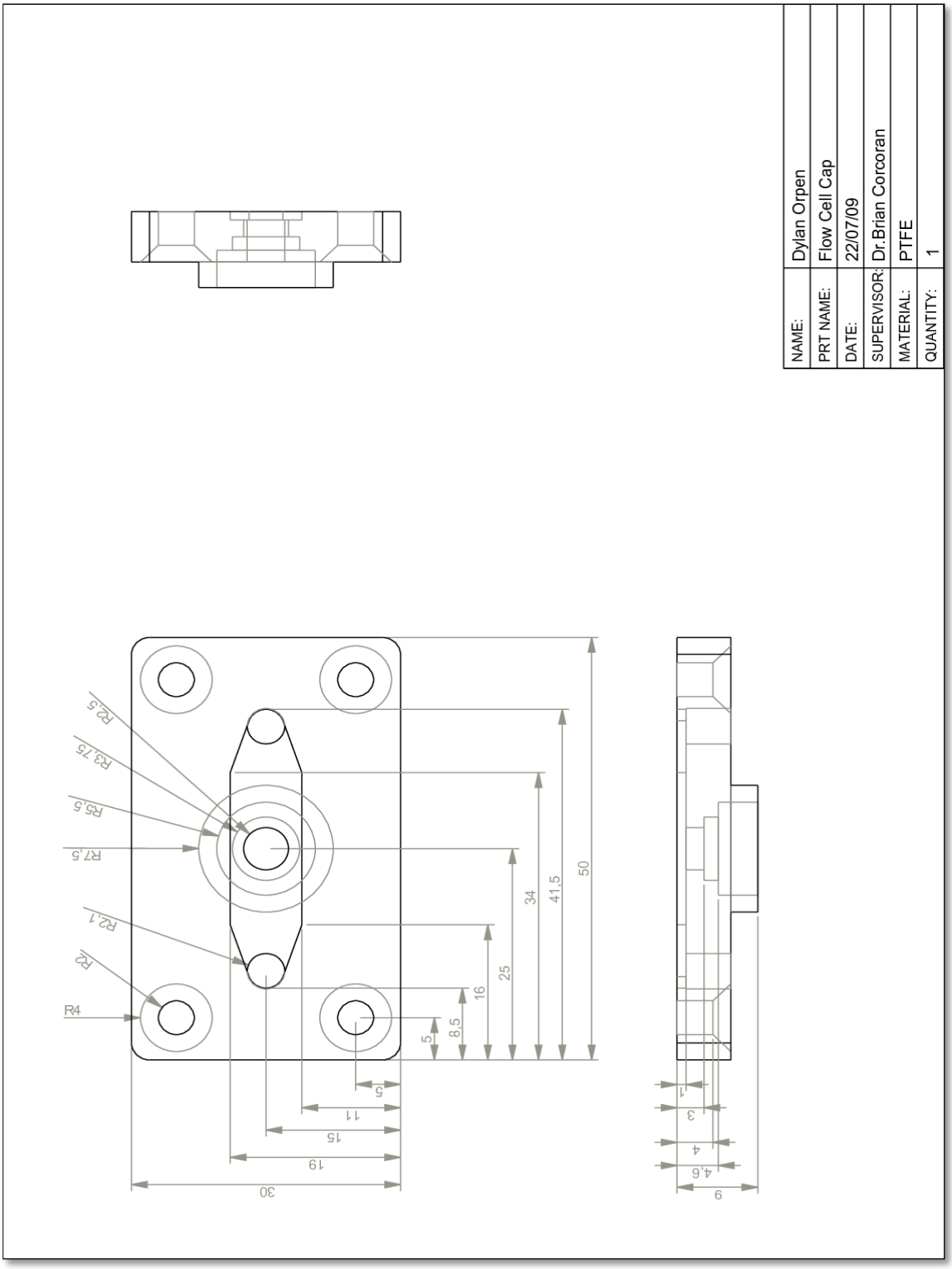
NAME: Dylan Orpen
PRT NAME: Flow Cell Cap
DATE: 22/07/09
SUPERVISOR: Dr.Brian Corcoran
MATERIAL: PTFE
QUANTITY: 1
R2,5
R3,75
R5,5
R7,5
R2,1
R2
R4
50
41,5
34
25
16
8,5
5
30
19
15
11
5
9
4,6
4
3
1

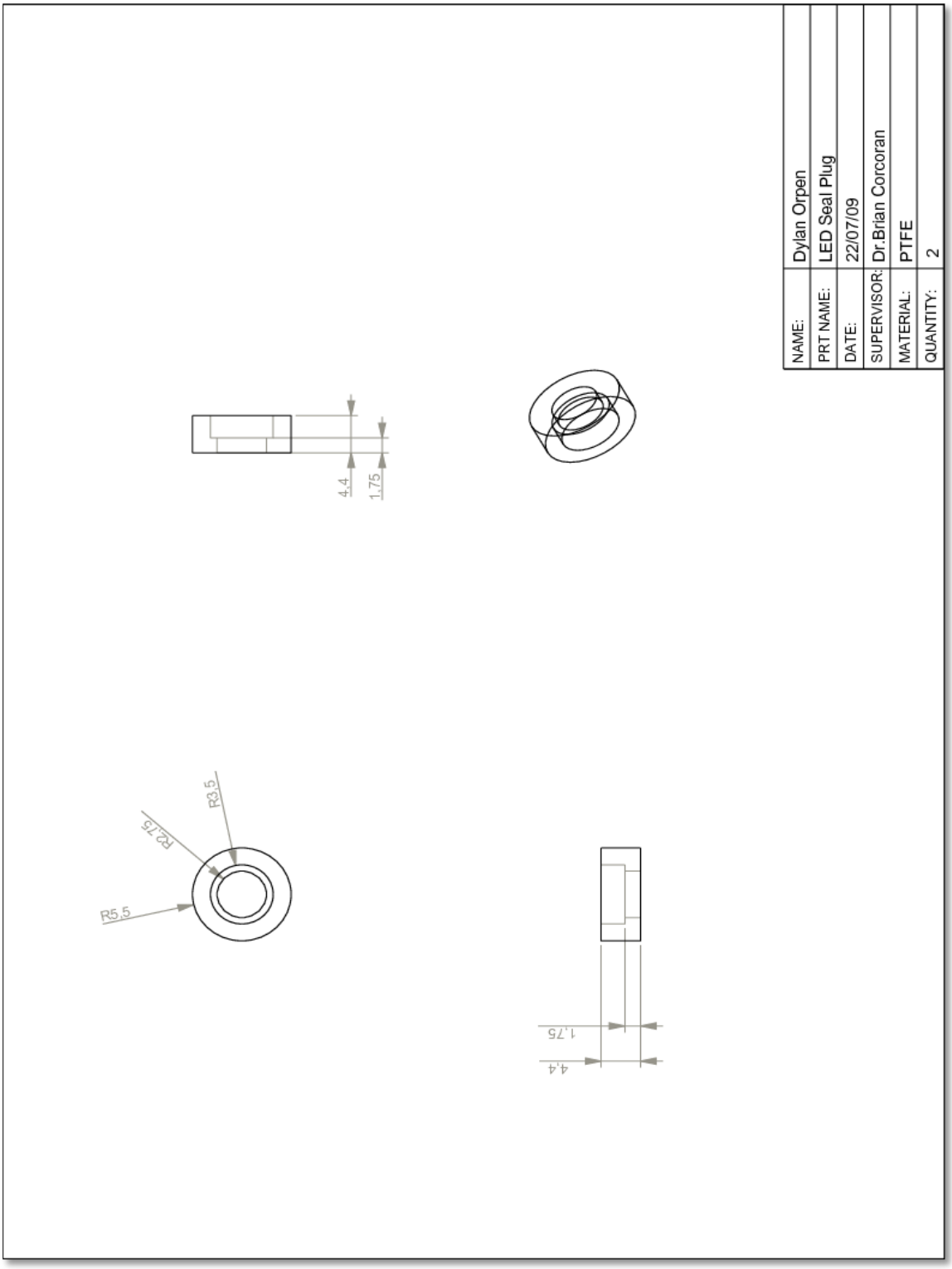
NAME: Dylan Orpen
PRT NAME: LED Seal Plug
DATE: 22/07/09
SUPERVISOR: Dr.Brian Corcoran
MATERIAL: PTFE
QUANTITY: 2
4.4
1.75
R3.5
R2.75
R5.5
1.75
4.4

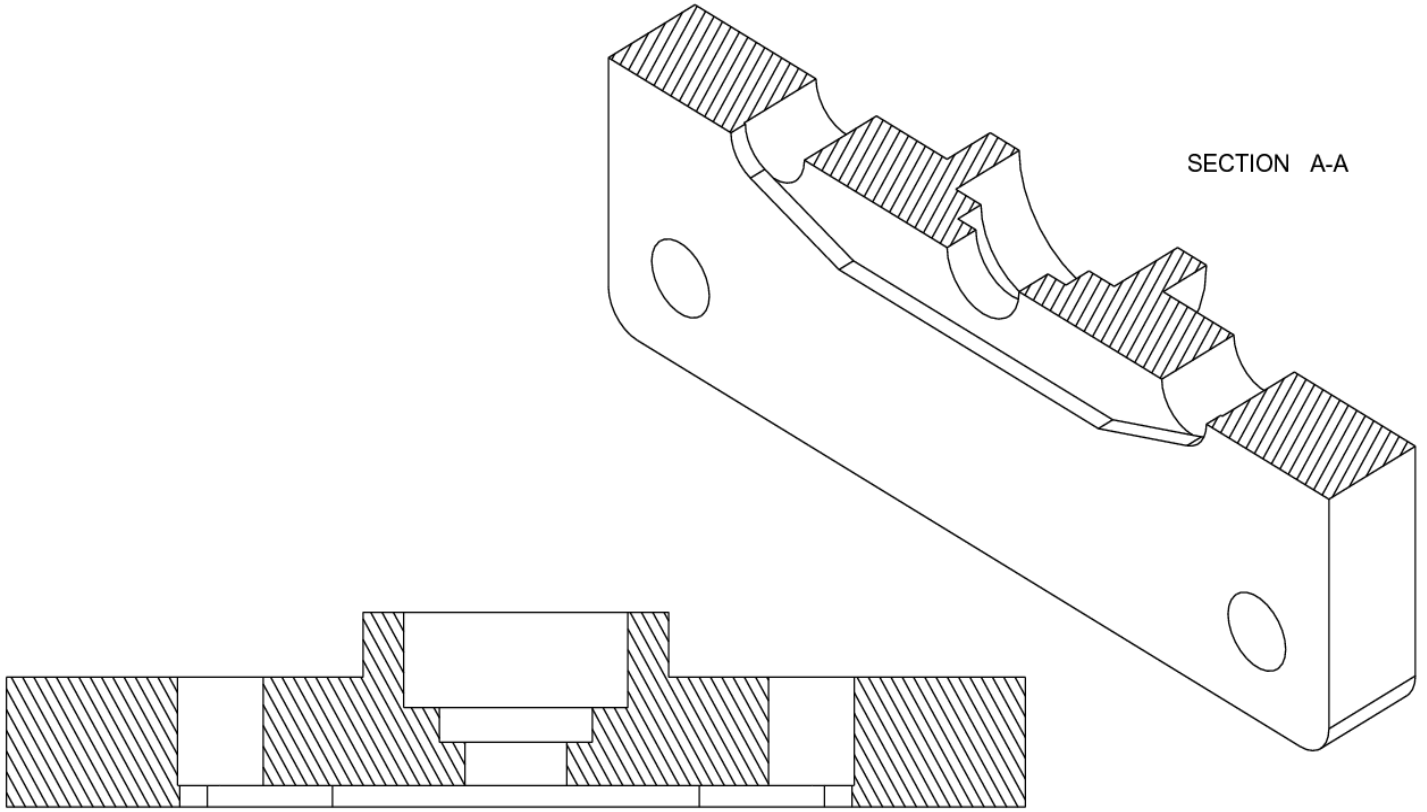

SECTION A-A

NAME:	Dylan Orpen
PRT NAME:	Flow Cell Cap
DATE:	22/07/09
SUPERVISOR:	Dr.Brian Corcoran
MATERIAL:	PTFE
QUANTITY:	1

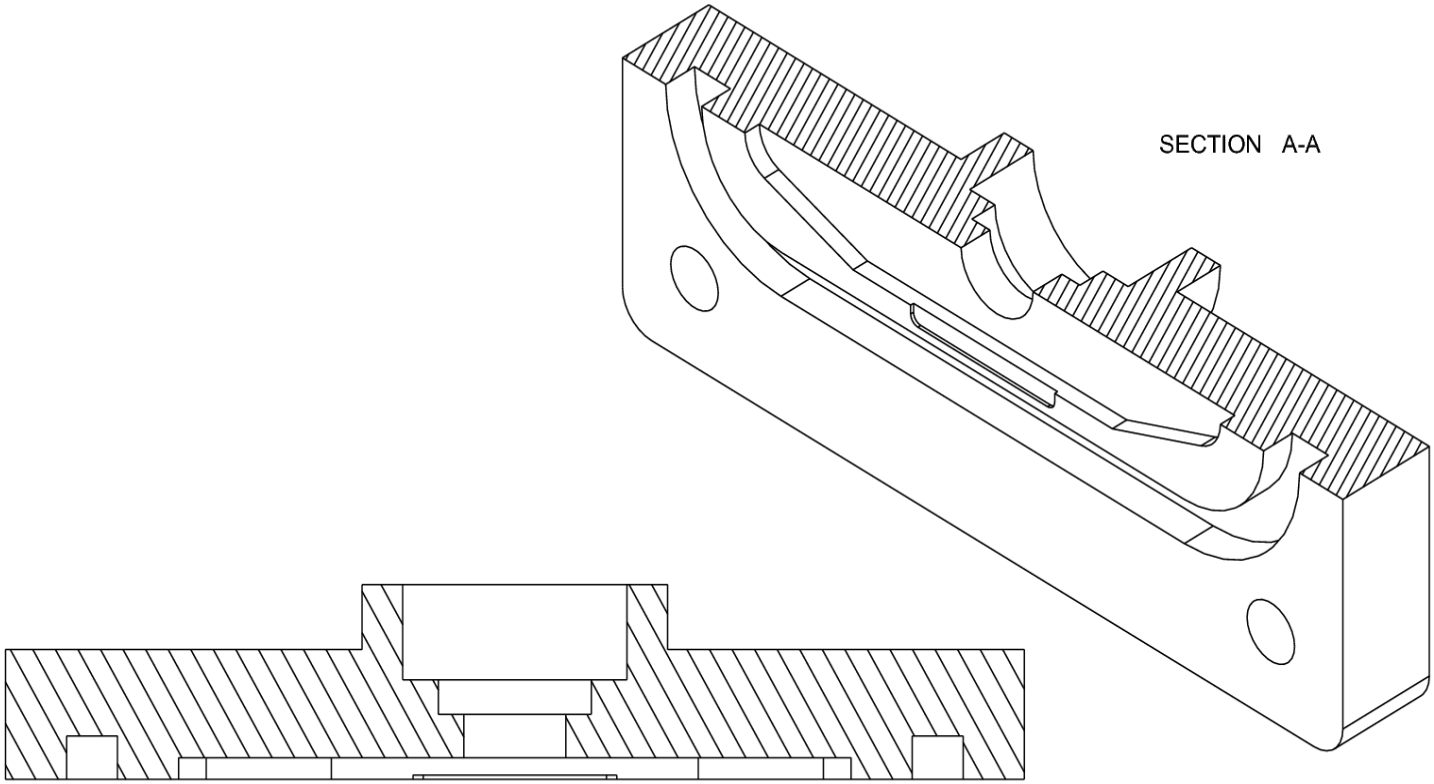

NAME:	Dylan Orpen
PRT NAME:	Flow Cell Base
DATE:	22/07/09
SUPERVISOR:	Dr.Brian Corcoran
MATERIAL:	PTFE
QUANTITY:	1

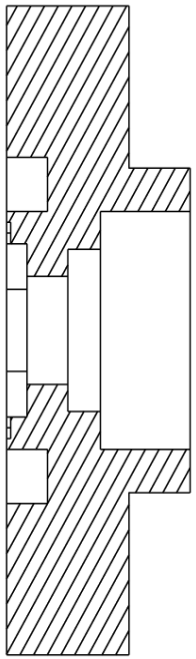

SECTION C-C

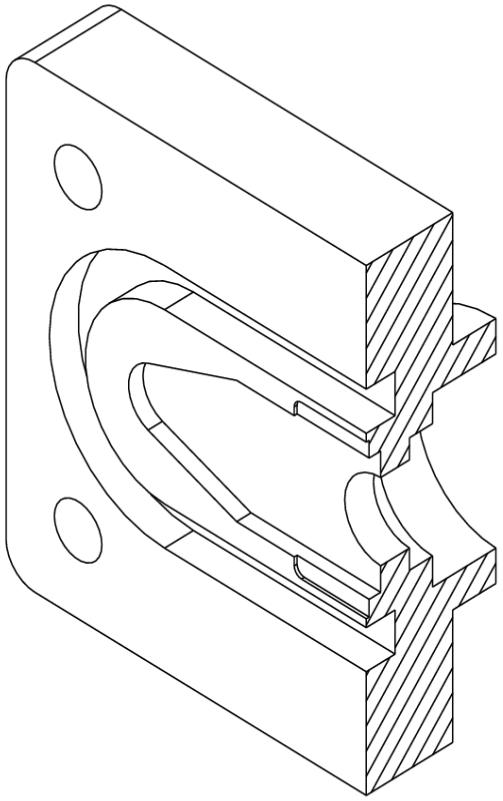

SECTION C-C

NAME:	Dylan Orpen
PRT NAME:	Flow Cell Base
DATE:	22/07/09
SUPERVISOR:	Dr.Brian Corcoran
MATERIAL:	PTFE
QUANTITY:	1

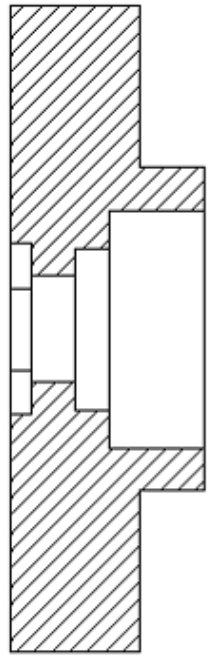

SECTION C-C

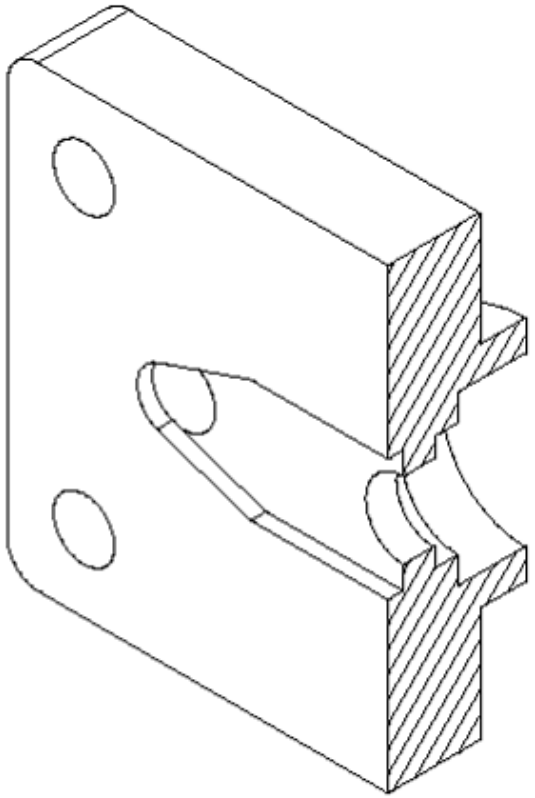

SECTION C-C

NAME:	Dylan Orpen
PRT NAME:	Flow Cell Cap
DATE:	22/07/09
SUPERVISOR:	Dr.Brian Corcoran
MATERIAL:	PTFE
QUANTITY:	1

Appendix - B

Operation code for the MATLAB® based collection program.

```
%% L.E.D. Reading & Adaptive Plotting
%% Dylan Orpen & Damien Maher 22-10-09

% create the serial object & open it
    serialPort = 'COM4';
    serialObject = serial(serialPort);
    set(serialObject,'DataBits',8)
    set(serialObject,'BaudRate',57600);
    set(serialObject,'RequestToSend','off');
    set(serialObject,'StopBits',1);
    set(serialObject,'FlowControl','none');
    set(serialObject,'terminator', 'LF/CR');
    set(serialObject,'InputBufferSize',40096,'OutputBufferSize',40096)
    fopen(serialObject);


% turn on IO 2 and set the device sampling
    fprintf(serialObject,'\r')
    fprintf(serialObject,'\r')
    fprintf(serialObject,'IO 2 ON')
    fprintf(serialObject,'ledFix 14000 5')
    fprintf(serialObject,'\r ')
    fprintf(serialObject,'\r ')


% setting up data collection & initializing loop variables
    stopTime = '01/18 17:10';
    serialObject.RecordDetail = 'verbose';
    serialObject.RecordName = 'calibrationtestfixed.txt';
    record(serialObject)
    data = 0;
    timenow = now;
    count1 = 1;
    CCC = [];
```

```
        while ~isequal(datestr(now,'mm/DD HH:MM'),stopTime);

            data1{1,count1}= fscanf(serialObject,'%*s''%f');
            CC = textscan(data1{1,count1}, '%f', 'delimiter', ' ');

            ind  = find(CC{1,1}(2:end-1)>50000);
            tmp = CC{1,1}(2:end-1);

            if ~isempty(ind)
                    tmp(ind) = [];
            end

            CCC = [CCC; tmp];

            if ~isempty(CCC)
               figure(1)
               plot(CCC)
            end

            if isnan(CCC)
               CCC= [];
            end
            count1 = count1 +1;

         end

      timend = now
      timediff=timend-timenow
      y = linspace(timenow,timend,length(CCC))
      y=y'



% %setting up plot window & plot result
colordef white
figure(1)
plot (y,CCC, 'r')
datetick('x',13,'keeplimits','keepticks')
figure(gcf)
set(gca, 'fontname', 'times')
set(gca, 'fontsize', 22)
xlabel('Time [s] ')
% ylabel('Processor Counts in Logic High')

grid on
hold on


% % plot moving average results
figure(1)
```

```
colordef white
[avgdata]=moving_average(CCC,25);
plot (y,avgdata,'b','LineWidth',3,'MarkerEdgeColor','k')
datetick('x',13,'keeplimits','keepticks')


% clean up the serial object turn off recording
record(serialObject,'off');
fclose(serialObject);
delete(serialObject);
clear serialObject;
```

Appendix – C

Table 12: Measured viscosity data from formulation given in Table 4

Sample 1	13.45
Sample 2	12.57
Sample 3	12.65
Sample 4	12.85
Sample 5	12.45
Sample 6	13.15
Sample 7	13.56
Sample 8	13.51
Sample 9	12.91
Sample 10	13.54
Average	13.06

Appendix - D

From the first mg/L concentration shown on page 61

Volume of acetic acid injection = 7 µl

Volume of test chamber = 13 L

1. Convert the injection to mass using its density

   Density of acetic acid = 1.049 g/cm^3

   $m = d.V$

   $= (1.049)(7x10^{-6})$

   $= (7.343 \times 10^{-6})$

2. Evaluate unit conversion

   $= (g/cm^3)(L)$

   $= (g/cm^3)(1000cm^3)$

   $= 1000\ g$

   $= Kg$

3. Now combine the to evaluate the mass of the acetic acid injection

   $m = 7.343 \times 10^{-6}\ Kg$

   $= 7.343 \times 10^{-3}$

   $= 7.343\ mg$

4. Now that we know the total mass of the acetic acid injection dividing my the chamber size of 13 litres will allow us to calculate how much acetic acid is in one L of ambient air.

   $= 7.343\ mg / 13\ L$

   $= 0.564\ mg/L$

Appendix - E

Example of a limit of detection calculation, done for drop cast sensor evaluated from Figure 32.

- The standard deviation in the sensor baseline was first evaluated through excel as stdev = 4.02849. This value is then multiplied by 3 to give 12.08415.

- Then using the same plot the amount of sensor response to the first 0.1 mg/L injection was calculated as 571.52 units.

$\therefore$ 571.52 units = 0.1 mg/L

1 unit = (0.1/571.52) mg/L

= (1.749×10^{-3}) mg/L

$\therefore$ 12.084 units = 21.13×10^{-3} mg/L

= 0.021 mg/L

= 0.021 p.p.m.

= 21 p.p.b.

Appendix - F

Table 13: Thickness data from an array of one sided printed sensor films

The Veeco Detak 8 Profiler	
9 Film Samples	
18 Measurements	
Thin Edge	Thick Edge
2.91	7.12
2.78	6.87
3.29	7.49
3.13	6.91
3.07	6.89
3.05	7.03
2.98	6.91
3.19	7.21
3.08	7.24
2.81	7.04

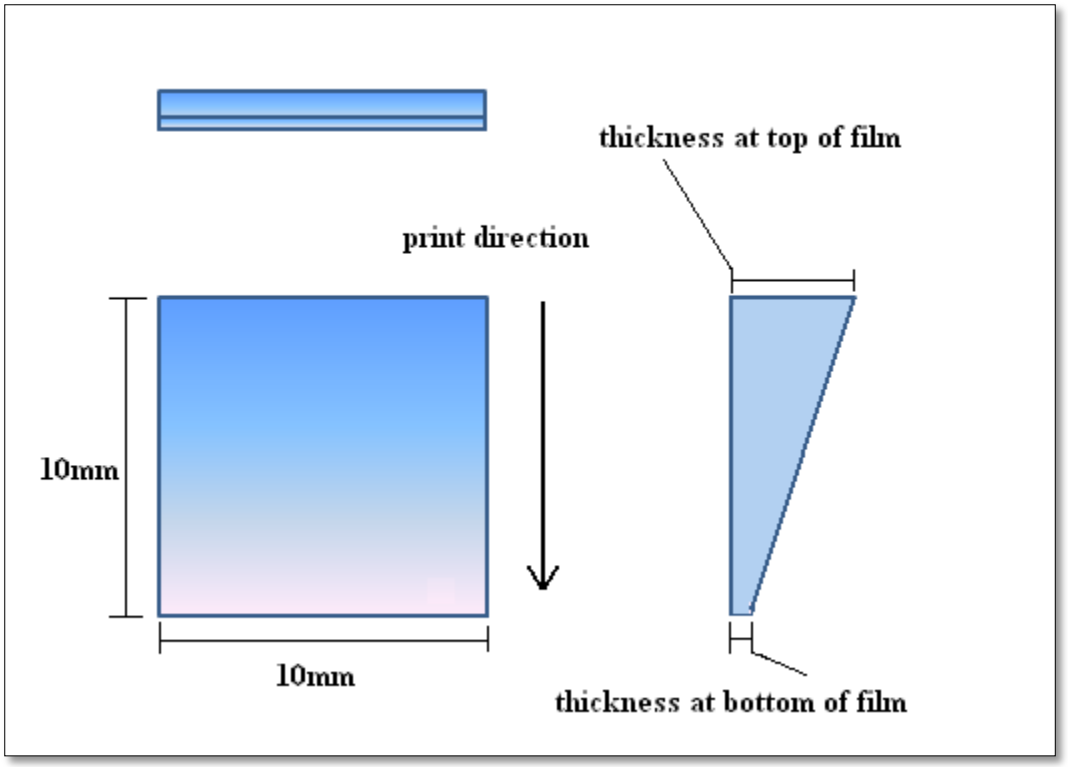

Figure 44: Graphical representation of gradient across printed slides

Appendix – G

Full collection of AFM scans of inkjet printed sensor slides, included feature distributions topography plots.

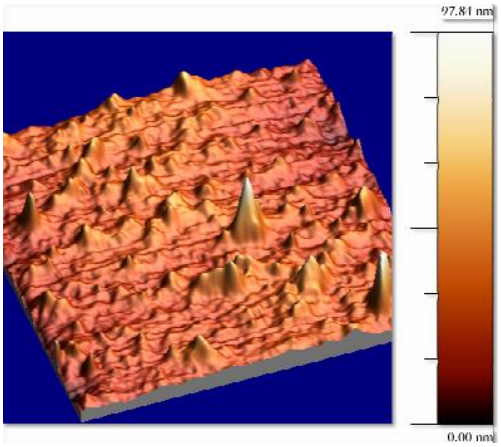

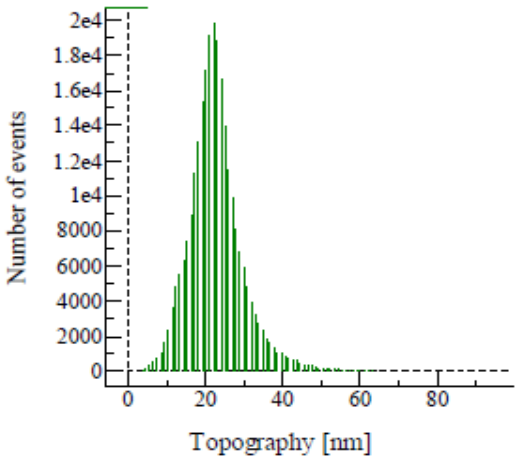

Area Size: 20 µm x 20 µm
RMS: 7.7594

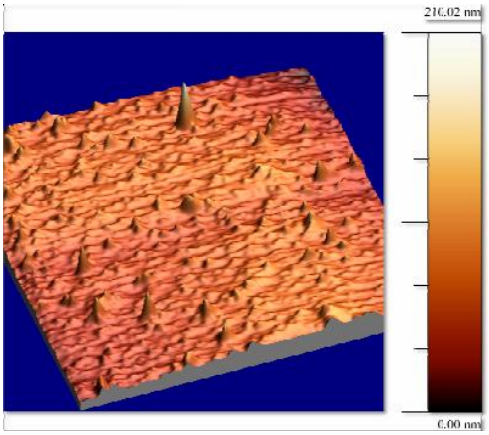

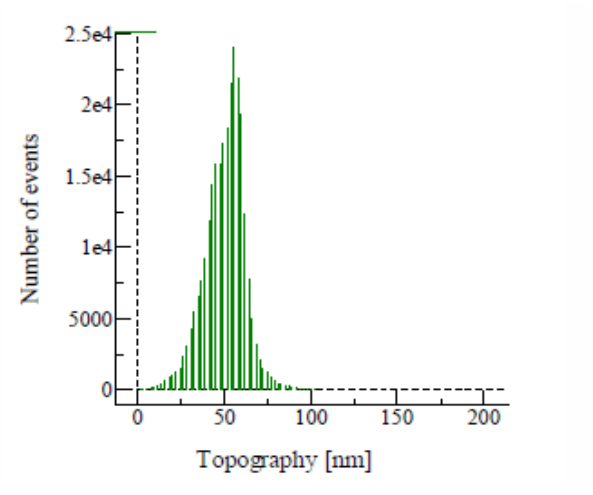

Area Size: 80 µm x 80 µm
RMS: 11.8351

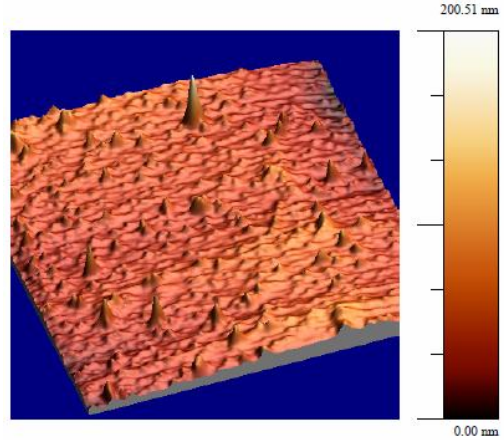

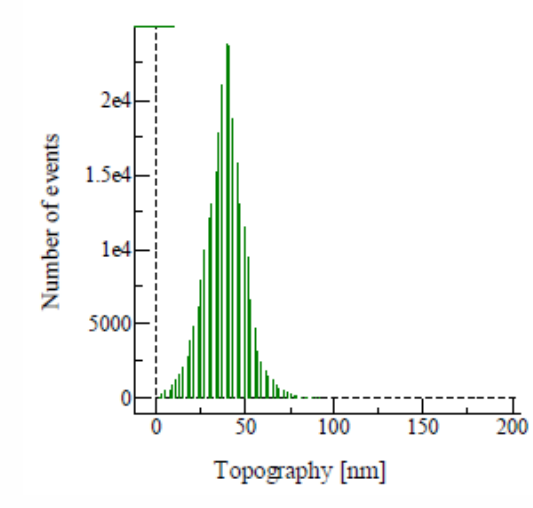

Area Size: 80 µm x 80 µm
RMS: 11.53

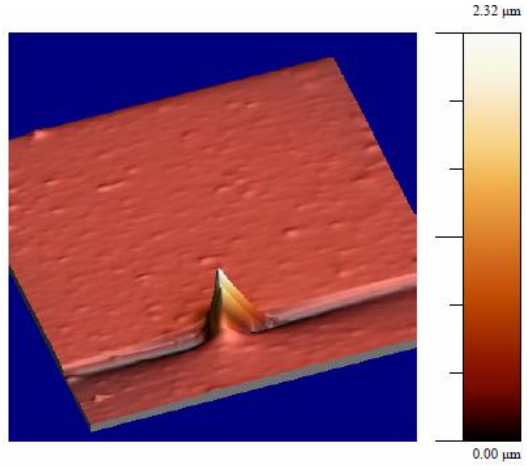

From this point on intereference is seen in the scans obvious in the topgraphy distrabution as lots of low amlitude noise. This has resulted in a distortion of the results and an appeared increase in RMS. It was most likely caused by inaccuracies in the replacement of the AFM tip.

Tip Crashed.

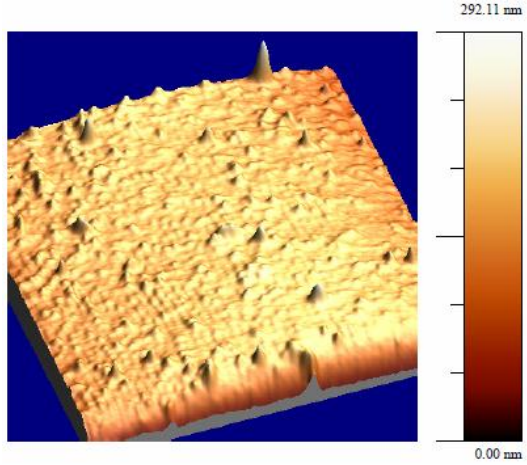

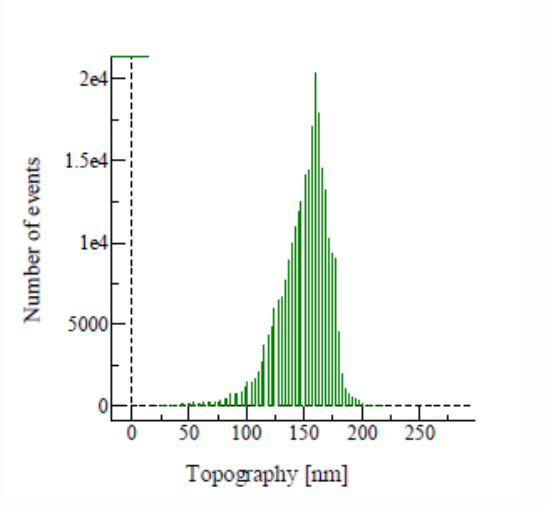

Area Size = 80 µm x 80 µm
RMS = 22.9

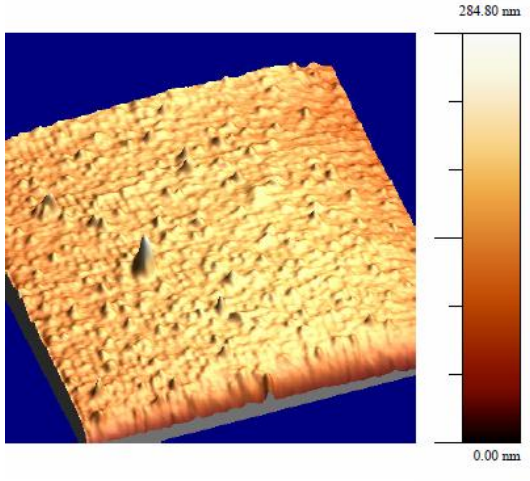

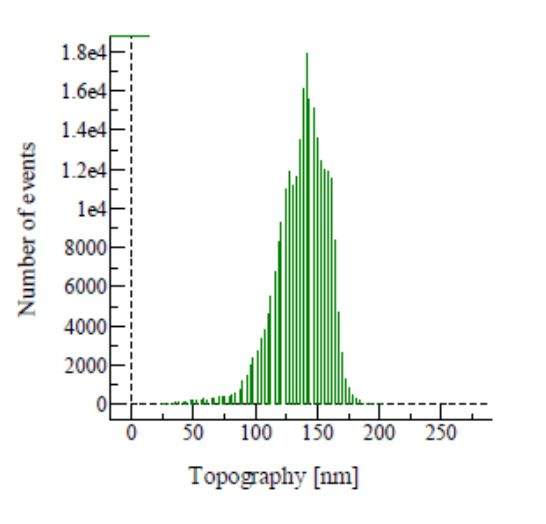

Area Size 80 µm x 80 µm
RMS: 21.9